University of Texas Rio Grande Valley
ScholarWorks @ UTRGV

Theses and Dissertations - UTB/UTPA

8-2015

Onboard load sensor prototype for use in freight railcar service

Thomas Michael Diedrich
University of Texas-Pan American

Follow this and additional works at: https://scholarworks.utrgv.edu/leg_etd

 Part of the Mechanical Engineering Commons

Recommended Citation

Diedrich, Thomas Michael, "Onboard load sensor prototype for use in freight railcar service" (2015). *Theses and Dissertations - UTB/UTPA*. 177.
https://scholarworks.utrgv.edu/leg_etd/177

This Thesis is brought to you for free and open access by ScholarWorks @ UTRGV. It has been accepted for inclusion in Theses and Dissertations - UTB/UTPA by an authorized administrator of ScholarWorks @ UTRGV. For more information, please contact justin.white@utrgv.edu, william.flores01@utrgv.edu.

ONBOARD LOAD SENSOR PROTOTYPE FOR USE IN FREIGHT RAILCAR SERVICE

A Thesis

by

THOMAS MICHAEL DIEDRICH

Submitted to the Graduate School of the
University of Texas Pan-American
In partial fulfillment of the requirements for the degree of

MASTER OF SCIENCE

August 2015

Major Subject: Mechanical Engineering

ONBOARD LOAD SENSOR PROTOTYPE IN

FREIGHT RAILCAR SERVICE

A Thesis
by
THOMAS MICHAEL DIEDRICH

COMMITTEE MEMBERS

Dr. Constantine Tarawneh
Co-Chair of Committee

Dr. Stephen Crown
Co-Chair of Committee

Dr. Robert Jones
Committee Member

August 2015

Copyright © 2015 Thomas Michael Diedrich
All Rights Reserved

ABSTRACT

Diedrich, Thomas M., Onboard Load Sensor Prototype for Use in Freight Railcar Service. Master of Science (MS), August, 2015, 124 pp., 4 tables, 62 figures, 14 references.

Determining the exact load carried by an individual railcar is crucial in the railroad industry. With an accurate load measurement, the filling process can be optimized to provide maximum cargo load without exceeding the loading thresholds set by the Association of American Railroads (AAR). In addition to optimizing the cargo load, an accurate load measurement will make it possible to identify any load imbalance in the railcar which has detrimental effects on bearing. Previous work conducted with a strain-gauge-based load sensor suspended between a thermoplastic steering pad and a bearing adapter provided accurate load data in the laboratory setting. This thesis details the work performed to optimize the load sensor for use in freight railcars, which includes developing a calibration procedure suitable for field service. The thesis also summarizes the efforts undertaken to produce eight load sensor prototypes in preparation for field testing on a freight railcar.

DEDICATION

I dedicate this work to my parents whom without my Masters' studies would not have become anything more than a dream. My dad, Thomas Martin Diedrich, for teaching me responsibility and work ethic, traits forever instilled in me. My mother, Ida Diedrich, for always being there as a person I could turn to when I needed help working through any issues. Their support had no limits, and for that I will always be grateful. Amy, thank you for always being there to put a smile on my face no matter the circumstance, you are a true guiding light in a dark tunnel.

ACKNOWLEDGEMENTS

I would like to thank my Co-Chair, Dr. Constantine Tarawneh, for providing a great research environment for students to take the knowledge gained in classrooms and applying that knowledge to real life problems. Not only is he a great leader, but a person who invests so much of his time into helping students become the best that they can be. Thank you for all the lessons you have taught me.

I would also like to thank my Co-Chair, Dr. Stephen Crown, for your infinite wisdom and always being available to bounce ideas off one another. Without your insight this project would not be near the final stage it is today.

Dr. Robert Jones, for being a great teacher in mechanical design, a subject that I hope to pursue in my professional career, as well as being an exceptional source of information whenever the research path dipped into the materials field.

I would also like to thank Lorenzo Saenz and James Bantz III for teaching me so many vital skills necessary to be successful in this project. A special thanks to the students in the Railroad Research Group for all the help and support, not only as colleagues, but great friends.

TABLE OF CONTENTS

Page

LIST OF TABLES

Page

LIST OF FIGURES

Page

CHAPTER I

BRIDGING THE GAP BETWEEN SEASONED SOLUTIONS AND CUTTING EDGE TECHNOLOGY

Transportation of cargo by rail is the most efficient method currently in use. According to CSX, "Trains can move a ton of freight over 480 miles on a single gallon of fuel." [1]. Although rail is arguably one of the most efficient methods of transportation, limitations do exist. For instance, all systems of the railcar must work in perfect unison to ensure the safety of the cargo as well as anyone in the proximity of the train. One of the main components of the suspension system that can suffer catastrophic failure is the tapered roller bearing. Current solutions are in place to monitor bearing health, however, studies have proven these methods to be crude and ineffective [2].

In order to fully characterize the health of a railroad bearing, three areas must be of focus: temperature monitoring, vibration analysis, and load measurement. The Railroad Research Group at the University of Texas-Pan American has dedicated years of research and testing to develop a complete bearing health monitoring system known as a Smart Adapter that incorporates all three of these areas. This thesis focuses on the design and implementation of a Smart Adapter Insert containing a strain gauge sensor capable of measuring the load applied to the bearing, as well as two analog temperature sensors that capture the temperature of the inboard and outboard curved portions of the bearing adapter. The insert will be a near-final stage

prototype that can be tested in the laboratory as well as field tested for accuracy and survivability.

1.1 Importance of Load Measurement

The rail industry would like to improve upon the traditional ways of filling a railcar with a higher accuracy than the crude method of filling a car up to the appropriate line, known as volume loading. A simple and accurate sensor could be used to inform the buyer, and seller, of the amount of cargo filled and use that information to bill the customer for the exact amount of goods that was loaded. The sensor would also be able to inform the loading personnel when the car has reached the maximum load during filling operations. This sensor would ensure that every car is loaded to its full capacity and the train is running in the most efficient manner possible.

Apart from knowing the amount of cargo that was placed in the car, the sensor would also be able to detect if any of the cargo is lost during transport or if a tanker car is leaking over a period of time. The latter is crucial information when transporting hazardous or combustible materials in the form of liquids or solids. In North America alone, four train derailments have occurred due to oil-related leaks from oil tanker cars. Once implemented, this sensor would be ideal for detecting leaks, and as a result, prevent derailments caused by dangerous material leaks.

The addition of an onboard load sensor would have the potential to identify and monitor wheels flats as well as track defects to ensure the entire system is safe for transportation. According to the Engineering Standard Rolling Stock (ESR) Wheel Defect Manual, railcars with defective wheels may cause damage to both the track and the vehicle or lead to derailment [3]. If the sensor is able to detect instantaneous spikes in load, which is a typical indication of wheel and track defects, the problem can be addressed before any major issues arise.

An advantage of the sensor's ability to output an accurate load measurement of the railcar is being able to incorporate that load measurement into other aspects of the car such as breaking pressure. A proportional breaking control system could be developed utilizing the sensor's load measurement of the railcar to determine and apply the appropriate amount of breaking pressure needed to subdue the momentum of the railcar. Applying the appropriate breaking pressure is imperative to the safety of the railcar and its cargo. If the wrong amount is applied, then wheel flats can develop, which can then lead to track or railcar damage. The current technology implemented in the field to determine breaking pressure simply outputs whether a car is empty or loaded, which can either under- or overestimate the required breaking force. Employing the information given by the sensor could determine the precise breaking force necessary to stop the railcar, which would contribute to increased wheel life.

The sensor's ability to accurately measure the load of a railcar provides endless possibilities of safety features that can be added to the railcar to produce the safest and most efficient trains on the tracks. Aside from efficiently transporting cargo across the nation, this sensor would also save the rail industry millions of dollars by eliminating the need to request cargo weigh-ins. Depending on the type of scale used to measure cargo load, the cost of weighing an individual car can range from $100 to $500 [4]. Not only would the sensor provide savings from weighing of individual cars, but prevent costly fines that would be applied to any accidental overloadings that occur. Overloadings that could also possibly damage the track and railcar making unsafe conditions for everyone.

1.2 Temperature Use

In addition to load measurement, the insert also has the capability of measuring the adapter's temperature in the inboard and outboard regions directly loaded by the rail car. This is

the region where the adapter and roller bearing cup make direct contact. An illustration of the curved portions can be seen in CHAPTER II Figure 4(b). These temperature sensors are capable of providing accurate temperature measurements without physically touching the bearing, and because of the location of the sensors, the lag experienced during a temperature change will be minimal.

Bearing temperature is typically a direct indicator of bearing malfunction. Some of the most common problems that tend to increase operating temperature include spall formations, grease deterioration, geometric inconsistencies of the bearing components, and overloading of the bearing. Although high bearing operating temperatures do not indicate the exact cause of the issue, it can be used as a warning indicator that suggests the bearing should be closely monitored and further analyzed. Also, in extreme cases, if the measured temperature reaches AAR thresholds, immediate action should be taken to prevent any train or cargo damage.

1.3 Positive Train Control

After the 1930's, the rail economy was on a sharp decline due to the fact that the investors' return on investments was always below 3% [5]. This problem was the result of the strict regulations the U.S. had placed on the freight rail industry. The regulations restricted the rail industry from controlling shipping rates, among other aspects of the industry, as well as making all business dealings public knowledge. However, thanks to the Stagers Act of 1980, the laws were changed allowing the railroad to base their rates on market demand and conduct confidential transactions. The act also recognized the railroad industry's need to make a profit. Although the Stagers Act of 1980 gave control back to the rail industry, congress still retained the authority to protect shippers from unreasonable railroad pricing to ensure the railroads were

honest [5]. The aforementioned boosted the rail industry economy and made it, once again, a service worthy of investment.

Although congress is a big supporter of rail, they are currently demanding better awareness of train cars to ensure that fewer accidents occur. To accomplish this, congress signed a legislation that mandated positive train control (PTC) be placed in all rail lines used for passengers and toxic materials by the end of 2015 [6]. Although the rail industry has asked for an extension to allow PTC to be further improved, the rail industry is still providing funding towards better technology that can be placed on railcars. With a push from Congress, PTC has provided a large market for advanced monitoring technology in rail.

1.4 Current Technology

One method to identify wheel impacts is the Wheel Impact Load Detector (WILD). This system is the industry standard for monitoring and measuring wheel impacts. The first generation WILD system was composed of strain gauges mounted directly on a section of rail. The strain gauges were used to measure the force applied by wheel defects that crossed the track. The strain gauge would then output a voltage that was correlated to the force seen by the particular wheel defect. A computer would then determine if the train needed immediate action or was able to continue operation. The second generation WILD system utilizes accelerometers, which are mounted to the track, to measure the vibration caused by a wheel impact. That measurement is then used to evaluate the size of the wheel defect. Figure 1 is a picture of the second generation WILD system. Along with the instrumented track, the WILD system also needs an on-site signal processor, a control PC, modems, Automatic Equipment Identification (AEI) and computers for local or remote diagnosis and monitoring [7].

Figure 1: WILD System, Wheel Sensor (Left circle) and Accelerometers Installed on Track (Right Circle) [7]

Weigh bridges are nearly identical to a WILD system with the exception that the bridges exclusively use strain gauges to measure the entire weight of the car. This information is stored in a database, and if any car is detected as overweight, then the data is sent to the appropriate personnel to ensure the railcar is still safe. The appropriate owner is also notified and receives a fine to ensure that future trains carry the appropriate weight, providing safety to the track, tapered roller bearings and wheels.

Volume loading is the simple process of taking a known commodity and filling the train car to an appropriate line that is typically used to approximate the full load. Although this method is not exact, it is used when the density of the products does not change significantly, such as grain or corn. This method rarely fills the train car to its maximum load because of the human error involved in spotting when the car is filled. In order for an operator to load corn

within a ±1% accuracy, they would have to correctly stop loading corn within 1.25 inches of the corresponding line every single time.

The breaking system on a railcar plays a very important role in cargo transportation. Functionality of the system can be the difference between a typical day and a catastrophe. In order for a train to achieve maximum breaking effectiveness, the breaking pressure must be adjusted according to how much load is carried by the train car. Safe transportation of goods relies heavily on the proper functionality of the components that make up the freight car, an example of such components are the wheels. Locking of the wheels could occur if too much force is applied during breaking, which is why applying the correct amount of breaking pressure to the wheels is of great importance. Current wheel breaking on conventional freight railcars is achieved by using a double break cylinder with compressed air acting on a large cylinder for a loaded railcar and switching to a small cylinder for a car in the unloaded state. An illustration of the double break cylinder is depicted in Figure 2. Although, this breaking system is simplistic, it can only be used for freight railcars operating less than 75 mph. For passenger trains, or high speed trains, a proportional breaking system is needed to account for the exact amount of weight applied to the train and apply a corresponding air pressure to ensure adequate breaking force. The appropriate air pressure is determined by the amount of deflection measured from the suspension springs [8]. This method of measurement can provide a close approximation to the amount of mass in the car, but cannot be used to achieve accuracies in the ±1% range.

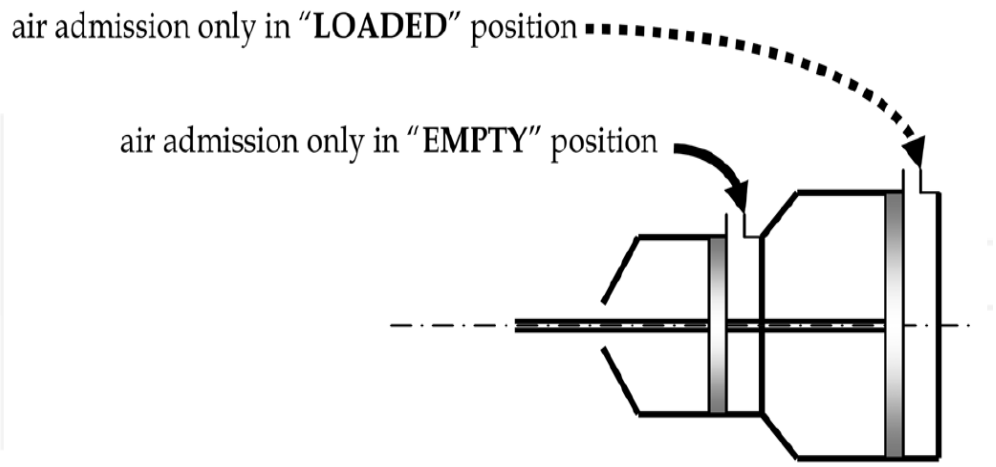

Figure 2: Double break cylinder [8]

A hot-box detector is an infrared based, non-contact, temperature measurement device that reads the bearing temperature as the train passes over the sensor. Although hot-box detectors were previously designed to flag bearings operating 170ºF above ambient for immediate removal, recent improvements to the system allowed for a comprehensive temperature examination of all the bearings on the train and flag the ones operating above the bearings' comprehensive operating temperatures [9]. These flagged bearings are known as "trended" bearings. Once a bearing is marked as "trended," the entire axle assembly is replaced. Then, at a later time, the trended bearings are removed, disassembled and inspected. "According to data collected by Amsted Rail from 2001 to 2007, an average of nearly 40% of bearing removals are *non-verified*. A non-verified bearing is one that, upon disassembly and inspection, is found not to exhibit any of the common documented causes of bearing failure such as spalling, water contamination, loose bearings, broken components, lack of lubrication, damaged seals, etc." [10]. With 40% of the bearings being possibly healthy, a tremendous amount of time, effort, money, and energy is wasted removing these possibly misdiagnosed bearings. If a new sensor were

developed that was capable of identifying high-temperature bearings while also determining whether that bearing was, in fact, defective, then there would be fewer removals of misdiagnosed, defect-free (healthy) bearings.

The goal of the Railroad Research Group at the University of Texas-Pan American is to incorporate all of the abovementioned precautionary safety methods into a single railcar monitoring device that can be placed on all railcars. This device will act as a complete health monitoring system capable of measuring the weight of a car, detecting wheel and bearing defects, while also monitoring bearing temperature. Once the device is manufactured, the Smart Adapter will make any train utilizing this technology, the safest train on the tracks.

1.5 Building Towards the Future

This thesis is a continuation of the work done by Saenz [11] at the University of Texas-Pan American, which created a working prototype of a load sensor that was able to produce a useable signal with a steel insert design. Although the prototype was able provide a clean signal clearly showing a response to the load applied to the bearing, the sensor still had room for improvement. This thesis will optimize the load sensor to produce a steady signal during use. A calibration procedure will also be devised to correlate the sensors output to the corresponding load applied. Also eight prototypes will be manufactured and calibrated for use in an upcoming field test that will validate the sensors performance and reliability.

CHAPTER II

LABORATORY SETUP AND INSERT DESIGN

Design changes and enhancements are imperative to improve upon the performance and design of a sensor until the best possible accuracy is achieved with the simplest of designs that lends itself to ease of manufacturability. However, determining what design changes will produce a more accurate and repeatable sensor requires extensive experimentation. The experiments must be completed on closely controlled test rigs capable of capturing the actual test conditions in order to produce usable data that can then be properly evaluated. Using the acquired data, educated decisions on the sensor development can be accomplished.

2.1 Experimental Setup

2.1.1 Typical Bearing Setup and Nomenclature

The main objective of the Smart Adapter is to produce a load sensor and two temperature sensors embedded in-between the AdapterPlus™ steering pad and the steel bearing adapter in a freight railcar. The final product will be a complete self-contained wireless unit reporting the sensor readings to a central location. The typical assembly of a freight railcar truck can be seen in Figure 3, where the AdapterPlus™ assembly is also highlighted. It should also be noted that a total of eight AdapterPlus™ assemblies are installed on a single freight railcar. Preferably every bearing would be equipped with a Smart Adapter to completely monitor each bearing as well as produce a real time response for any load imbalances or shifts during operation on gradients and around curves.

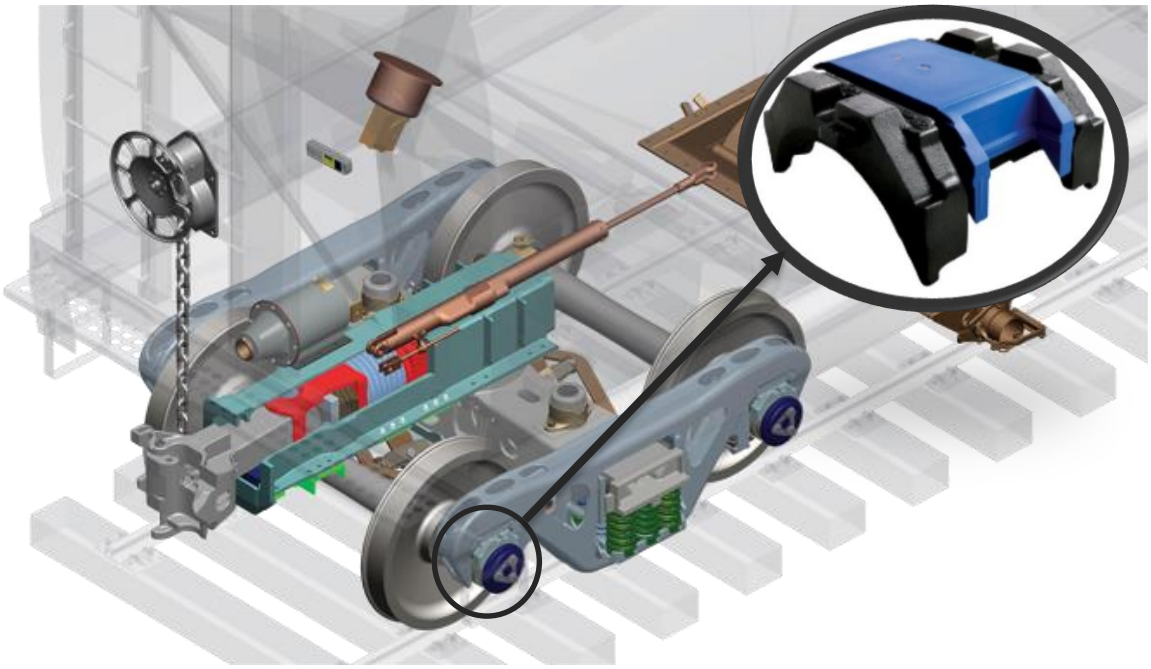

Figure 3: Freight Railcar Components with AdapterPlus™ Steering Pad and Steel Adapter Close-up [12]

The key to the success of the Smart Adapter Insert lies in the placement of the sensors. For an accurate load measurement, the sensor must be placed directly in the path of the applied load. In the assembly shown in Figure 3, the load passes directly through the steering pad to the steel adapter and then finally to the bearing and wheel. By placing the smart insert directly between the steering pad and the steel adapter, a portion of the applied load can be measured by the sensor. The temperature sensors also need to be placed as close to the bearing as possible to ensure an accurate thermal response. The AdapterPlus™ steel adapter is a cast iron component that is in direct contact with the outer surface of the bearing cup (outer ring) via the curved inner machined portions shown in Figure 4 (b). By placing the temperature sensors on the top side of the adapter directly over the curved portions, the majority of the heat can transfer to the temperature sensors with minimal thermal lag, thus, producing accurate temperature measurements.

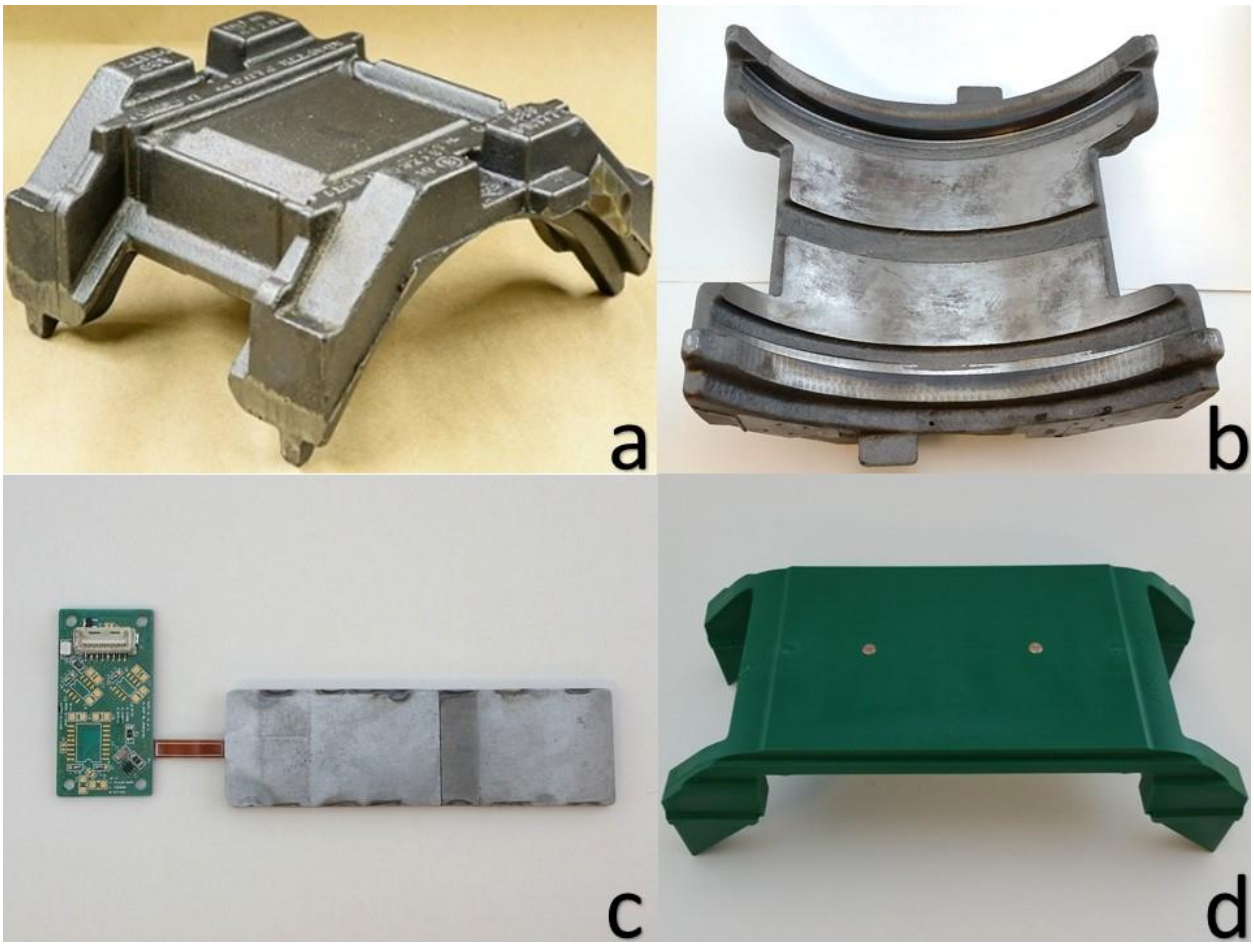

Figure 4: (a) AdapterPlus™ Bearing Adapter, (b) Bottom Side of Bearing Adapter Showing Curved Portion, (c) Smart Insert Prototype, (d) AdapterPlus™ Steering Pad

2.1.2 Single Bearing Tester

Experiments were conducted on the Single Bearing Test Rig at the University of Texas-Pan American. The Single Bearing Tester, referred to as SBT, has many advantages that made it the most suitable laboratory setup for conducting controlled experiments on the Smart Adapter Insert. The SBT is capable of simulating conditions a railroad bearing would experience in field service. The SBT allows for static testing as well as dynamic testing at speeds varying from 5 to 85 mph. Additional field service conditions can be simulated such as impacts due to wheel flats or track defects, and lateral loading resulting from a train negotiating a curve. To apply the

typical load a bearing experiences at 100% load capacity (34,400 lb_f or 153 kN), a hydraulic cylinder is utilized. This hydraulic cylinder, along with additional equipment, known as the load controller, was designed and fabricated at the University of Texas-Pan American. The load controller provides an accurate and constant load by monitoring the output of the load cell and actuating the hydraulic cylinder to maintain a specified load. The load controller can also actuate the hydraulic cylinder to simulate the filling process of a freight railcar at different loading rates ranging from slow filling (> 7 min) to fast filling (< 7 min). The hydraulic cylinder, load controller, and other components of the SBT are pictured in Figure 5.

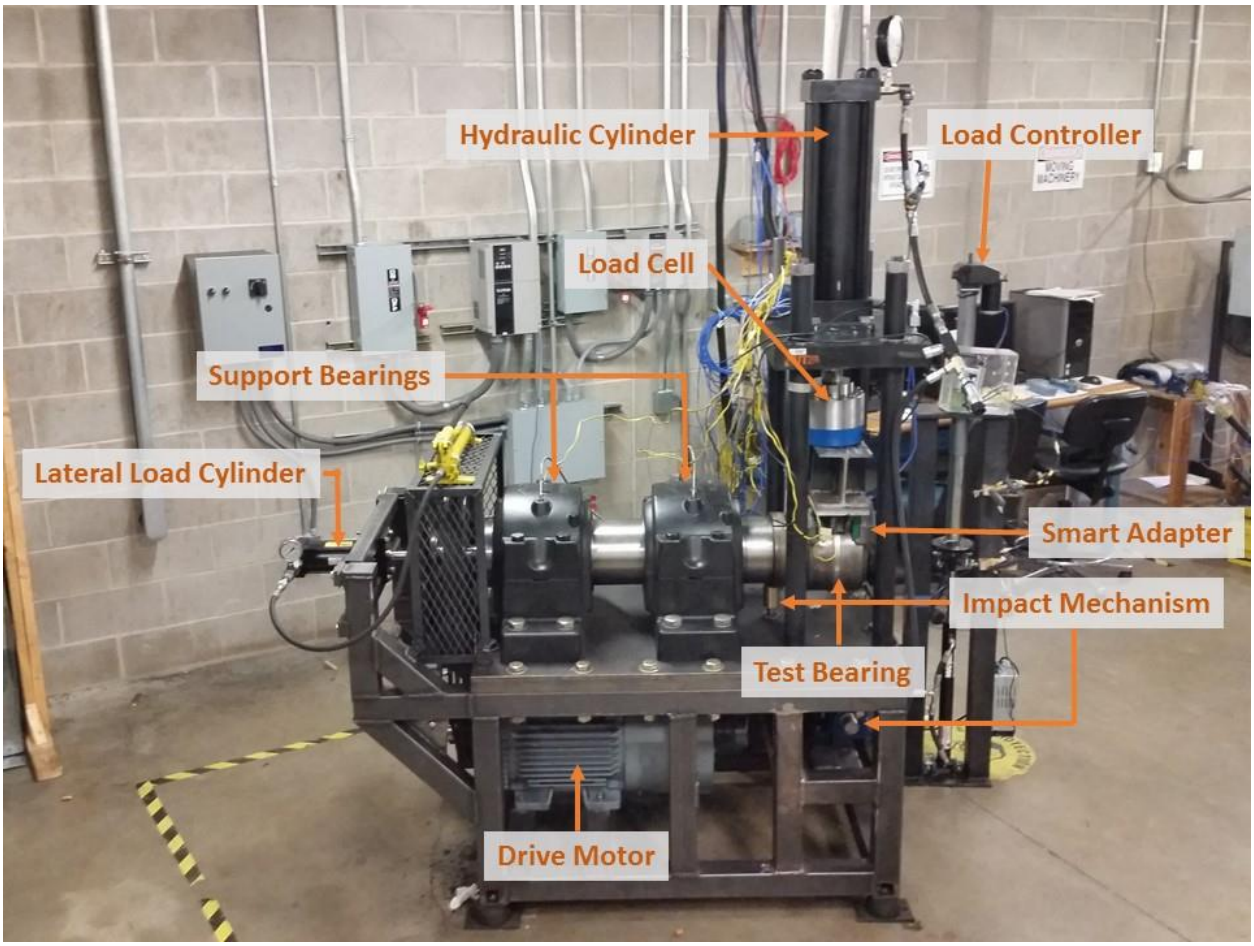

Figure 5: Single Bearing Test Rig with Annotations

2.1.3 Data Acquisition System

All data was collected with a National Instruments™ cDAQ-9474 USB chassis along with a NI 9205, 32 channel, ±10V, analog input module. Data acquisition for the strain gauge and temperature sensors were carried out at a rate of 50 Hz and post processed with a moving average of 2 seconds or 100 data points. The cDAQ-9474 chassis can be seen in Figure 6, as well as the additional slots where additional cards can be installed to provide a versatile data acquisition device.

Figure 6: NI cDaq-9474 USB Chassis with Removable Card

2.1.4 Load Controller

One of the difficult tasks of preforming controlled experiments was the ability to hold a constant load on the SBT. The fluctuations in load were caused by the thermal expansion and compression of the hydraulic fluid in the hydraulic cylinder. Initially, the load is set by pumping an appropriate amount of hydraulic fluid to provide the pressure that corresponds to the desired load setting. However, although the hydraulic cylinder valve is properly closed, changes in the ambient conditions or in the overall temperature of the test rig would result in an increase or decrease in the force applied to the bearing due to aforementioned thermal effects of the

hydraulic fluid. In order to mimic the conditions the sensor would experience in the field, a solution to the load fluctuation problem was needed.

The typical solution to provide a constant pressure in a hydraulic cylinder found in the industry is to attach an accumulator to the line. A hydraulic accumulator is a pressure storage device where the hydraulic fluid is held under pressure by a compressed gas. Thus, the accumulator provides a constant pressure to the cylinder which, in turn, produces a steady force on the adapter. However, this system would need to be manually adjusted for every change in pressure, and requires expensive parts along with high pressure gasses.

Due to the complexity of the hydraulic accumulator, additional options were examined. The ideal system should be capable of increasing or reducing the hydraulic fluid in the cylinder by small amounts. Additionally, if the pressure could be controlled by a computer in order to run a detailed testing plan, it would result in a much more accurate experiment. The devised solution is to use a 1-½ inch bore hydraulic cylinder to pump the small changes in hydraulic fluid to the system. The hydraulic cylinder is driven by a linear actuator which transforms the rotational movement of a DC motor to translational movement through a threaded rod. The system is able to determine the load measured by the load cell, and determine whether the pressure should be increased or decreased, then by sending a high or low signal to the motor controller the corresponding amount of hydraulic fluid is pumped into the system to maintain the desired load. The complete system is pictured in Figure 7 (Left) with annotations of the main components. The motor driver which is the interface between the motor and the computer signal is shown in Figure 7 (Right). The complete system is capable of providing a steady, accurate load to within 100 lb_f, and can execute a preprogrammed test plan that consists of several loading and

unloading cycles performed at different loading rates. The latter allowed testing to be conducted after-hours and during the weekends, independent of continuous human supervision.

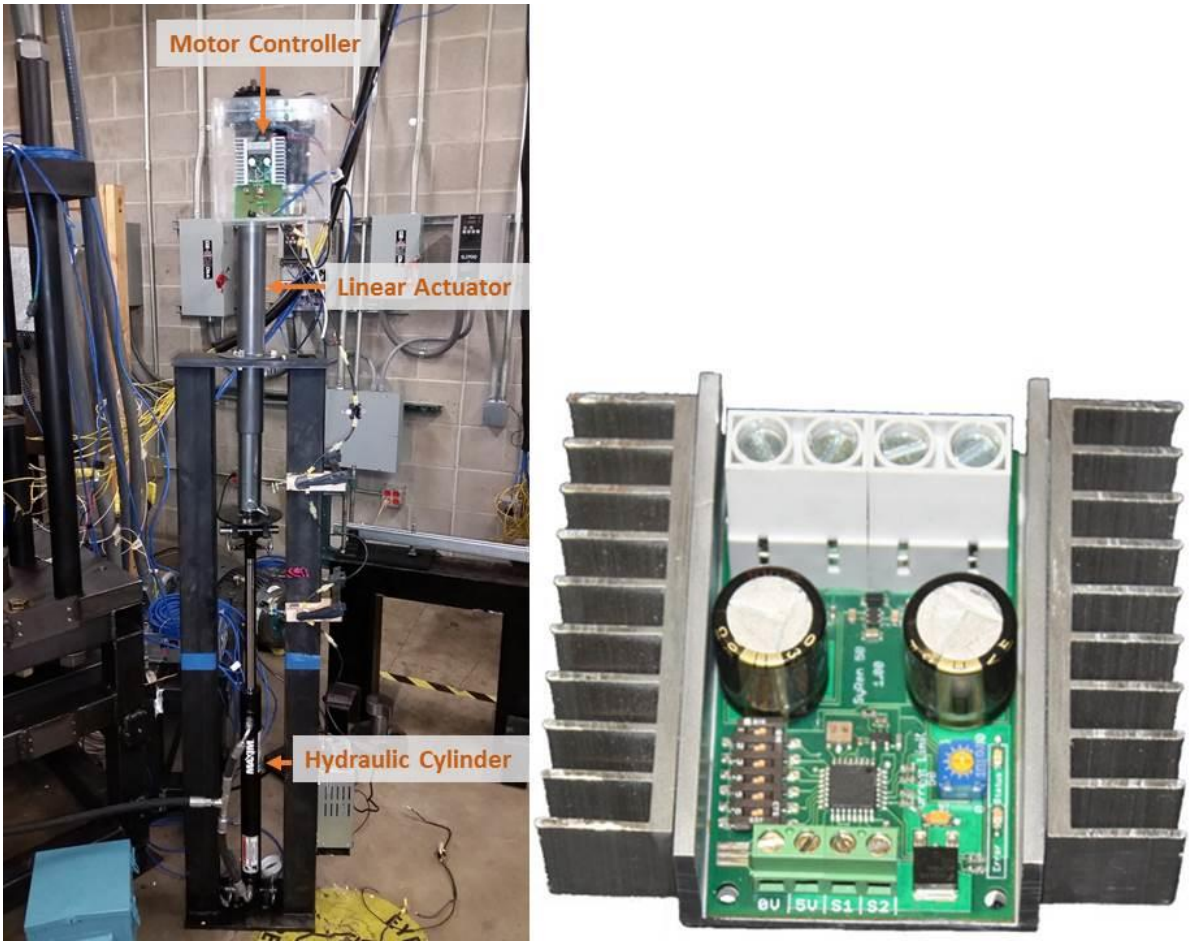

Figure 7: Load Controller with Component Annotations (Left), and SyRen 50 Amp Motor Driver (Right) [13]

2.2 Smart Insert Design

2.2.1 Strain Gauge

The basic premise behind the load sensor is a beam with both ends fixed and a distributed load applied to the entire length of the beam. Any deflection in the beam is measured by the strain gauge that is mounted to the side in tension. When the beam is deflected, a voltage change is measured and can then be related to the load applied to the bearing. The strain gauge used is a

full bridge, transducer class strain gauge with 350 ohm nominal resistance manufactured by Micro Measurements. The basic schematic of the full-bridge transducer is seen on the left of Figure 8, along with the strain equation that is capable of calculating the strain experienced by measuring the voltage output of the sensor. For additional information on using the equation refer to Saenz [11].The dimensions of the strain gauge, wire leads and labeling of the resistors on the sensor is depicted on Figure 9. It can be seen that the full bridge is made up of four individual resistors that change resistance based on strain experienced on the surface of the material to which the gauge is mounted. Two of the resistors are the active gauges that measure the strain experienced in the bending direction of the sensor; these resistors are labeled as R2 and R4. R1 and R3 act as temperature compensation for the material and will cancel out any changes in the signal due to thermal expansion, through the appropriate wiring of the circuit.

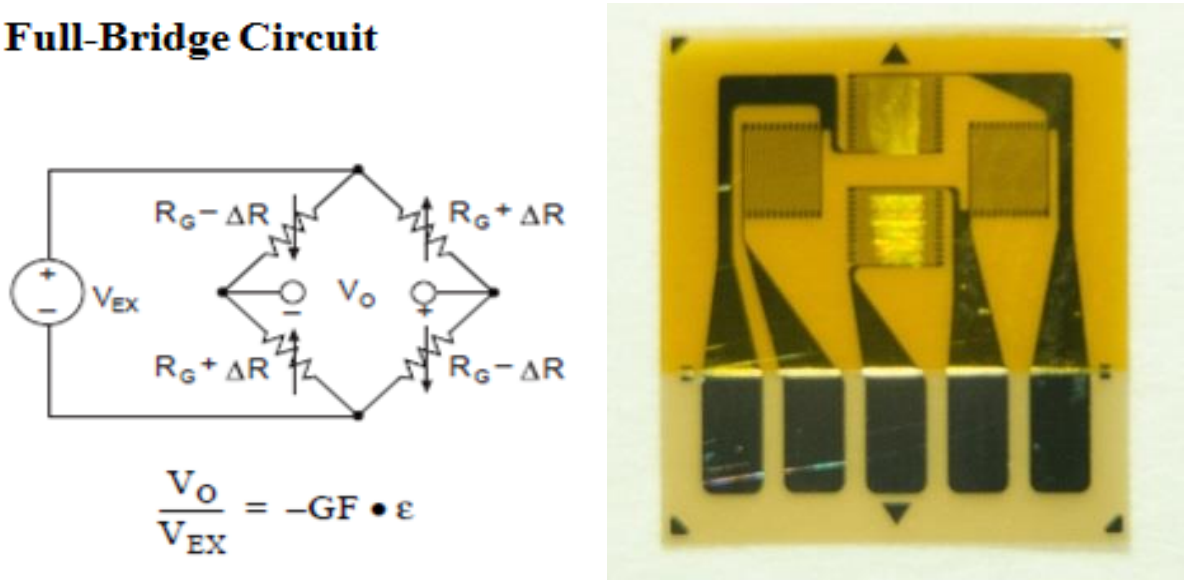

Figure 8: Full-Bride Circuit (Left) and Full-Bridge Transducer (Right) [11]

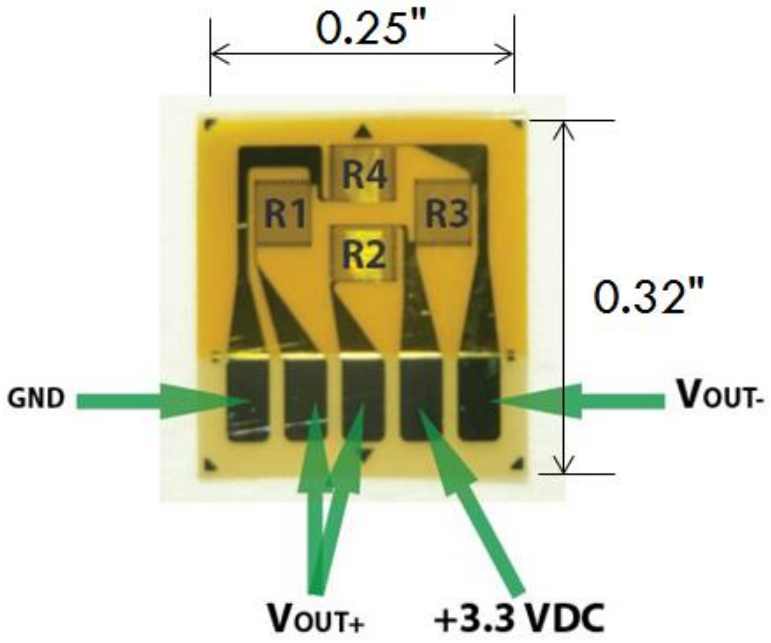

Figure 9: Full-Bridge Transducer Solder Pad Identification [11]

2.2.2 Previous Design

The final insert design (see Figure 10) developed by Saenz [11] was able to produce accurate results in a static test, though the data required an additional correlation due to a logarithmic increase in the sensor output over time. The additional step to correlate the static load would require advanced computation on the unit, which would result in increased system cost, and more energy consumption, thus, shortening the battery life of the unit once the wireless capabilities were implemented. With a reduced battery life, the usefulness of the sensor is compromised.

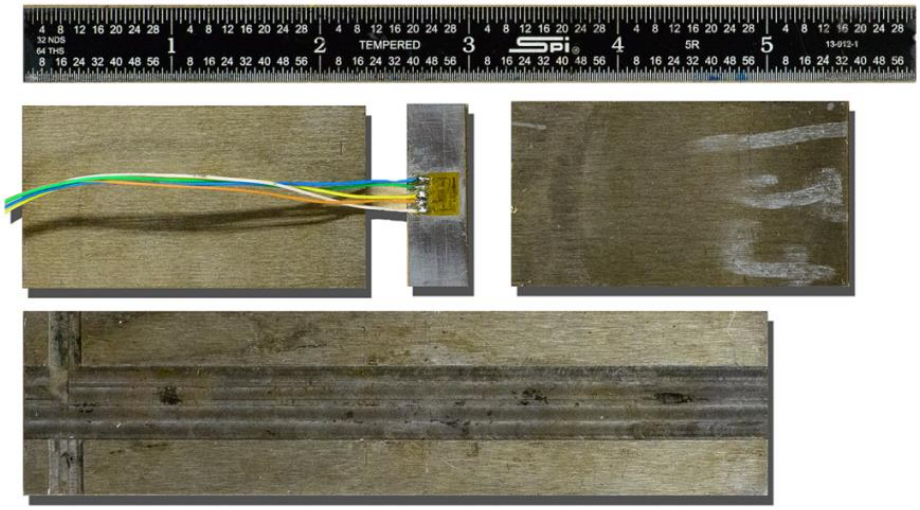

Figure 10: Load Sensor Insert Prototype Developed by Saenz [11]

The transient increase in the sensor output can be noticed in Figure 11. By monitoring the output voltage of the sensor when the load was held at 70,000 lb_f, the sensor voltage should remain constant. However, when looking at the data between 5.25 and 7.25 hours, the voltage appears to have a logarithmic function with the voltage and does not remain constant. Saenz [11] believed that the logarithmic function was caused by the creep of the elastomer pad, which gives the appearance that the sensor experiences an increase in load although the load was held constant throughout the test.

It was also observed that the sensor designed by Saenz was not accurate at loads under 50% of full load. Although the design by Saenz met the requirements which called for the load to be read accurately (within 3%) at loads ranging from 70 to 100% of full load (25,000-34,400 lb_f), a sensor capable of measuring the full load range, including an unloaded (empty) railcar (17% of full load), is preferred.

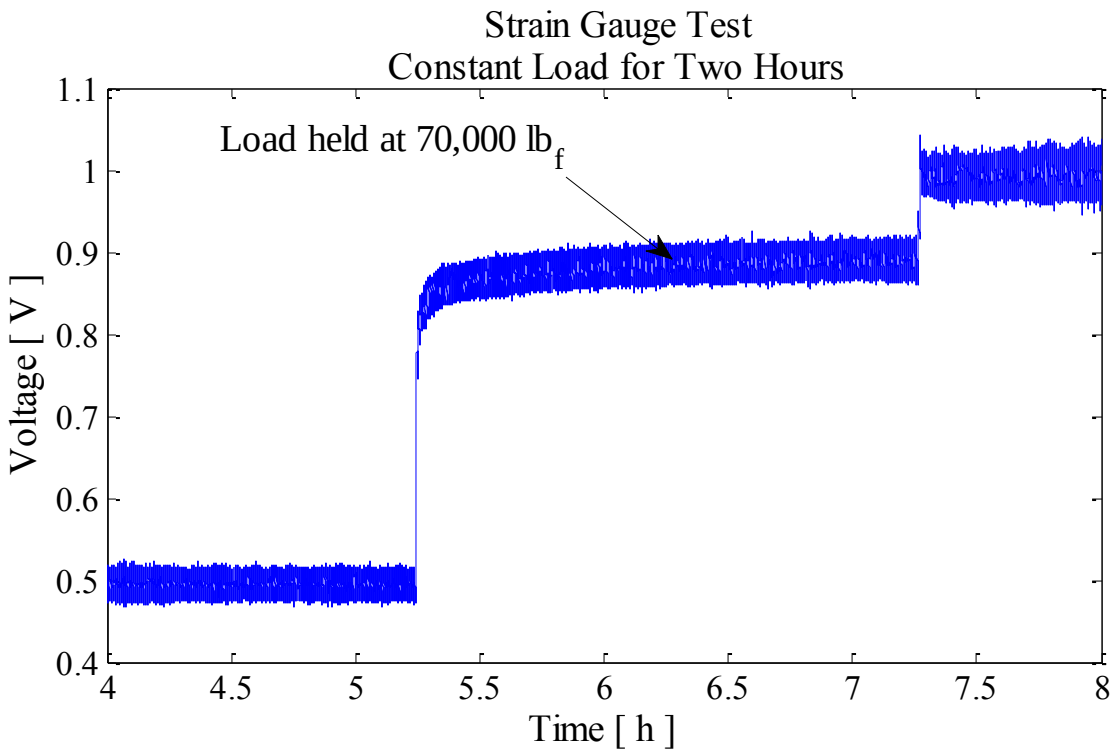

Figure 11: Load Insert Prototype Two Hour Sustained Load [11]

2.2.3 Resolving the Elastomer Pad Creep Problem

In order to resolve the creep issue, the mechanism for creep must first be understood. Creep is one of the modes in which a material can respond to an applied external force. It is described by Vincent [14] as: "In a physically stressful environment, a material can respond to external forces by [feeding] the energy into large changes in shape and flow away from the force to deform either semi-permanently or permanently." With the design of the AdapterPlus™ Steering Pad, two areas experience the majority of the load. These high stress locations create an area where the elastomer needs to find a low stress environment for the material to flow. The Steering Pad is depicted in Figure 12 with the high stress locations marked in red, and the direction of where the material is believed to flow is illustrated by the arrows.

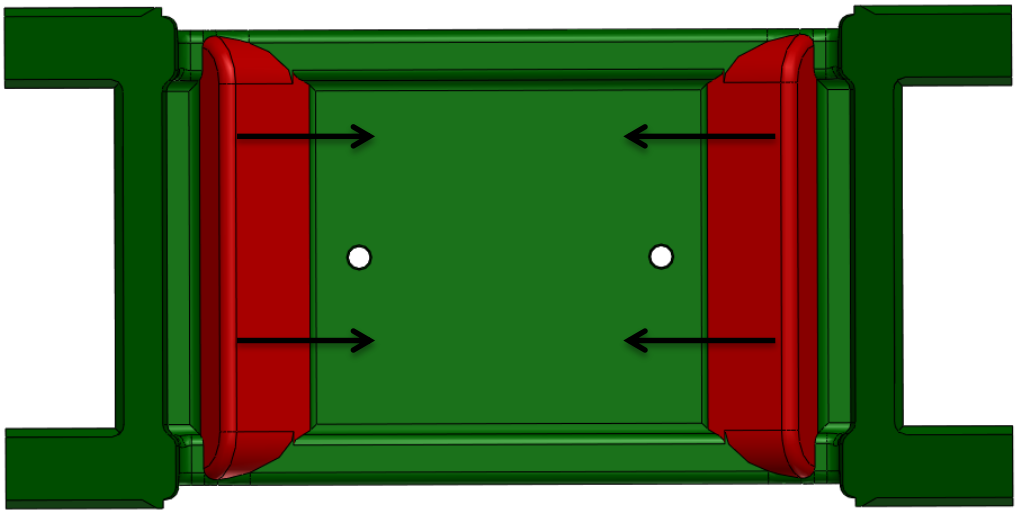

Figure 12: AdapterPlus™ Steering Pad with High Stress Locations (Red) and Arrows Point to the Direction of Predicted Creep Flow

A special film by Sensor Products, Inc. Fujifilm Prescale® (referred to as pressure film), was used to map the pressure distribution between the AdapterPlus™ Steering Pad and the Steel Adapter. The pressure film is composed of two sheets, one sheet acts as the activator and has tiny capsules embedded on the surface, and the second sheet absorbs the dye that is released when the capsules rupture. Using a color scale, the pressure experienced in the area of contact with the sheet can be estimated visually by the intensity. The film can also be sent to Sensor Producs, Inc. to have a more detailed analysis conducted on the sample. The illustration of the resulting films at various instances can be seen in Figure 13. The pressure film shows that at 50% load, the majority of the load is carried by the interlocking ridges which are the red portions of the AdapterPlus™ Steering Pad shown in Figure 12. What is also illustrated by the scan of Figure 13 (b) is that a minimal force is seen in the center of the AdapterPlus™ Steering Pad, where the sensor is placed. Examining the scan of Figure 13 (d), at 100% of full load, the interlocks still carry the majority of the load, however, a portion of the load is now distributed in the center.

With the use of the pressure film, the scans provide evidence in support of the hypothesis that the creep of the elastomer material was the cause of the increase in the sensor output during a constant load condition.

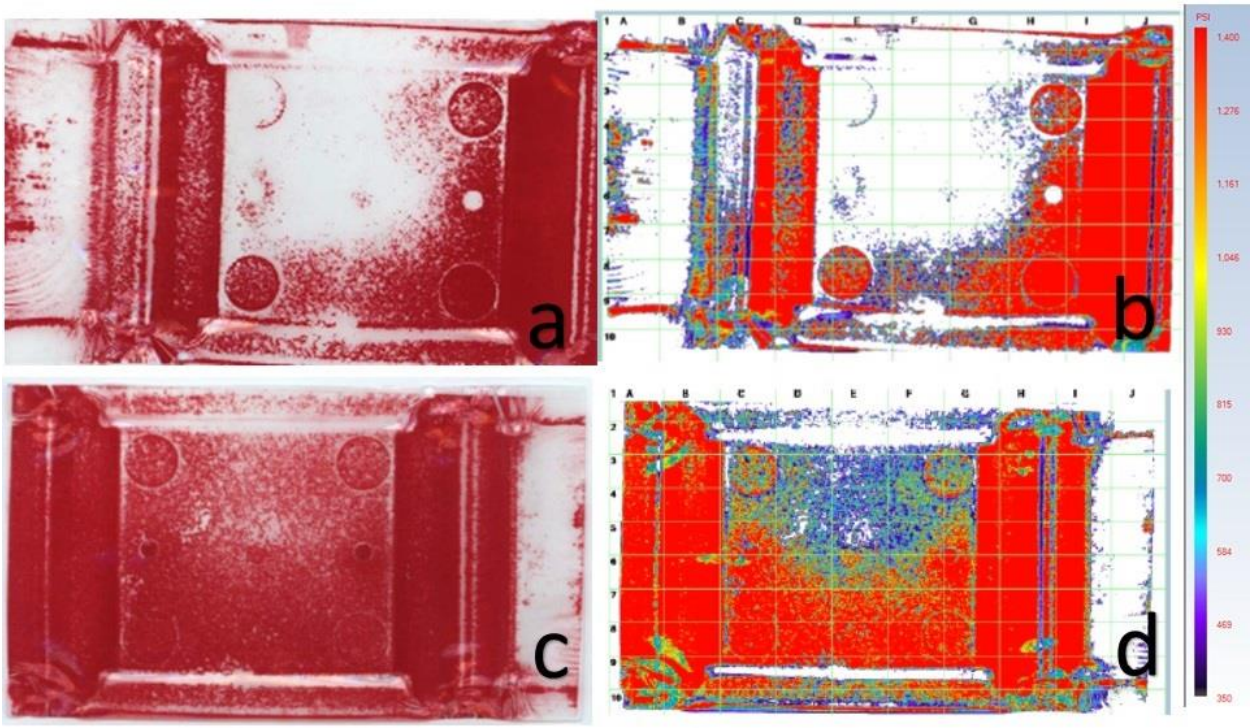

Figure 13: Pressure Film and Corresponding Scan. (a) 50% of Full Load Pressure Film, (b) 50% of Full Load Pressure Profile Map, (c) 100% of Full Load Pressure Film, (d) 100% of Full Load Pressure Profile Map [Courtesy of Sensor Product, Inc.]

In order to improve the sensor performance at loads under 50% and produce a signal that is not affected by the elastomer pad creep, the insert required a redesign. The initial thought was to increase the height of the sensor relative to the surface of the steel adapter; i.e., rather than having the sensor even with the surface of the adapter, a shim would be placed under the load insert to raise it above the steel adapter surface. In order to determine the appropriate height above the surface that would yield the best sensor response, different thickness shims were utilized ranging from 0.305mm to 0.405 mm (0.012 inches to 0.016 inches). The results of the testing are provided in Section 4.1 Shim Testing.

2.2.4 Flex Circuit

The flex circuit was designed to provide the essential wiring for a prototype design for the smart insert. The insert design created constraints that the flex circuit needed to account for in order to ensure reliability and functionality. One of the main functions of the flex circuit is the location of the temperature sensor. The temperature sensors must be placed as near to the center of each raceway of the bearing adapter as possible. The temperature sensors are also surface mount parts which require copper pads to be placed so the sensors can be soldered in place. Even though the flex circuit is a thin strip, it requires sufficient clearance in-between the top and bottom parts of the insert to ensure that it does not get damaged by the high loads experienced in operation.

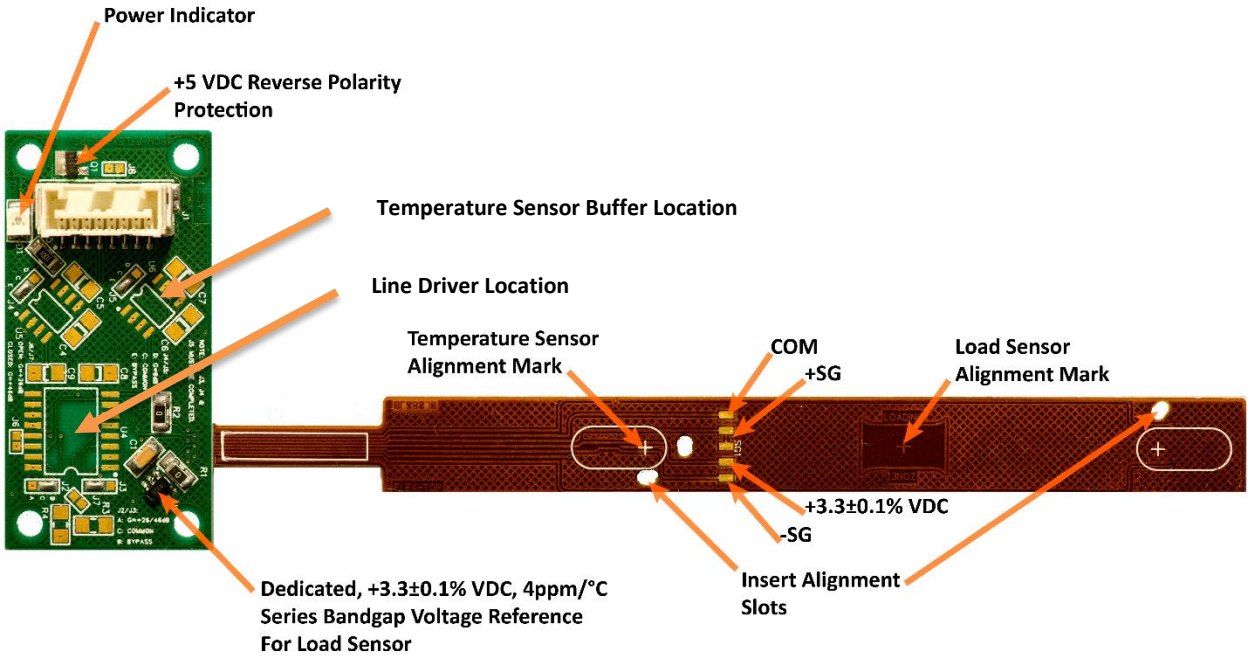

Figure 14: Top View of Flex Circuit with Annotations [Courtesy of James Bantz]

The manufactured and partially assembled flex circuit can be seen in Figure 14 and Figure 15. The pictures also include annotations describing the important features of the flex

circuit. The top view of the flex circuit shows the unmounted locations of the differential line driver for the strain gauge output as well as the locations for a buffer for each of the temperature sensors. These components will aid in pre-amplification of the strain gauge signal which will further decrease any noise in the signal. For further understanding of these components, refer to Section 3.1 Load Amplification Schematic. Although the flex circuit contains mounting locations for temperature buffers and line driver, they can be left unmounted to simplify wiring and power requirements. A complete list of all pinout for the flex circuit is provided in Table 1 along with a brief description of each of the wire functions. At this point, it should be noted that the flex circuit design was done by James Bantz an electrical engineering graduate research assistant, who was assisting with the instrumentation and signal conditioning needs of the research team.

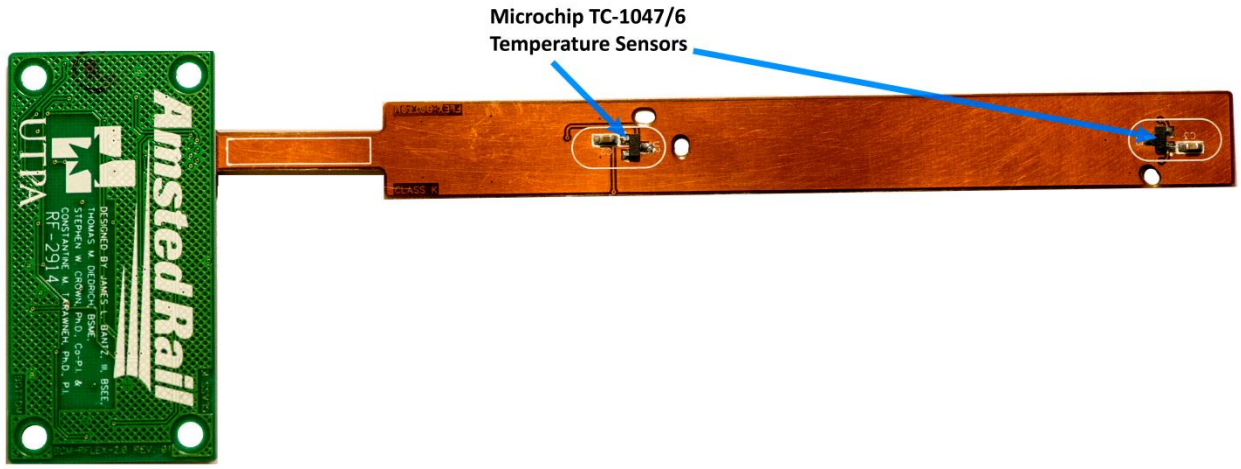

Figure 15: Bottom View of Flex Circuit with Annotations [Courtesy of James Bantz]

Table 1: Flex Circuit Pinout with additional Notes.

Pin Number	Wire Color	Function	Note
1	White Orange	+5 Volts	Power for strain gauge and temperature sensors
2	Orange	Common	Ground
3	White Green	+7.5 Volts	Required for line drivers (Optional)
4	Green	-7.5 Volts	Required for line drivers (Optional)
5	White Blue	SG out (+)	Positive differential signal for strain gauge
6	Blue	SG out (-)	Negative differential signal for strain gauge
7	White Brown	TS Outboard	Positive single ended signal for temperature sensor with respect to Ground
8	Brown	TS Inboard	Positive single ended signal for temperature sensor with respect to Ground

2.3 Final Insert Design

With the favorable results obtained by the latest modification to the Smart Insert determined in a later section (4.1 Shim Testing), a redesign of the sensor was appropriate. A sensor redesign allowed for many improvements to the insert, such as a slight adjustment in temperature sensor placement, optimization of machining time, and reducing raw materials. The Smart Insert also needed modifications for the flex circuit to mount inside. The temperature sensors were a critical issue, with slots needing to be machined to allow the temperature sensor to be located as close to the adapter surface as possible. The insert also had an unnecessary amount of material that protruded past the temperature sensor. Although the previous design was symmetrical, the additional material was unnecessary. The new design reduced the length of the insert to 4.15 inches from the previous 5 inch length. The reduced material also required less machining to be conducted to the steel adapter. The dimensions of the lower plate of the insert

can be seen in Figure 16. Additional dimensions of the Smart Insert as well as CAD drawings can be found in APPENDIX G.

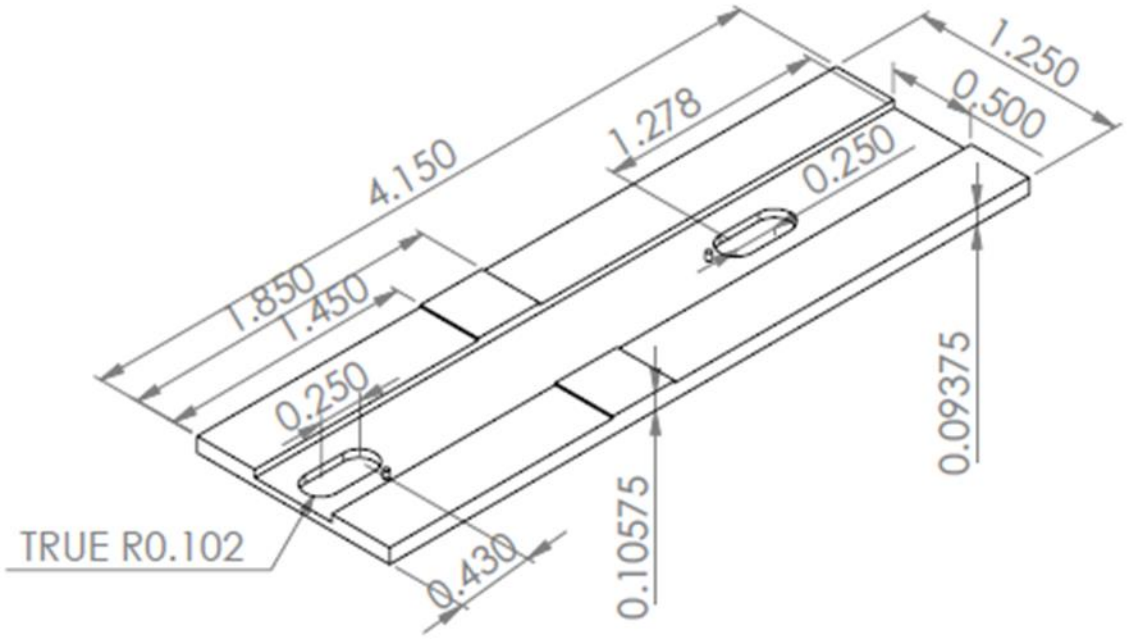

Figure 16: Final Lower Plate Insert Design with Dimensions

Once the insert is machined the Smart Insert can be assembled. The flex circuit is aligned with the machined dowel pins in the lower insert and adhered in place. The strain gauge, mounted on the top portion of the insert, is soldered to the flex circuit and the entire assembly can then be welded together. In order to weld the top plates to the lower plate great care must be taken to ensure the heat from welding does not damage the flex circuit embedded in the insert. In order to prevent heat from traveling to the flex circuit the smart insert was clamped between two pieces of aluminum in order to act as a heatsink (Figure 17). The completed insert can be seen in Figure 18.

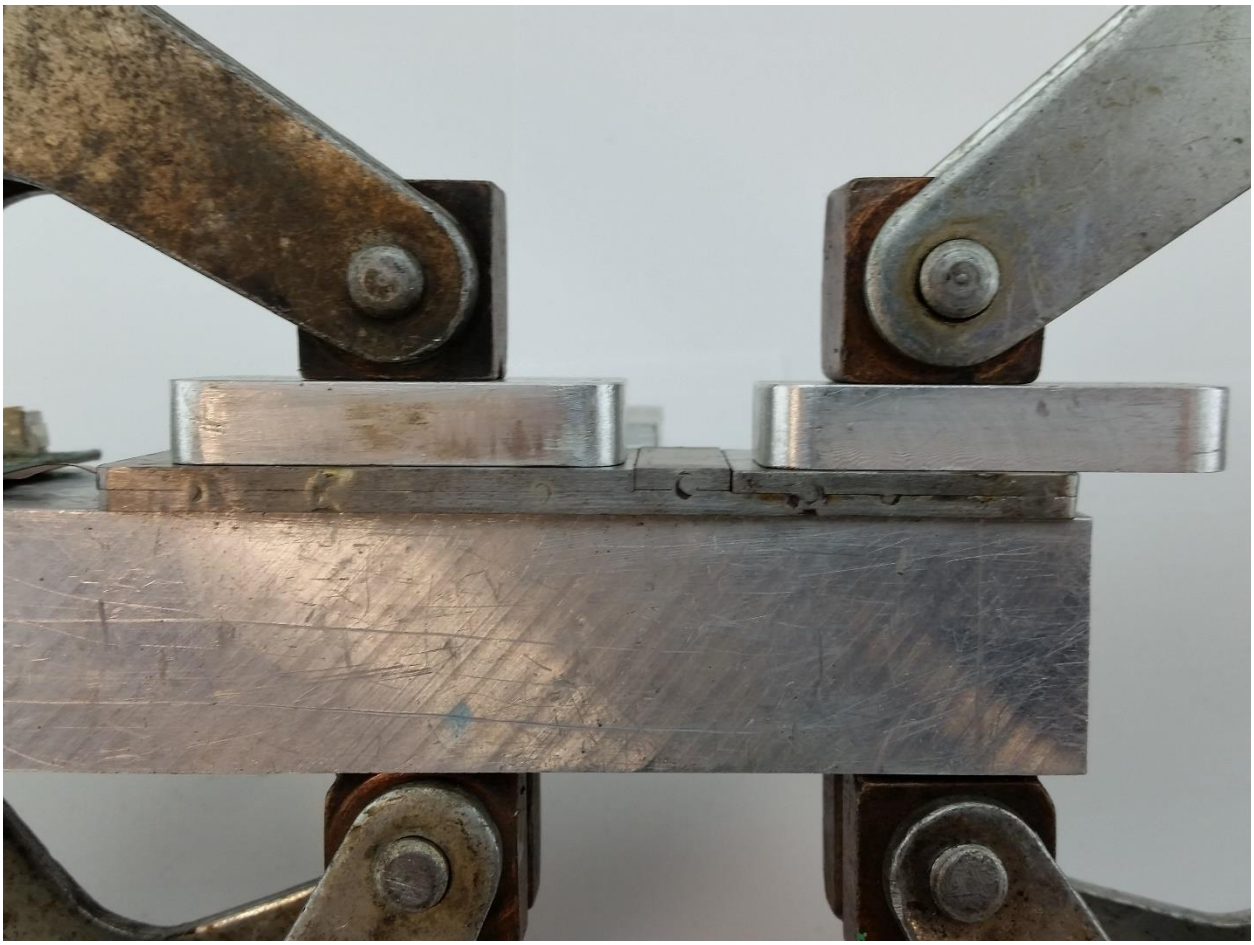

Figure 17: Aluminum Heatsink Used for Welding

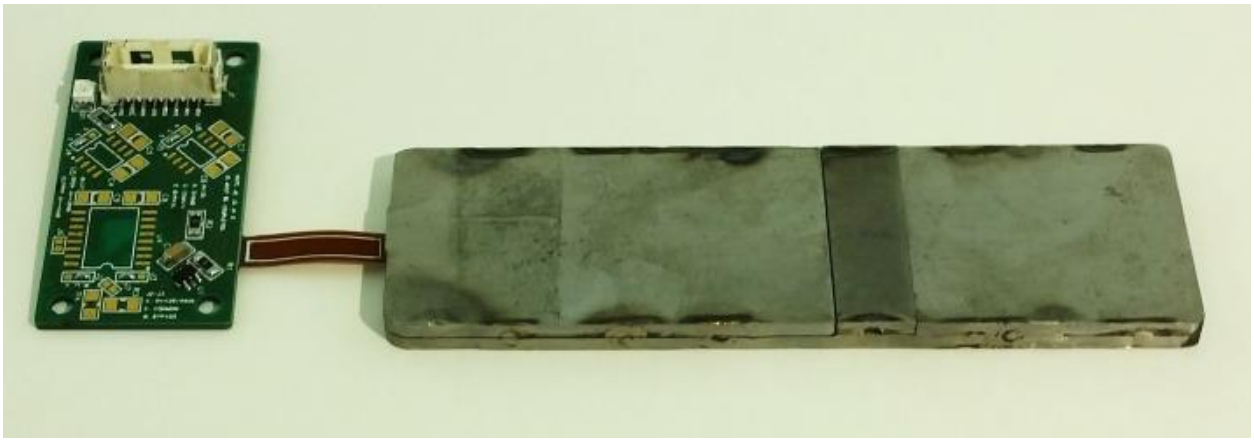

Figure 18: Final Smart Insert Design Welded Insert with Flex Circuit

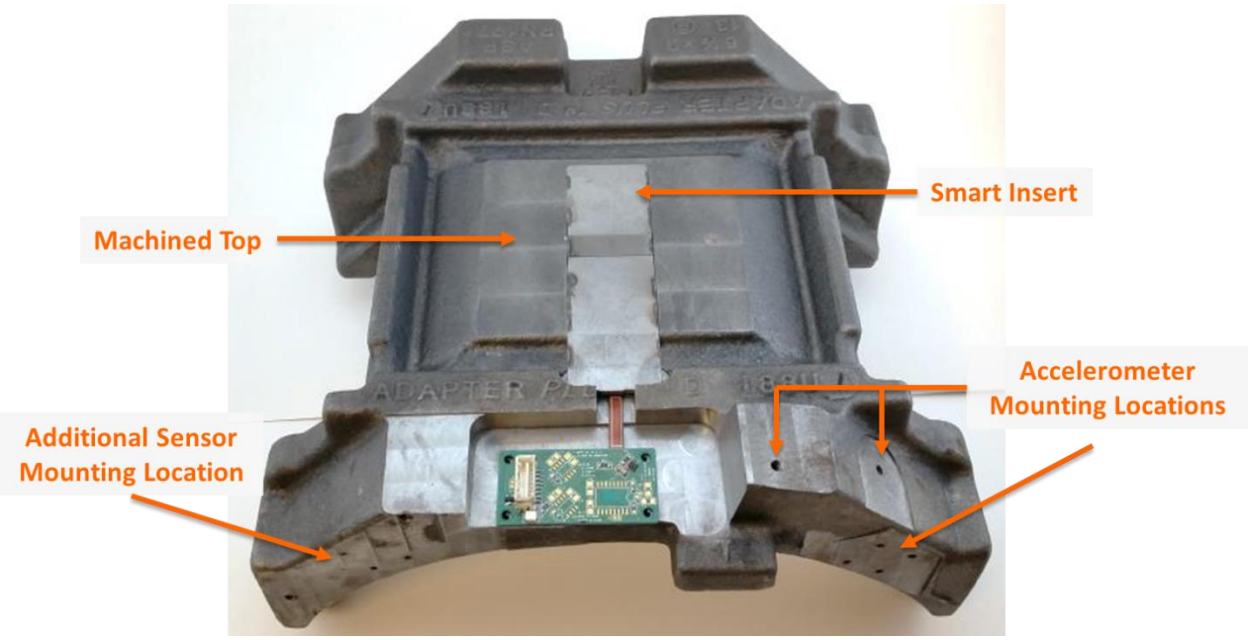

Figure 19: Machined Class K AdapterPlus™ Steel Adapter with Annotations

The steel adapter had a series of machining operations conducted to accept the Smart Insert. A critical machining operation preformed was surfacing the top of the adapter where the insert will be embedded. The surfacing of the adapter was needed to provide an accurate reference used to machine down to the appropriate depth with a high accuracy. The steel adapter also required additional mounting locations to be machined for various other sensors used to record data in the laboratory and field. The machined adapter along with annotation of the sensor mounting locations is pictured in Figure 19.

Eight individual steel adapters and Smart Insert assemblies were machined and built for the upcoming field test. Three of the assemblies were used to provide the results seen in this thesis labeled Adapter A, B, and C.

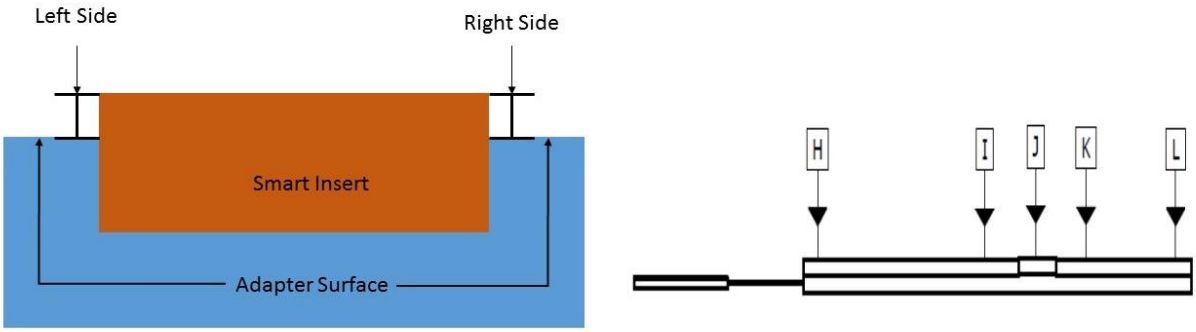

Figure 20: Measurement Location for Insert Height Above Surface of Adapter (Left), Insert Thickness Dimension Location on the Insert (Right)

Table 2: Measured Insert Dimensions

	Height Above Surface of Adapter (Thousandths of an Inch)			Actual Dimensions Measured* (Thousandths of an Inch)				
	Left Side	Right Side	Average	H	I	J	K	L
Adapter A	9	12	10.5	189	193	203	197	186
Adapter B	8	9	8.5	189	189	198	191	187
Adapter C	8	10	9	189	190	201	190	187
Targeted Value	12	12	12	188	188	200	188	188

* For Location of Measurement Refer to Figure 20

Even with extreme care taken during the manufacturing of the sensor to ensure proper dimensions of the insert, final inspection of the insert revealed slight variations. In some locations such as dimension “I” (see Figure 20), the insert of Adapter A was found to have a five thousandths of an inch difference from the targeted value shown in Table 2. Another location in the insert that was found to vary from the targeted value was the measured height above the surface of the adapter. This is the critical dimension that provides the compensation effect for the creep of the pad material. Each of the inserts in the respective adapters should measure 12 thousandths of an inch above the surface of the adapter, however the average height was measured to be 9 thousandths of an inch.

CHAPTER III

SMART INSERT CIRCUITRY AND CALIBRATION

A redesign of the instrumentation circuitry was triggered by the need to test eight Smart Adapter Inserts simultaneously on a freight railcar for an upcoming field test. The redesign allowed for several improvements to be carried out over the previous version. One of the main disadvantages of the previous circuitry is the complexity of the system, needing extensive knowledge of the hardware to install and setup. Additionally, the previous instrumentation circuitry is only capable of handling two load sensors per board and the amplifier gain is fixed at 200 V/V. The new instrumentation circuitry offers a larger gain and improved sensitivity to compensate for that lost when the sensor insert was welded together. Furthermore, the instrumentation circuitry redesign allows for the signals to be transmitted through 80 feet cables from the sensor insert to the data acquisition device without a considerable voltage drop that degrades the signal.

3.1 Load Amplification Schematic

The initial schematic as well as component selection for the load amplification circuit was completed by James Bantz III (a fellow electrical engineering graduate research assistant). After the initial schematic was drafted, it was transferred into DipTrace, a printed circuit board (PCB) design software, in order to create a clear schematic that could then be transformed into a PCB to be manufactured. Once the initial schematic was generated, a few changes were made. First, the gain of the load sensor was designed to be selectable by a jumper that could be

switched from 400 V/V to 600 V/V. The second modification was to place a capacitor capable of setting the cutoff frequency for the filter, or by moving a jumper, a clock frequency could be applied in order to have an adjustable cutoff frequency. The final step of designing the load amplification board was to replicate the circuit four times in order to make a single board capable of handling four Smart Sensor Insert prototypes. The final schematic of a single load sensor amplification channel is provided in Figure 21 and the complete circuitry of the board is given in Appendix A.

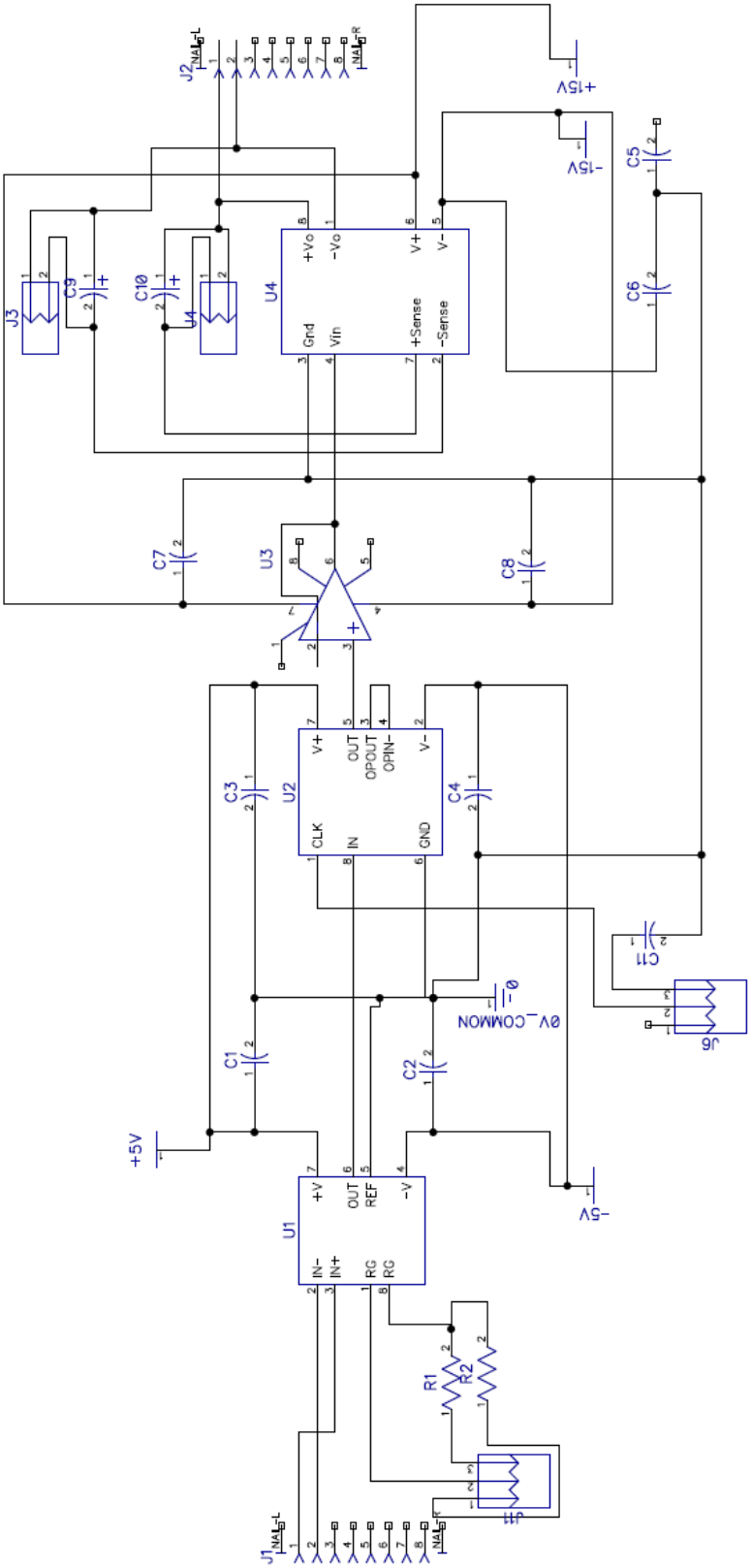

Figure 21: Single Load Sensor Amplification Circuit

3.1.1 Amplifier

In order to generate a useable signal from the strain gauge of the load sensor, the signal needed to be amplified. The amplifier of choice was the INA 129 instrumentation amplifier from Texas Instruments. The INA 129 is a low power, high accuracy amplifier with an adjustable gain set by a single resistor. The change from the INA 131 to the INA 129 was prompted by the need to increase the gain from the previous 200 V/V to an adjustable gain of up to 600 V/V. Recommendations for the optimal gain setting will be discussed in CHAPTER V. The location of the INA 129 can be seen in Figure 21, the integrated circuit (IC) labeled U1.

3.1.2 Filter

After the signal is amplified, the next step in the signal conditioning chain is the filter. For filtering, the MAX 294 8^{th} order, low pass filter designed by Maxim Integrated Products Inc., is used. Figure 21 shows the filter IC labeled as U2. The filter is responsible for removing any 60 Hz interference in the signal that is produced by the AC power in the laboratory testing environment. The cutoff frequency of the filter can be set by one of two ways; either by placing a capacitor to the corresponding pin of a designated value determined by the datasheet, or by applying a clock frequency to the clock pin of the amplifier. Additional information pertinent to the filter can be found in APPENDIX D which contains the Max 294 datasheet. The benefit of using a capacitor to set the cutoff frequency is the simplicity of design requiring only one additional component; although, this permanently locks the cutoff frequency. By using a clock frequency produced by a microcontroller, it is possible to adjust the cutoff frequency at any time by changing the programming embedded in the microcontroller. The current design is flexible in that it allows for further adjustments of the cutoff frequency to be investigated by applying the cutoff frequency to an additional pin on the board. However, during normal operation, it is best

to have the 60 Hz cutoff frequency set by a capacitor. It should be noted though that the filter may be unnecessary in the final sensor design which will be powered by a battery; hence, not be subject to 60 Hz noise found in the laboratory. It is highly recommended that the choice of electronics utilized here be re-examined once the final self-contained wireless insert is produced.

3.1.3 Line Driver

With the smart insert located on a railcar, the signal must be sent to a data acquisition unit located on the instrumentation car, which is the next railcar ahead of the test car. The signal from the strain-gauge-based load sensor was not designed to provide a signal further than 20 feet. However, a railcar is over 60 feet long, so the signal conditioning box must ensure that a solid signal can be sent a distance of 80 feet to the data acquisition system in the instrumentation car. The final component that the signal passes through before it is sent down the 80 foot cable is the DRV 134 line driver produced by Texas Instruments. The function of the line driver is to improve the strength of the signal through the long cable length to ensure that the correct voltage is recorded. Due to the fact that the line driver requires a high current signal into the integrated circuit (IC), an operational amplifier (OPA 177 from Texas Instruments) was used to buffer the voltage in order to provide the required current. The operational amplifier and line driver are represented, respectively, as U3 and U4 in Figure 21.

3.1.4 Strain Gauge Instrumentation Circuitry

Integrating all the components, described in the previous sections, into a dual sided printed circuit board (PCB) was the final step taken to accurately test the strain gauge in the sensor insert prototype with the integrated flex circuit. The board is composed of a signal input connector from which the signals are split and sent to the corresponding signal chain providing the ability for four load sensors to be measured simultaneously from a single board. Finally, the

signals are sent out through a connector on the opposite side of the board to the data acquisition unit. The board contains a large connector used to provide all the necessary power for the circuit. The complete board is pictured in Figure 22 along with annotations of each of the main components, as well as, an individual signal chain highlighted by arrows.

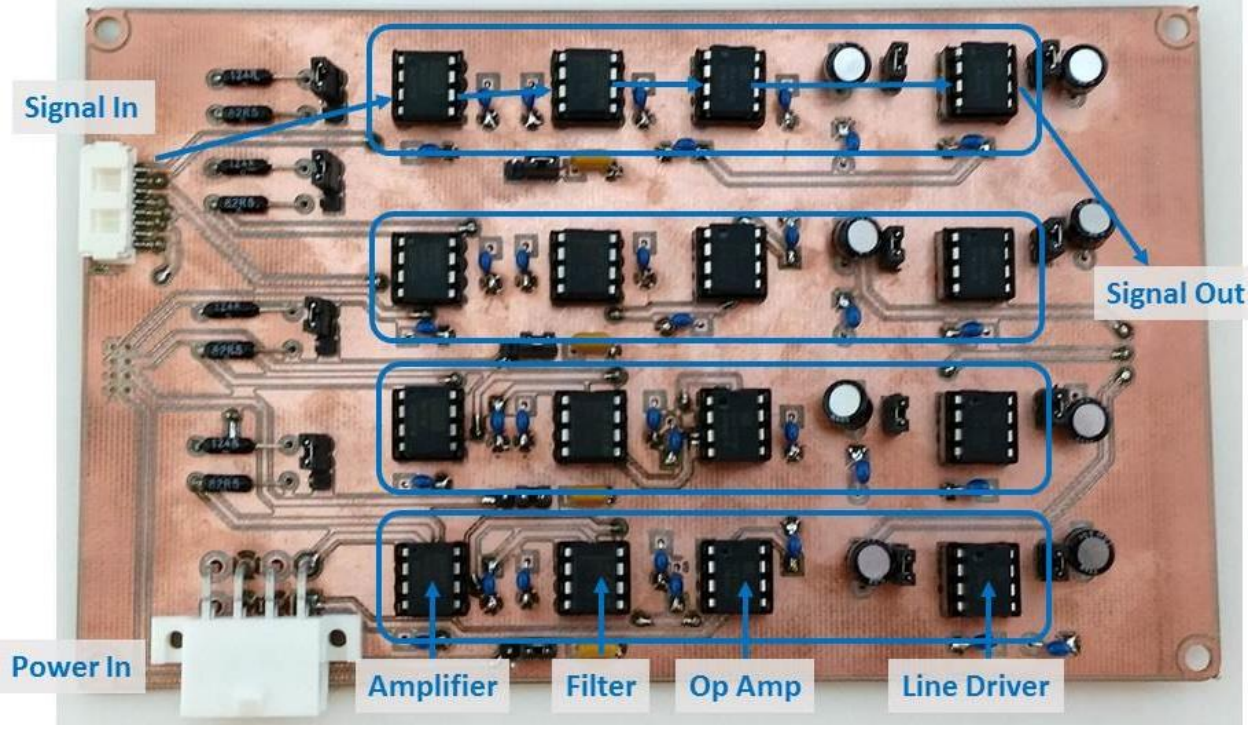

Figure 22: Load Amplification Board with Annotations

3.2 Analog Temperature Sensor Circuitry

The circuitry for the TC 1047 analog temperature sensors was less complex than the previously discussed circuitry for the load sensor. The temperature sensors output an analog voltage that directly correlates to the measured temperature. However, by sending the signal over 80 feet of cable, the voltage drop would manifest as a decrease in the insert temperature, as well as, have additional background noise picked up in the line. In order to negate the aforementioned effects, additional circuitry must be placed between the sensors and the data acquisition unit.

3.2.1 Line Driver

Similar to the line drivers used in the strain gauge circuit, the same integrated circuit (IC) was used to boost the signal to account for the voltage drop that occurs over the 80 foot cable. The line driver also transforms the single ended signal into a differential signal that is less susceptible to background noise. Similar to the load amplification board, the sensor output must first pass through an operational amplifier to buffer the voltage before it can be sent to the line driver.

3.2.2 Temperature Sensor Signal Conditioning Board

The temperature sensor circuitry was built using a similar design to that utilized for the strain gauge amplification board. The temperature sensor signal conditioning board is capable of monitoring four Smart Inserts, each of which house two temperature sensors, for a total of eight temperature sensors. Each channel requires two ICs to provide the proper signal conditioning seen in Figure 23, which also depicts the final board along with annotations of the main components.

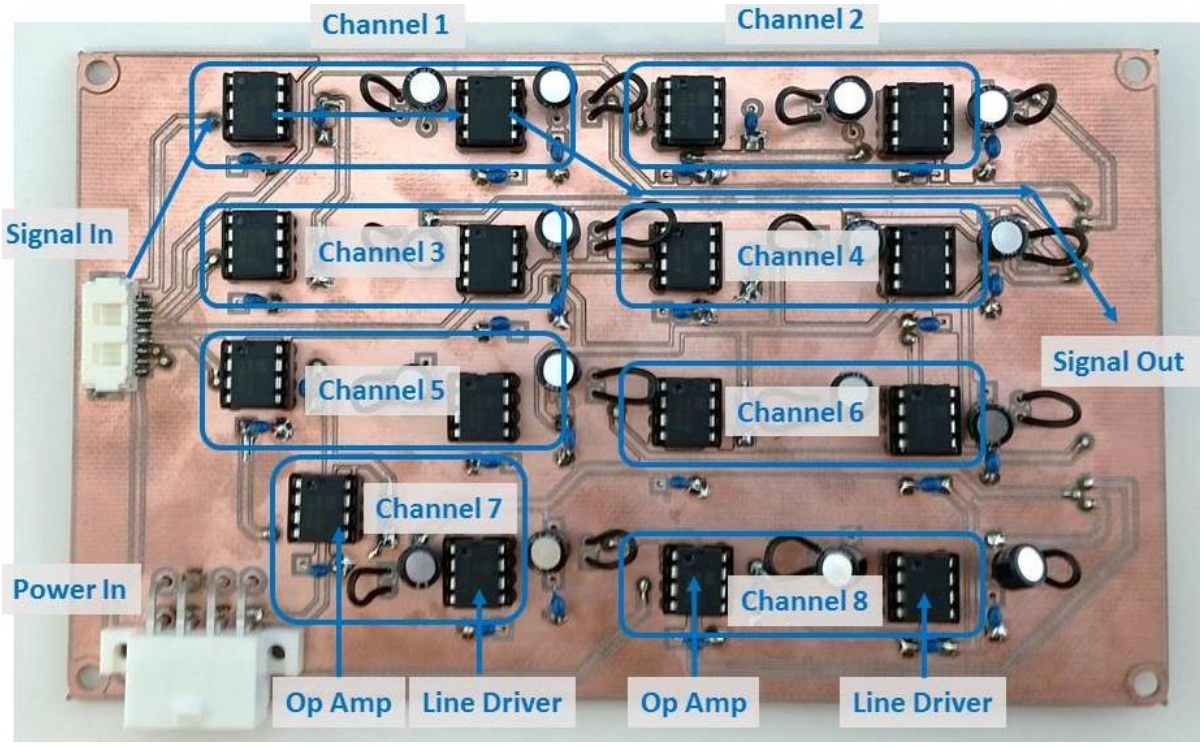

Figure 23: Temperature Sensors Signal Conditioning Board with Annotations

3.3 Calibration Methodology

Without a proper calibration, a sensor would output an inaccurate signal. In order to transform the signal sent from the sensors into a comprehensible unit of measurement, a calibration must be completed. Typically, a calibration for a load sensor is accomplished by monitoring the sensor output while it is placed under several known load conditions. The data is then recorded and a correlation is created that relates the signal output to the known loads. Since the current system is a complicated assembly that involves multiple variables, the calibration process is complex and requires several steps. The procedure used to properly correlate the known load to the sensor output is explained in the following sections.

3.3.1 Pad Settling

Before any calibration can be conducted, the AdapterPlus™ steering pad must be allowed to properly settle into the steel adapter. In order to allow for the pad to settle, the assembly is installed on the test rig and is placed in the fully loaded position (34,400 lb_f or 153 kN) for 24 hours. The settling allows the elastomer material of the pad to deform into the final shape during usage, providing a steady signal output. Alternatively, the settling process can be completed in a shorter period by operating the test rig dynamically at a speed of 50 mph for a minimum period of four hours. The elevated temperatures seen in high speed operation allow the elastomer pad to settle at a faster pace, which allows for more frequent laboratory testing to be performed.

3.3.2 Static versus Dynamic Testing

Dynamic testing is required when the desired use of the sensor is during operation. Dynamic testing can cause instantaneous readings of the sensor to fluctuate over 1% of full load; however, a one minute moving average of the sensor value can be taken to get a signal that is typically within 0.5% of full load. Static testing, on the other hand, can produce a much more constant reading (variation of 0.1% of full load) because the inherent vibrations and small changes in load are not seen in a static condition. Testing in a static condition is consistent with the typical loading or filling process experienced by a freight railcar. For example, a train pulls up to a loading station, halts movement while the first railcar is loaded, and once it's loaded, the train slowly moves forward to allow the next railcar to be loaded. The aforementioned process is repeated until all the railcars are full, then, the train proceeds to the desired destination for unloading. Loading is never done while the train is in motion and, thus, the testing and calibration should mimic as closely as possible the intended application of the sensor.

3.3.3 Calibration Data Points

Depending on the desired application of the sensor, a calibration plan can be devised to encompass the intended range of the signal. A second order calibration is used to correlate the sensors output voltage to the known loads. In order to properly calibrate the sensor, a minimum of three unique data points must be acquired. For the sensor to produce the highest possible accuracy at full load, a three step loading calibration of 95%, 100%, and 105% load steps should be used. The three previous loads will give the best accuracy for the sensor at full load, but that would come at the expense of reduced accuracy for loads under 70% of full load. For the purpose of developing the most versatile sensor, a full range calibration that is skewed to the higher loads was used for the testing conducted for this thesis. The loads used for the calibration of the sensor were 17%, 80%, and 100% providing a full range of the loads experienced by the sensor with slightly better accuracy for the higher loads that fall between 70 and 100% of full load.

CHAPTER IV

LABORATORY TESTING AND RESULTS

4.1 Shim Testing

In order to counter the effects seen by creep, the Smart Insert was raised above the surface of the adapter in order to create a stress concentration in the center of the steering pad. The stress concentration was an attempt to stop material from traveling toward the sensor under steady loads due to creep at the interlocks, where stress concentrations were the highest. The two opposing stress concentrations minimize creep at the sensor providing a constant signal proportional to the total load. The predicted stress concentrations as well as the predicted direction of the elastomer creep flow are shown in Figure 24.

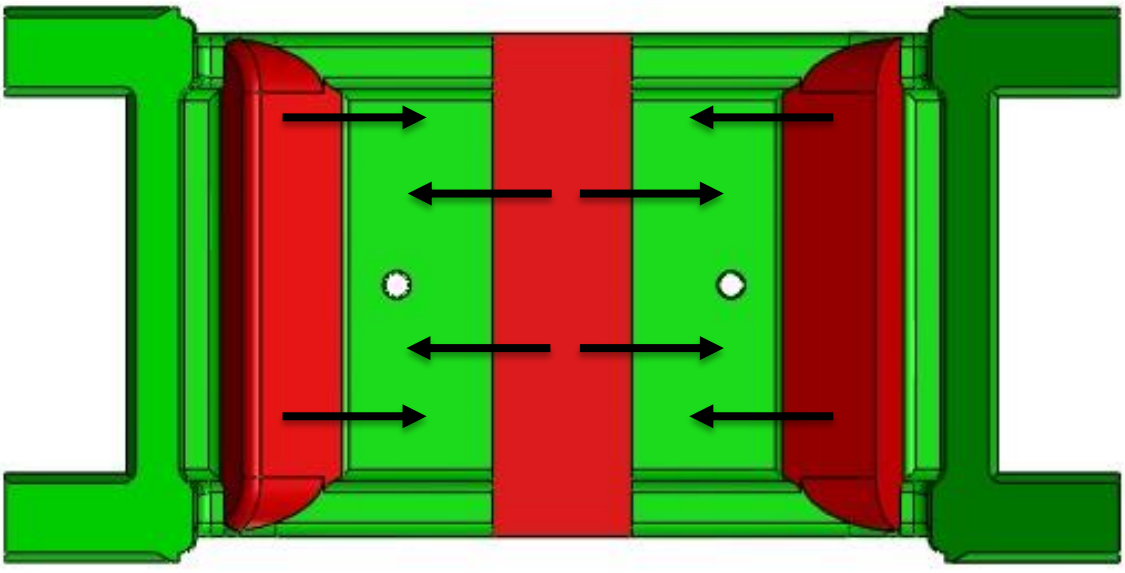

Figure 24: Steering Pad with Stress Concentrations and Predicted Creep Flow Directions

4.1.1 Shim A

The first set of testing was conducted using a shim with a thickness of sixteen thousandths of an inch (0.405 mm) which raised the entire insert above the adapter surface. A picture of the shim can be seen in Figure 25 and 26 showing the entire insert slightly raised above the adapter surface. The sensor was held in an unloaded state of 17% load (5,850 lb_f or 26 kN) for 30 minutes and then increased to 100% load (34,400 lb_f or 153 kN) and held for four hours. The test was conducted to monitor the step response of the sensor and to compare the output to the previous sensor design. In the following graphs, the blue and red lines represent the correlated strain gauge voltage and the load cell output respectively. Looking at the sensor's output, Figure 27, an initial overshoot is apparent immediately after the load was increased to 100% load. Following the initial overshoot the predicted load returned to an accurate steady state value.

Figure 25: Shim A, 0.016 Inch Thick Aluminum Sheet

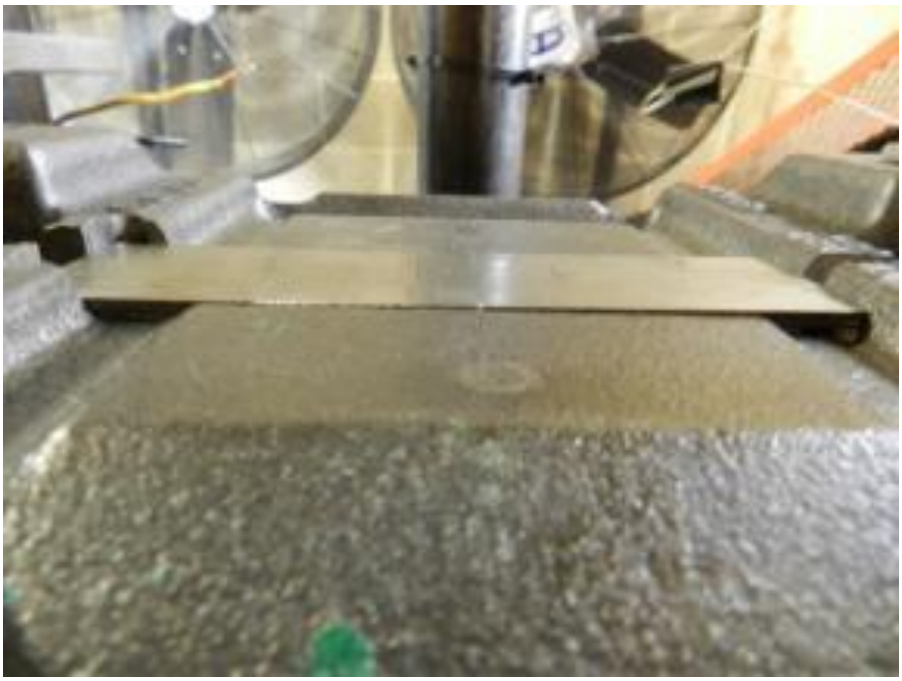

Figure 26: Shim A Installed with Adapter and Insert

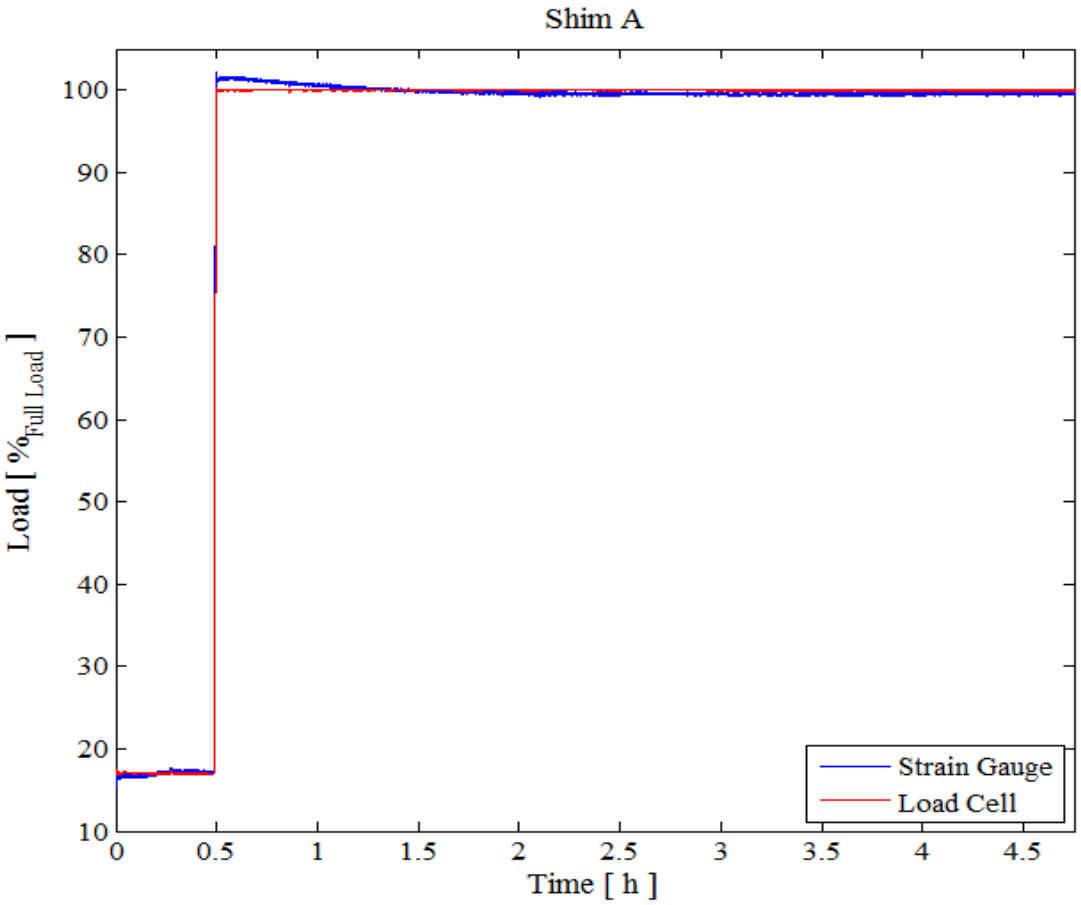

Figure 27: Shim A Response Due to 100% Load Input

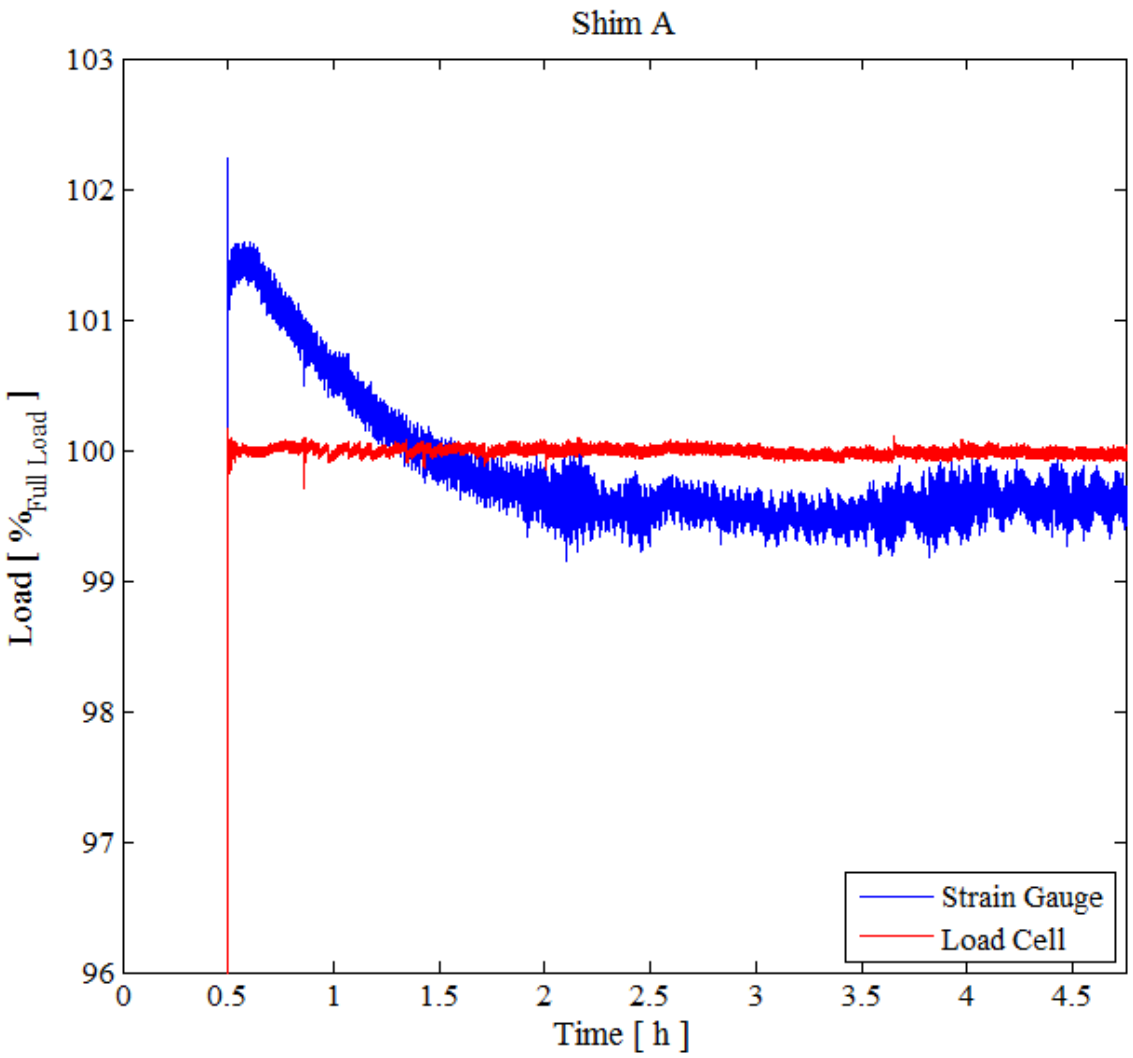

Figure 28: Shim A Performance Expanded View

Figure 28 shows the overshoot portion of the same signal in greater detail. The figure clearly shows that the Smart Insert initially experiences a 1.5% overshoot in load and then proceeds to decrease to a steady state value. It can also be observed that approximately 30 minutes after the load reached 100%, the Smart Insert was within the targeted 1% error value. The test showed that material creep in the elastomer pad, which introduced significant error with the previous design, was mitigated with the addition of the shim.

4.1.2 Shim B

With the excellent results obtained by Shim A additional testing was performed with a slightly thinner shim with a thickness of twelve thousandths of an inch (0.305 mm). A decrease in thickness was used in order to attempt to produce similar results as Shim A, but with less overshoot and a decrease in the 1% settling time. The aluminum shim can be seen in Figure 29.

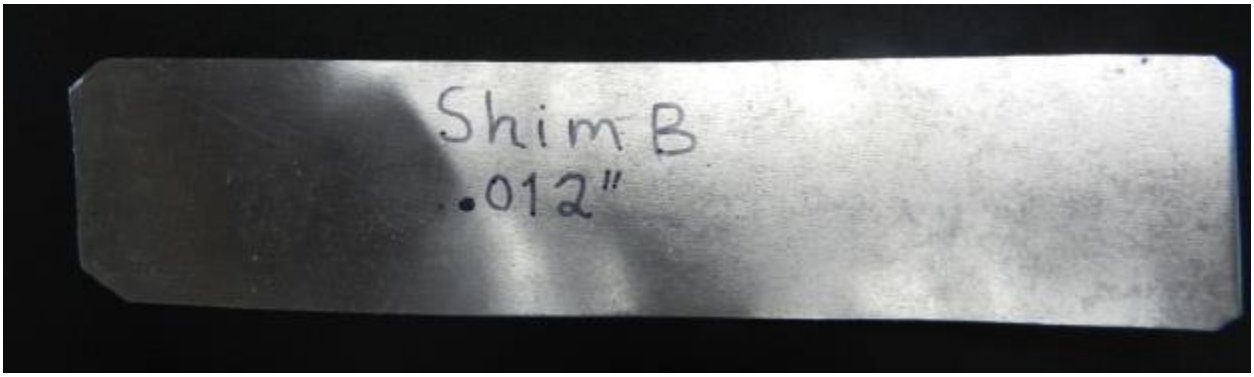

Figure 29: Shim B, 0.012 Inch Aluminum Sheet

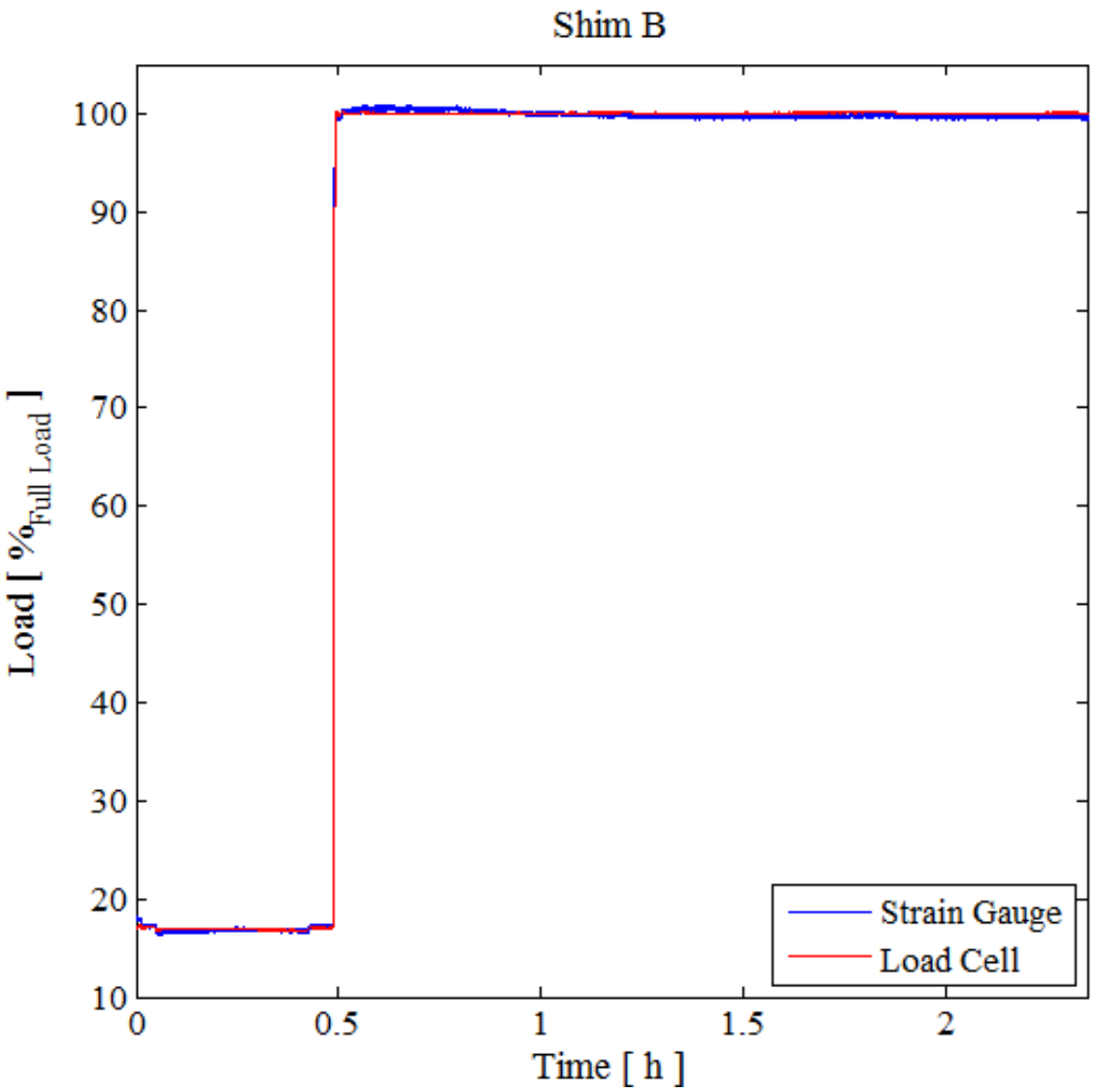

Figure 30: Shim B Performance

The correlated output obtained with Shim B (Figure 30) is similar to Shim A. However, the initial overshoot was limited to a 1% error rather than the 1.5% seen previously with Shim A. Figure 31 provides a closer look at the output where the entire portion of the test conducted at 100% load was held within the targeted 1% error.

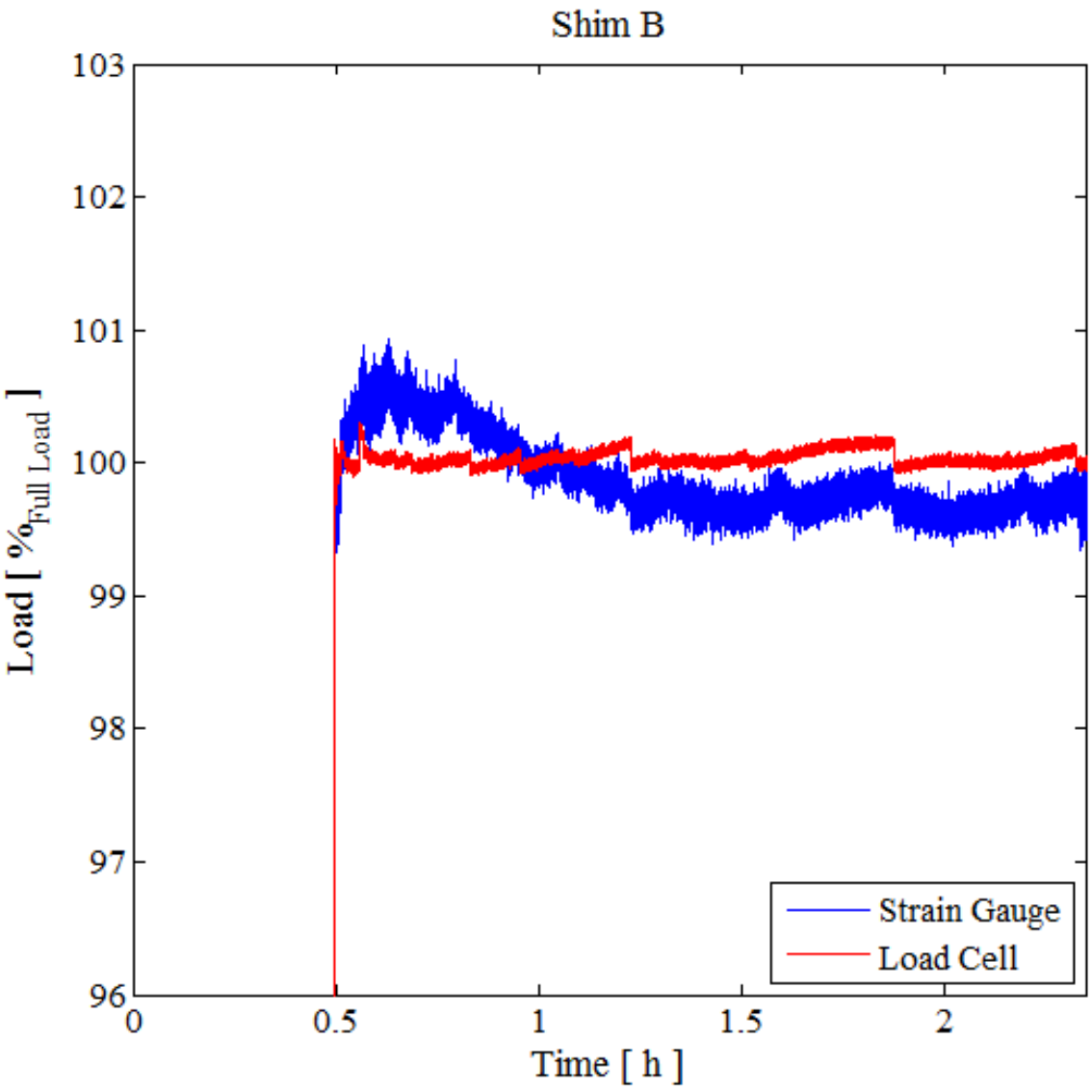

Figure 31: Shim B Performance Expanded View

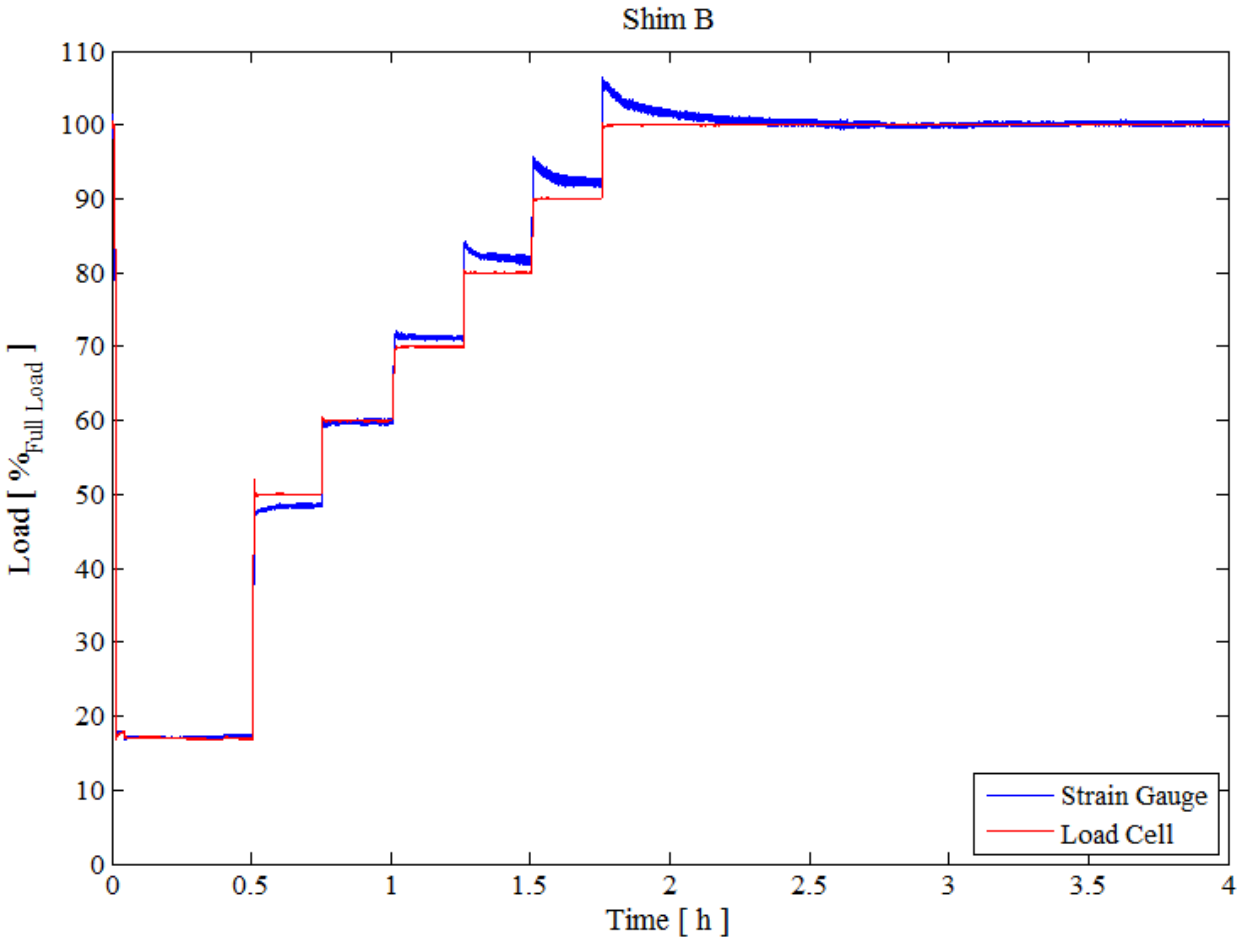

Figure 32: Shim B Step Response

With favorable results obtained with testing going from the unloaded to loaded step test, additional testing was done to determine the sensors response to intermediate load conditions. The multiple step test was used to determine the static values of intermediate loads used in a correlation. The first step from a steady unloaded car condition to 50% of full load was held for 15 minutes and then increased by 10% load every 15 minutes. The first results (Figure 32) show a large overshoot when the load is increased at loads over 70%. The overshoot at these loads are observed to be 4% or greater. The sensor also appears to experience a transition in response. For the 50% load the sensor output increases slightly to the steady value, while at 70% the sensor's output is relatively flat and ideal. However, once the load applied is over 70% of full load the

output produces a 5% overshoot and then settles to a steady state value. A possible explanation for the overshoot was the large area experiencing the stress concentration above the insert.

4.1.3 Shim C

Due to the unintended overshoot during step testing with the use of Shim B a new design needed to be considered to reduce the unintended effects. In order to reduce the size of the stress concentration above the center section of the insert, only the center section of the insert was raised with a shim twelve thousandths of an inch thick (0.305 mm). The shims installed on the insert are shown in Figure 33. It was predicted that the modified design with a more localized stress concentration in the center of the pad, as illustrated in Figure 34, should produce similar results but with less overshoot for the higher loading conditions.

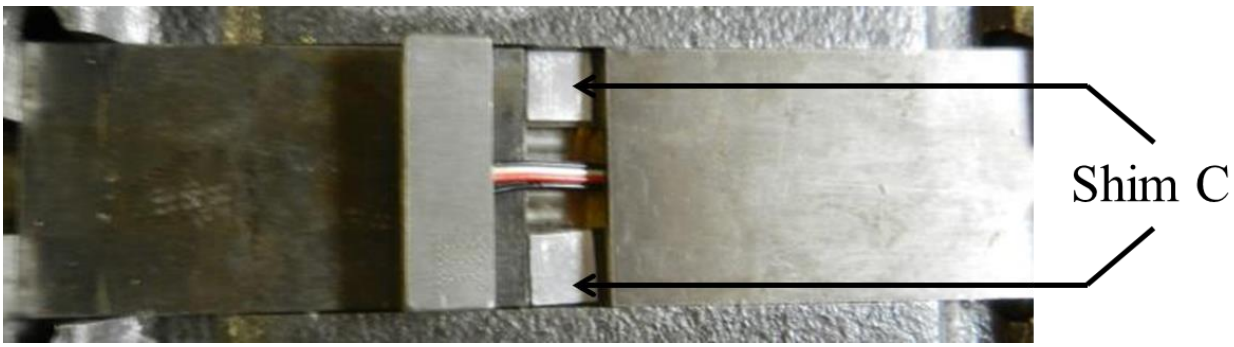

Figure 33: Shim C Insert Only

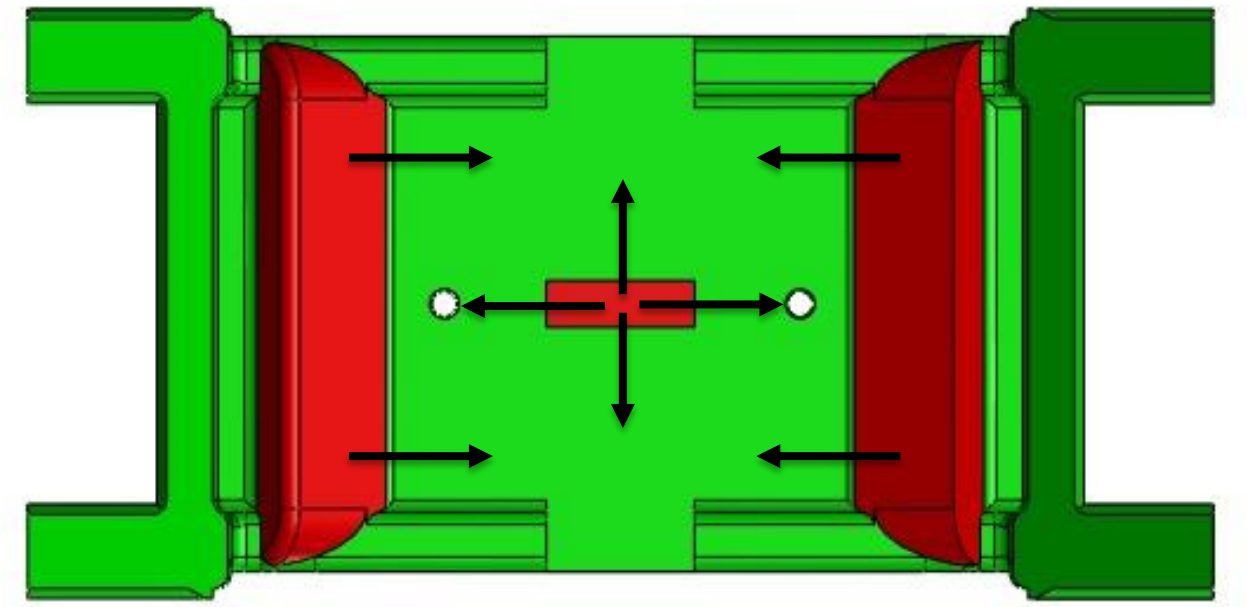

Figure 34: AdapterPlus™ Steering Pad with Stress Concentrations and Predicted Creep Flow Directions for Shim C

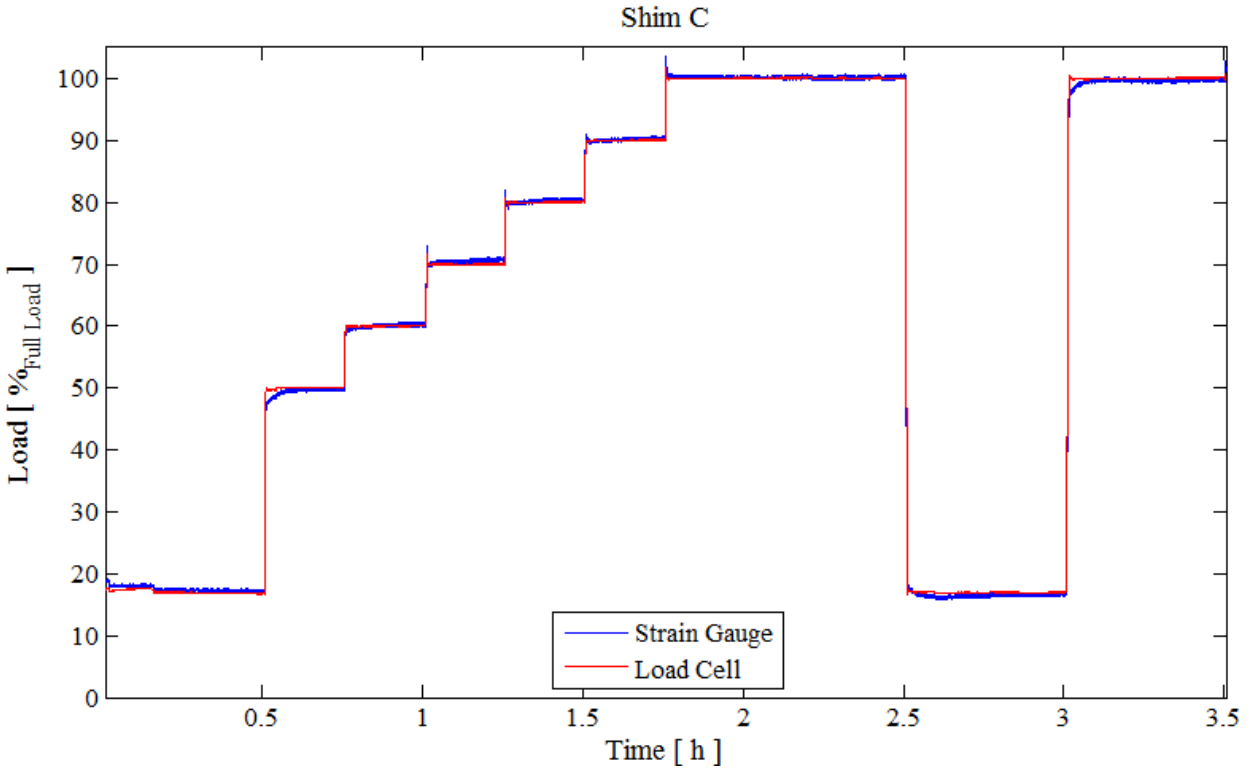

Figure 35: Shim C Performance

The multiple step test for the modified design is shown in Figure 35. The data shows that for loads of 70% of full load and over, an initial overshoot is present, however the overshoot is short lived and a steady state value can be seen after 30 seconds. The output of the Smart Insert provided a signal that correlated much more accurately, with all the steps held to within ±1% error. The last portion of the test contained the step from 17% to 100% load. The sensor produced a slightly different output then that of the shim A and B. Rather than having an overshoot and then decreasing down to a steady value, the sensor slightly under predicted the load, but within 5 minutes the sensor read an accurate steady state value.

4.2 Laboratory Testing

The typical test used to calibrate the final Smart Insert prototype consisted of a settling portion, dynamic testing, followed by static testing. The test covered the entire range of loads from 17% to 100% load with a focus on the loads over 70%. All the ramping rates were based on a 7 minute ramp time from 17% to 100% or 4,080 lb_f/min (18.15 kN/min). The unloading time was based on a 3 minute ramp from 100% to 17% or -9,520 lb_f/min (-42.35 kN/min). The loading and unloading rate was provided by Amsted Rail® as typical rates in the rail industry for the loading and unloading of grain. The settling period required a minimum of 18 hours at full load while the tester was in operation at 25 mph. Once the settling was completed the dynamic portion of the testing was conducted. The dynamic portion consisted of 3 loaded steps of 80%, 95%, and 100% held for 18 hours each. In-between each of the loaded steps, a 17% step was held for 6 hours. Five minutes before any change in load, the test rig was halted. After the load was changed, the test rig remained in a static condition for an additional five minutes. This was an attempt to simulate a train coming into a loading station. The dynamic portion of the test was used to calibrate the sensor. The static portion consisted of multiple loading and unloading cycles

with dwells between 1 and 12 hours. Loading steps of 80% and 100% were used with a 17% load applied between steps. The static portion simulates the sensors response while the train is stationary, as well as, to determine the sensor's ability to measure the load instantaneously during a loading condition.

4.2.1 Adapter A

The results of the dynamic test for Adapter A show that the sensor produced a steady signal for the loaded steps (Figure 36). The only portion of the test that contained notable errors was the initial 100% step with an initial error of 3%, although the error dropped to a steady value after 3 hours of operation.

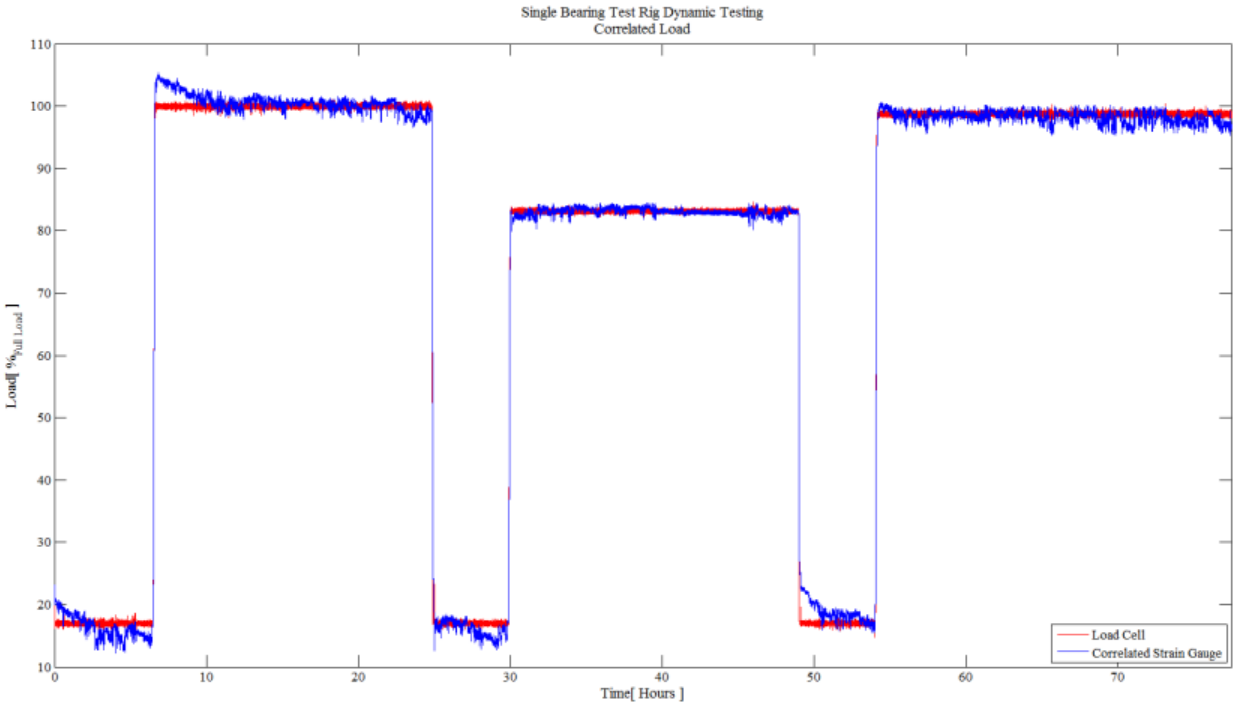

Figure 36: Adapter A Dynamic Testing at 25 mph

After approximately 77 hours of dynamic testing the static portion of testing was conducted to monitor the sensor's response (Figure 37). Upon inspection, the results shown for the static test provide evidence of a large overshoot for the 80% and 100% steps of

approximately 2.5% error. The 17% load step produced an error of almost 10%. Although the error at the unloaded step is not critical the error is significant if the sensor is purported to be accurate over the full range.

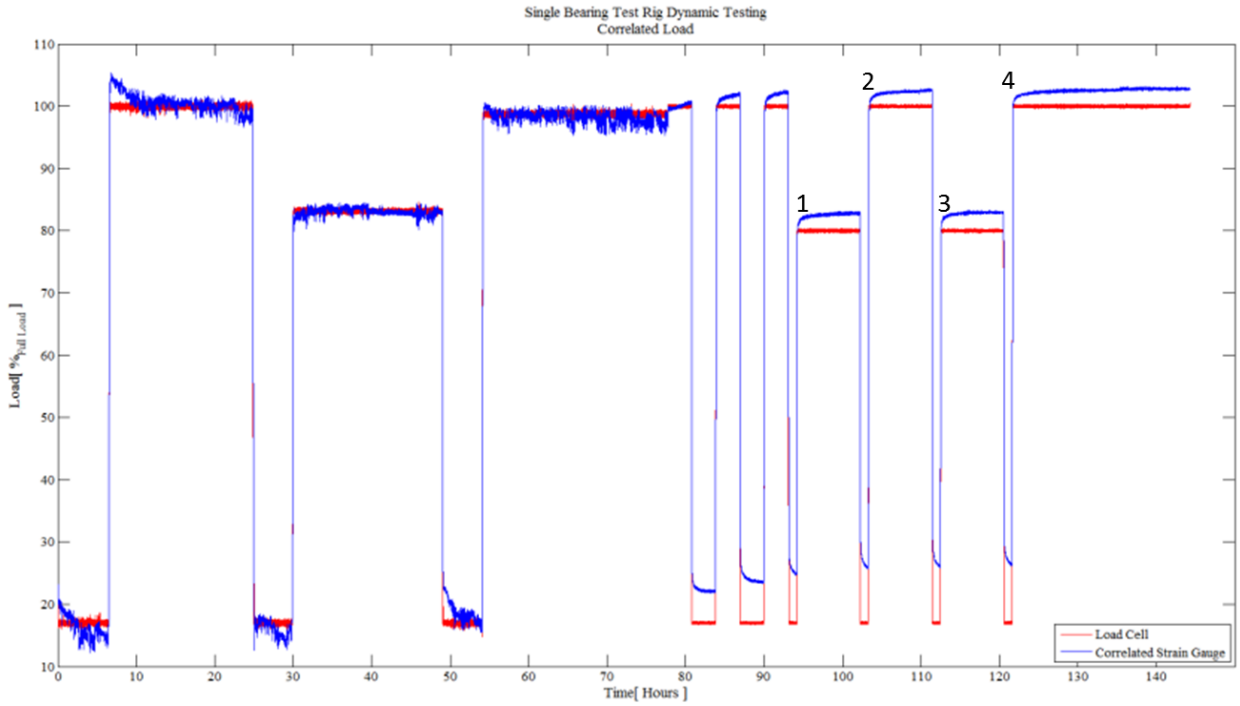

Figure 37: Adapter A Complete Test

Figure 37 shows four loading steps that are labeled from 1 to 4. These four loading steps were further analyzed to determine the sensors response during the loading portion of the test. The ramps were first analyzed with a 3 to 5 minute window after the ramping was complete to determine the error at different instances in time. Upon inspection Figure 38 shows the 80% step of Ramp 1 with the errors labeled at various points in time after the ramp was completed. The error immediately after the loading was completed was -1%. One minute after loading the error was at -0.3% and after two minutes after loading the error was found to be 0.3%. Examining Ramp 2 for the 100% loading ramp an initial error of -1% was found, but within one minute the error was down to -0.2%. Two minutes after reaching full load, the error was at 0.1% and started

to slowly increase to a maximum error of 2.5%. Similar results were found for Ramps 3 and 4 as shown in Figure 39. For additional time periods after the loading portion has been reached along with errors refer to APPENDIX H.

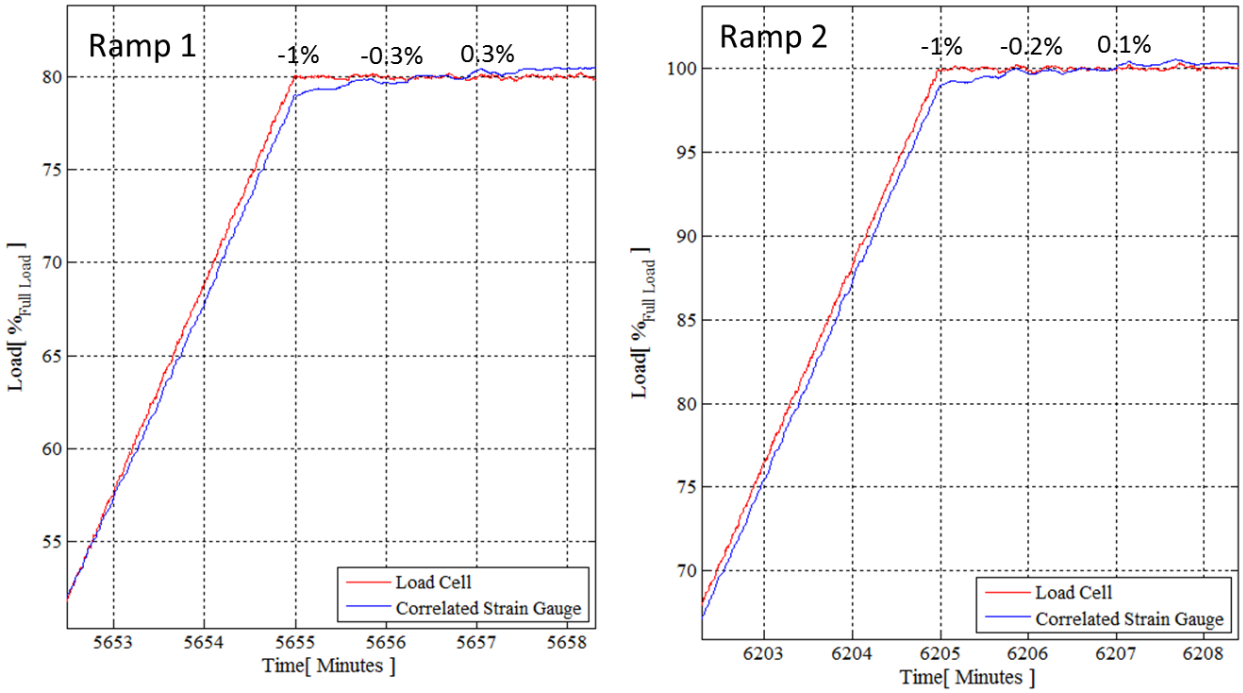

Figure 38: 5 minute view of Ramp 1 (80% Load), and Ramp 2 (100% Load) for Adapter A

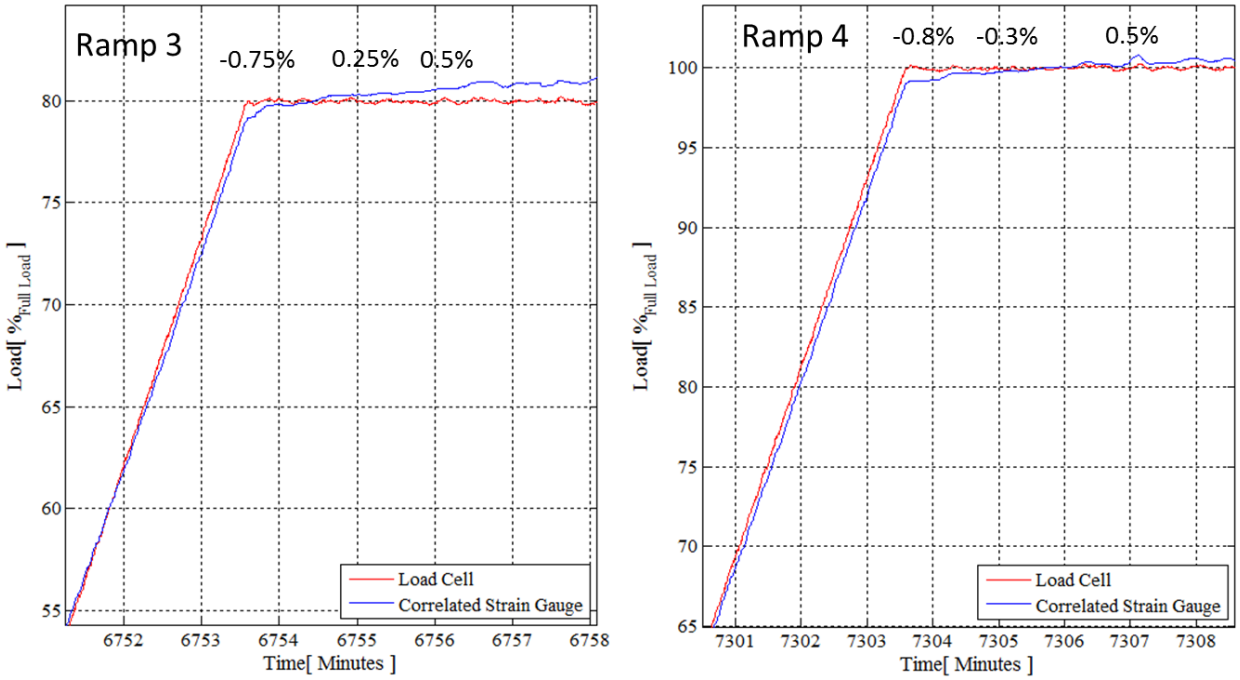

Figure 39: 5 minute view of Ramp 3 (80% Load), and Ramp 4 (100% Load) for Adapter A

4.2.2 Adapter B

With promising results collected with Adapter A, similar testing was completed with Adapter B. Due to time constraints in testing the unloaded step between the 95% load and the 100% load step was not conducted. The loaded steps for Adapter B showed a much more consistent reading over Adapter A (Figure 40). However, the beginning of each step had a small overshoot and then settled within an hour to the steady state value. The 17% load steps for Adapter B were also more consistent than the previous adapter and had a much higher accuracy with fluctuations of 3% as compared to 5% for Adapter A.

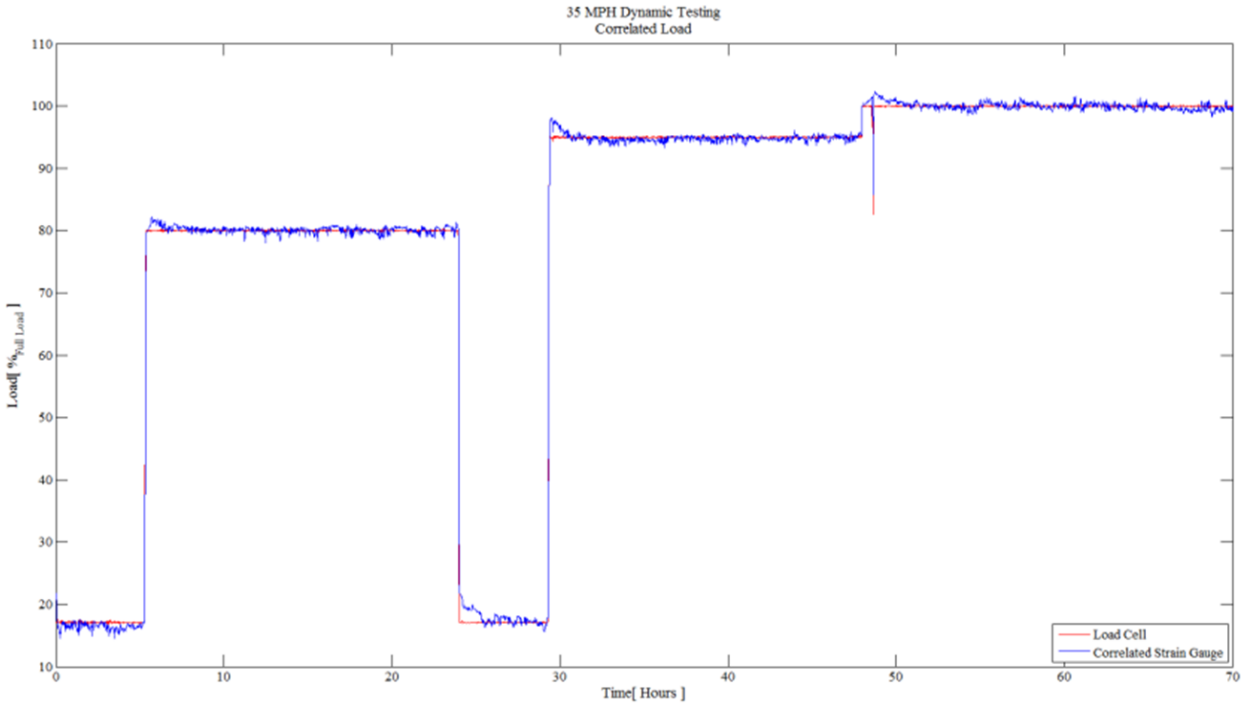

Figure 40: Adapter B Dynamic Testing at 35 mph

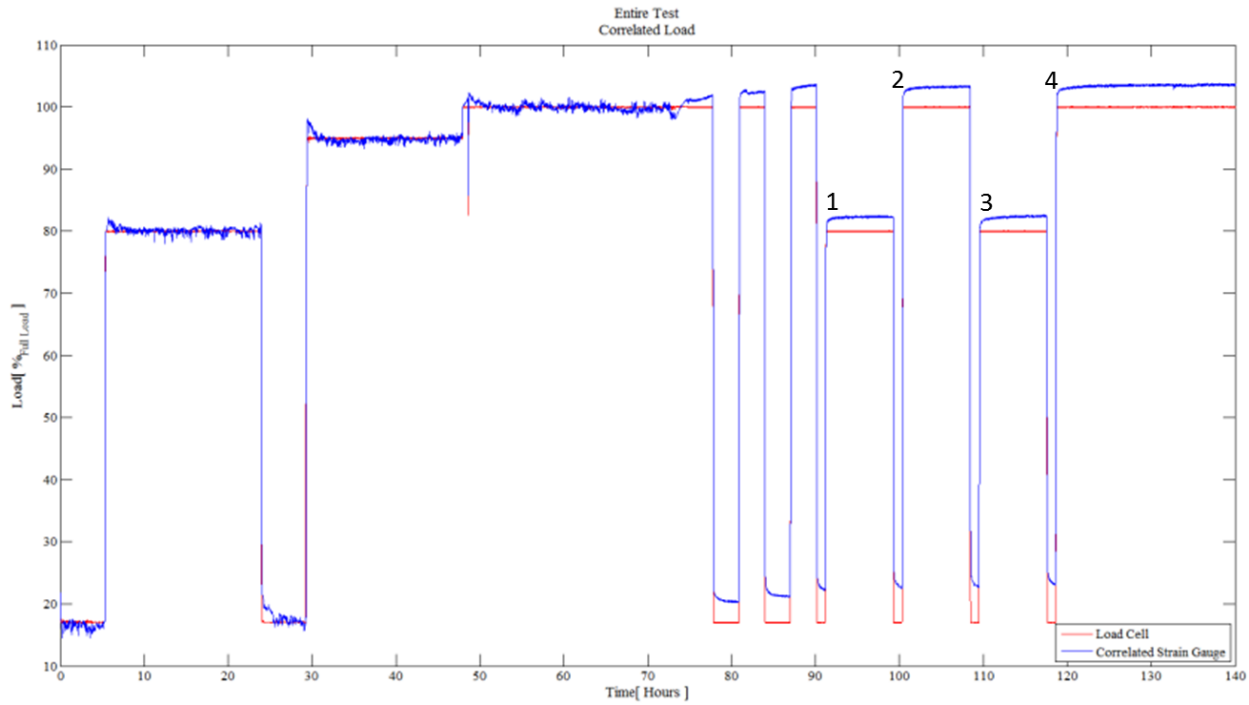

Figure 41: Adapter B Complete Test

Although a higher accuracy was obtained at the full range of the sensor for the dynamic portion of the test, looking at the static section of the test, the sensor experienced a higher overshoot of about 3% error for the 80% and 100% steps (Figure 41). Similar to Adapter A, the 17% load portion of the static test experienced an increase in the predicted load of approximately 6% over the actual load.

The ramping portions of the test can be seen in Figure 42 and Figure 43. Ramps 1 and 3 show the 80% steps and are seen to have the most accurate results almost immediately after the step has been completed. Ramps 2 and 4 represent the ramp for the 100% step and showed an overshoot in the predicted load of 0.7% and 1% respectively. The overshoot is in contrast to the results for Adapter A which undershot the actual load. In order to examine the response of the sensor at additional time intervals after the ramping portion additional graphs can be found in APPENDIX H.

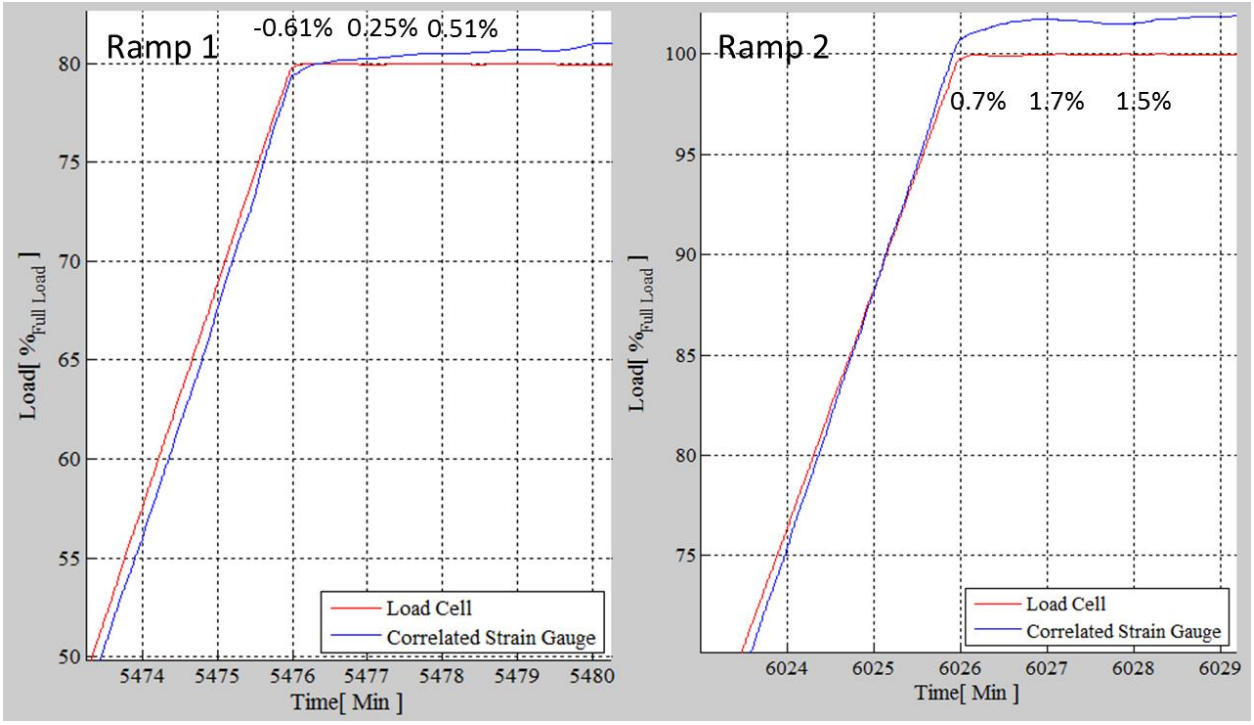

Figure 42: Ramp 1 (80% Load 5 minute view) and Ramp 2 (100% Load) for Adapter B

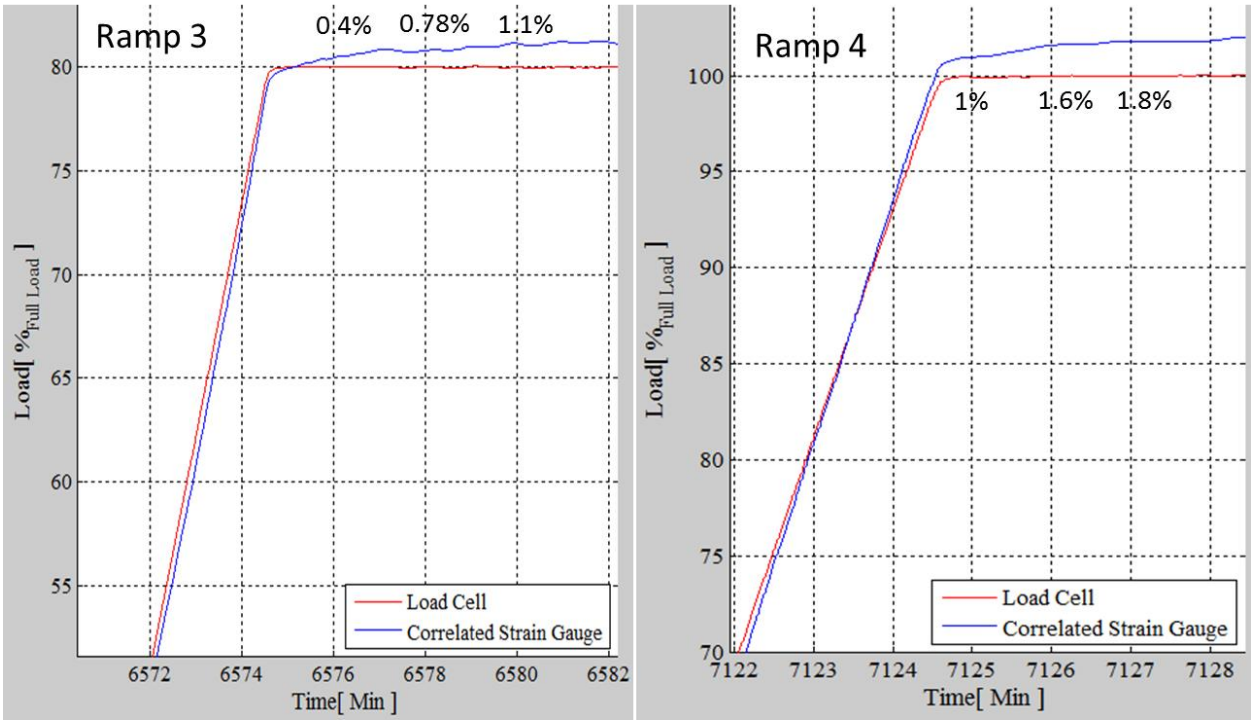

Figure 43: 5 minute view of Ramp 3 (80% Load) and Ramp 4 (100% Load) for Adapter B

4.2.3 Adapter C

Adapter C was the final adapter tested to determine the Smart Insert's reliability and performance. The dynamic testing provided an accurate output for the insert that matched the load cell value (Figure 44). The insert only experienced a slight overshoot for the 95% and 100% load step. The 17% load data appeared to have an increased standard deviation, although when a five minute average was taken the error was within ±1%.

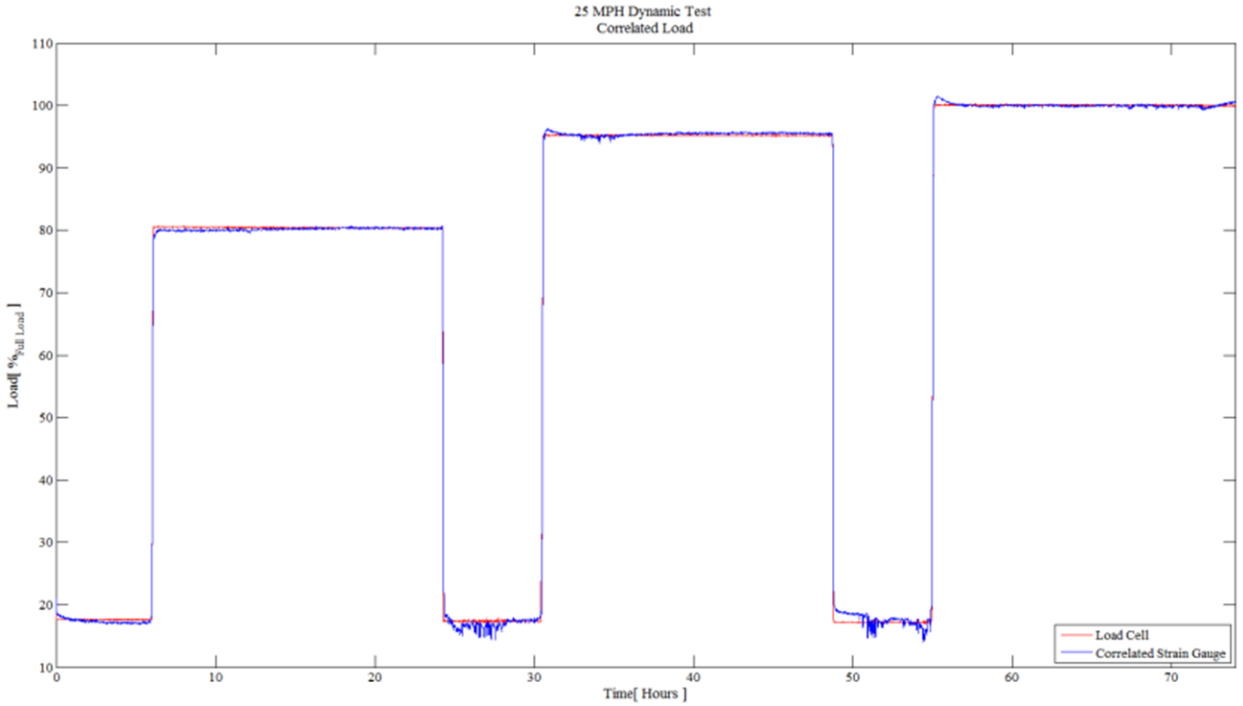

Figure 44: Adapter C Dynamic Testing at 25 mph

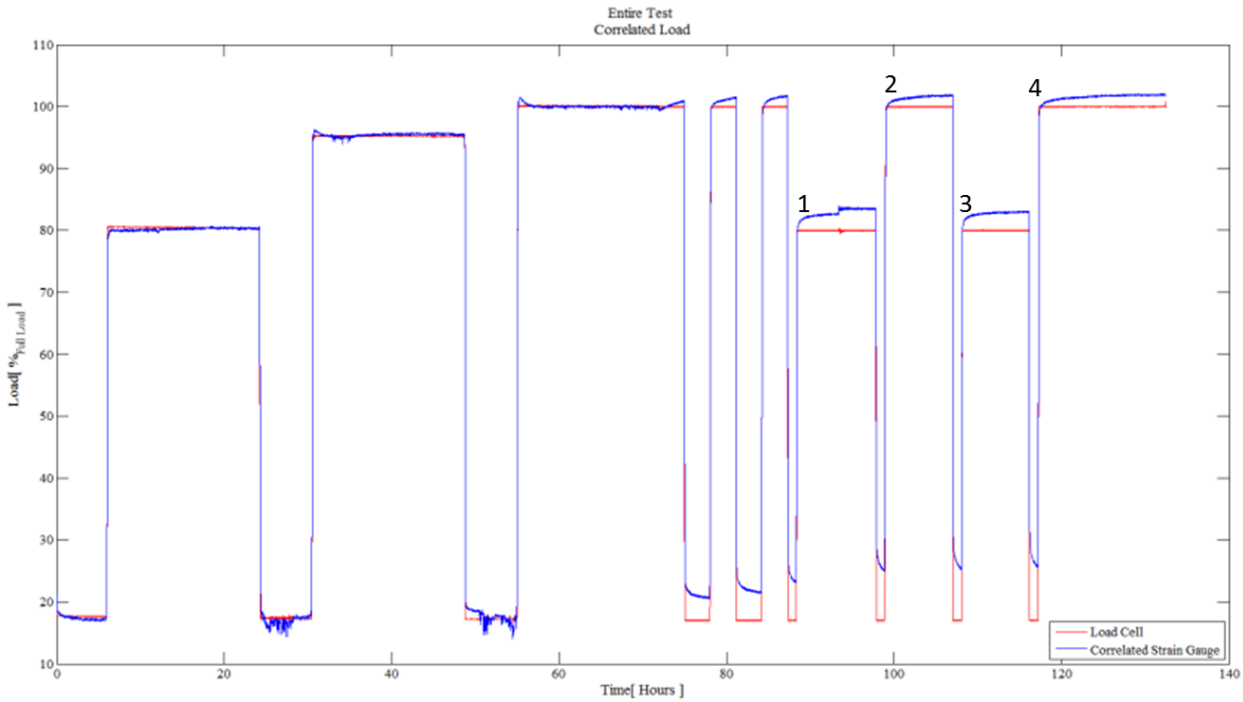

Figure 45: Adapter C Complete Test

The entire test conducted on Adapter C can be seen in Figure 45 along with the labeling of the ramping portion of the test. Adapter C produced a 2% overshoot for the 100% load static portion of the test, the smallest overshoot seen from any of the adapters. For the 17% step Adapter C produced similar results to Adapter A with almost 10% error. Although the overshoot was considerably better for the long term static portion of the test the results came at the cost of increased error in the ramping portion. Examining Figure 46 and Figure 47, the initial errors immediately after the ramping occurred for the 80% steps of Ramp 1 and 3 were -2.5% and -1.4% respectively. The sensor did provide an accuracy of 1% or better within one minute after the load was reached. Inspecting the 100% loaded step, Ramp 2 and 4 had an initial error of -1.7% to -2% error and required 3 minutes and 4.5 minutes respectively to reach within the targeted 1% error.

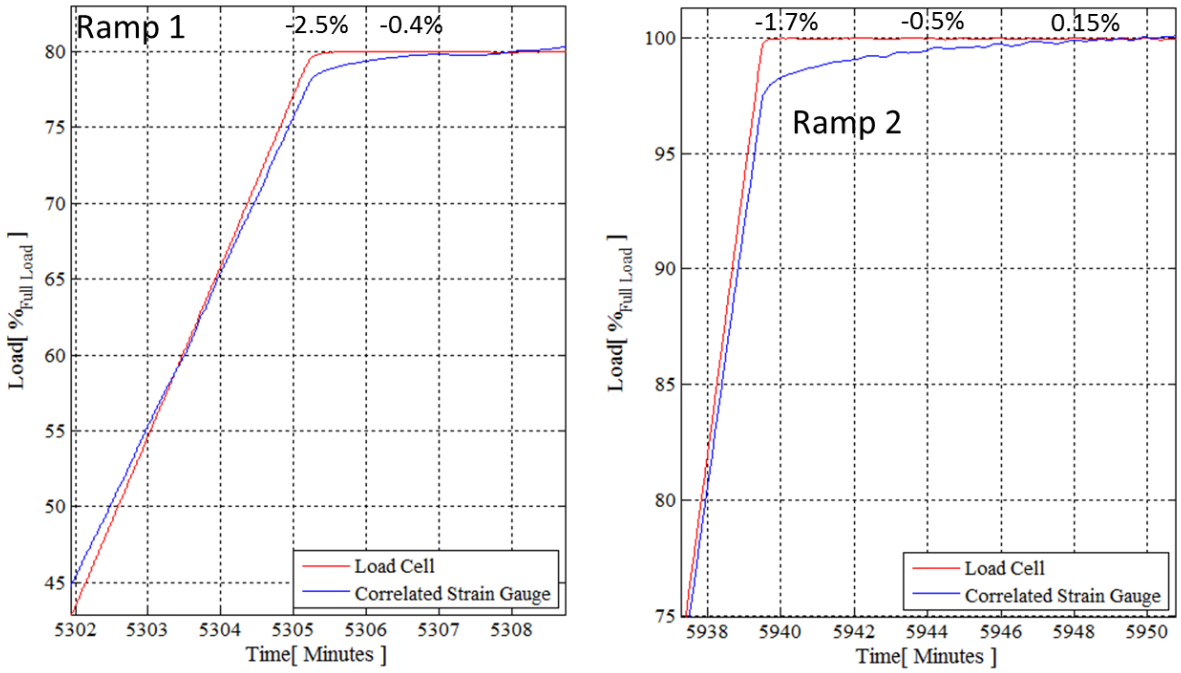

Figure 46: Ramp 1 (80% Load 5 minute view) and Ramp 2 (100% Load 12 Minute View) for Adapter C

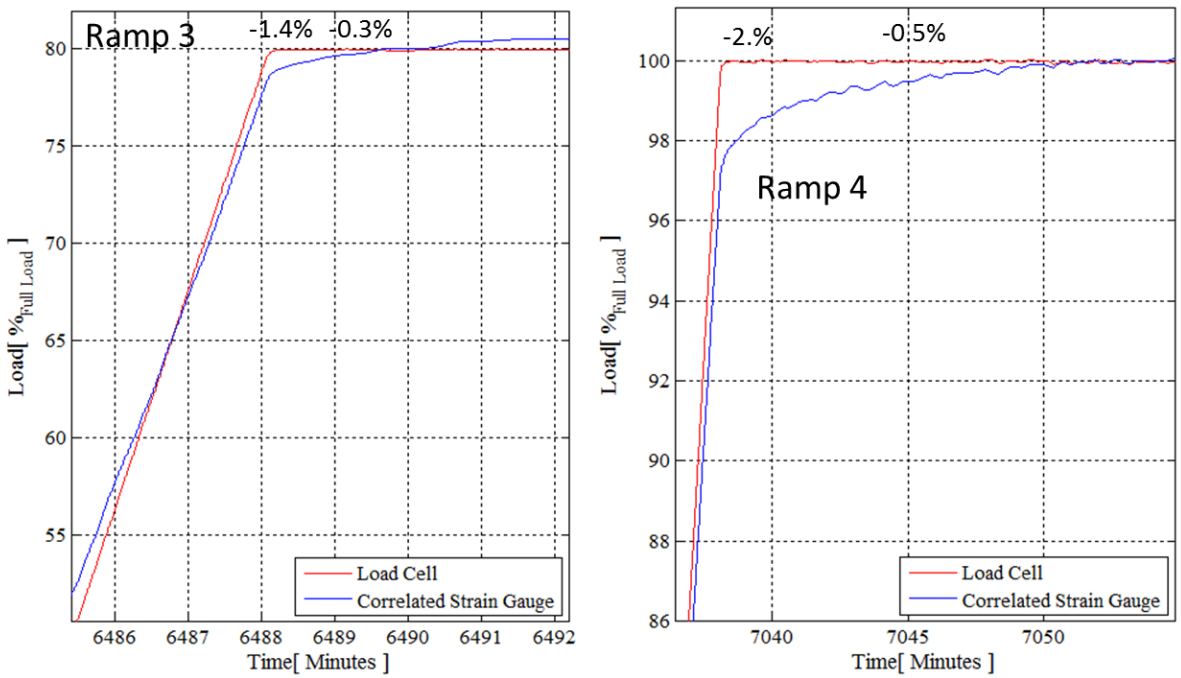

Figure 47: Ramp 3 (80% Load 6 minute view) and Ramp 4 (100% Load 12 Minute View) for Adapter C

4.2.4 Summary

In order to better compare the data collected from the three individual Smart Adapters Table 3 was compiled with all the errors. The top portion of the table contains the average errors for the dynamic steps for each of the adapters. The lower portion of the table contains the error determined for varying time intervals after the loading was completed. The time intervals used are 1, 2, and 5 minutes. All the errors are highlighted by one of three colors. The green highlighted cell means the value was within the targeted 1% error, the yellow highlighted cell was within an error of 1% to 1.5%, and the red highlighted cell was within 1.5% to 2% error. All of the adapters were within the targeted value of 1% for the dynamic testing for all of the loaded steps. Adapter A also produced errors of less than 1% for the ramping portion. For Adapters B and C the errors for the 80% steps were also within the target of 1% however, the 100% step provided errors ranging from 1% to 2%.

Table 3: Adapter Testing Error Summary

Dynamic Step (%Full Load)	Adapter A Average Error (%)			Adapter B Average Error (%)			Adapter C Average Error (%)		
80		0.07			0.14			-0.26	
95		-0.50			-0.13			0.23	
100		0.55			-0.02			-0.09	
Ramping Load	%Error*			%Error*			%Error*		
	1 Min Avg	2 Min Avg	5 Min Avg	1 Min Avg	2 Min Avg	5 Min Avg	1 Min Avg	2 Min Avg	5 Min Avg
80	-0.50	-0.26	0.21	0.04	0.23	0.58	-0.54	-0.37	0.00
80	-0.19	0.06	0.53	0.21	0.42	0.70	-0.54	-0.27	0.20
100	-0.53	-0.31	0.08	1.48	1.56	1.78	-1.56	-1.33	-0.93
100	-0.56	-0.37	0.04	1.19	1.43	1.74	-1.94	-1.68	-1.21
	0-1% Error			1-1.5% Error			1.5-2% Error		

*Static Ramping Error: Average error determined after specified time once target load was reached.

4.2.5 Insert Response Due to Variable Speeds

The majority of the testing previously conducted occurred at a constant load and speed. The sensor would also have to operate in the field with varied speed of operation while the load was held constant. In order to test how the speed affected the sensor performance, the sensor was placed under a constant load condition with the speed of operation varied. The resulting test can be observed in Figure 48. The figure illustrates the constant load held at 100% while the correlated strain gauge is shown to vary between 4.5% of full load shown by the horizontal green lines. The figure is sectioned and labeled for each portion of the test that experienced a different operating speed. The speed was varied randomly from 5 mph to 50 mph with each step lasting approximately 30 minutes.

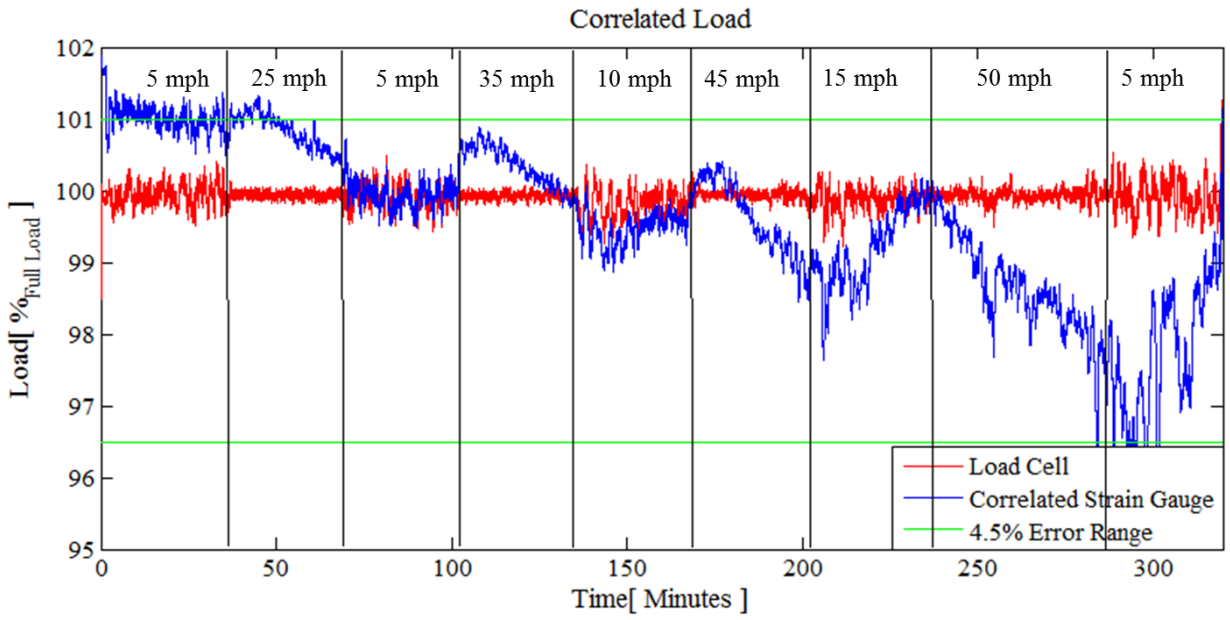

Figure 48: Adapter C Variable Speed Response

As the speed is varied the sensor experiences a change in load, however there does not appear to be a clear indication as to why the sensor output would remain constant at some speeds and decrease or increase at another. One of the previously unexplored variables of the sensor was the temperature of the bearing pad assembly. With two temperature sensors embedded in the Smart Insert the temperature effect could be explored. The correlated strain gauge output was plotted along with the temperature recorded from the Smart Insert. The temperature axis on the right side of Figure 49 was inverted to illustrate how the two signals track. Looking at the figure it is apparent that the bearing temperature has some effect on the sensors output.

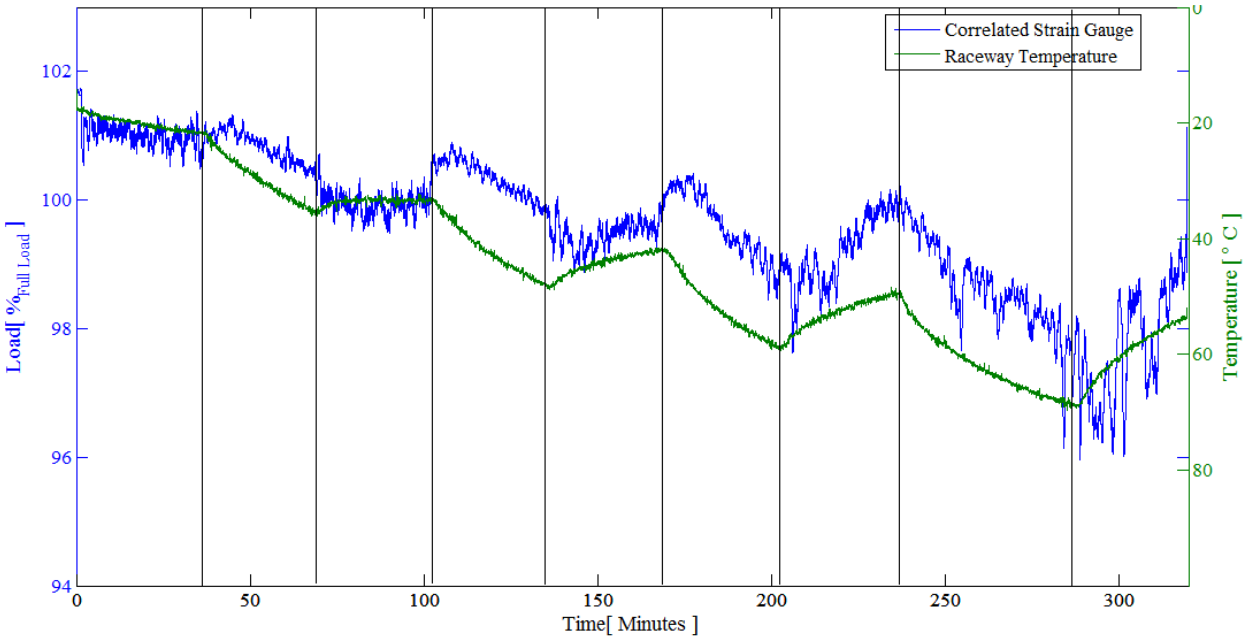

Figure 49: Adapter C Response with Temperature Plot

In order to integrate the bearing temperature into the correlation of the Smart Insert a multivariable linear regression was created. The multivariable linear regression took the strain gauge voltage, as well as the bearing temperature to create a correlation that was capable of predicting the load applied to the bearing. The correlation was then applied to the same data set and shown in Figure 50. With the use of the multivariable linear regression the entire signal was able to be almost completely contained within 0.25% accuracy as shown by the horizontal black lines in the figure.

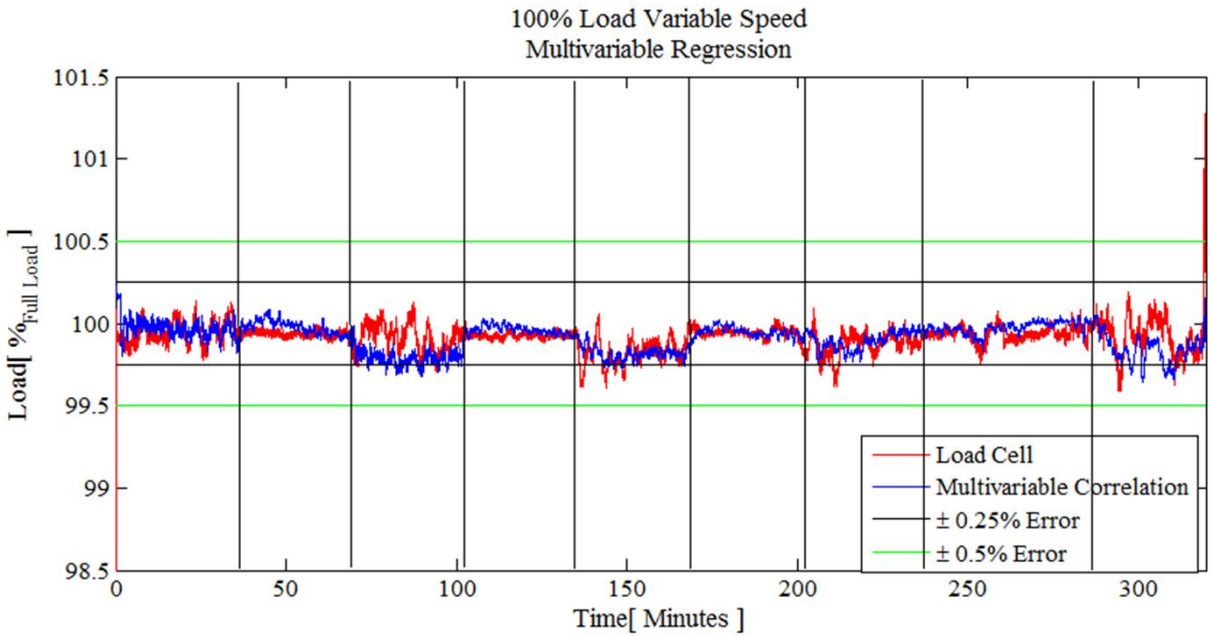

Figure 50: Adapter C Multivariable Linear Regression

CHAPTER V

CONCLUSION AND FUTURE WORK

Eight Smart Inserts were manufactured and tested to provide a steady signal in dynamic testing at 25 to 35 mph in laboratory settings. The accuracy of the sensors was within the targeted range of 1% with respect to full scale load. The electronics needed to continuously monitor eight of the load sensors simultaneously was also built and tested to ensure a successful field test, which will validate the accuracy and correlations obtained in the laboratory.

The current sensor design is a versatile unit capable of measuring static and dynamic loads applied to a freight railcar bearing. Depending on customer specifications the sensor can be calibrated to measure most accurately loads from 90% to 110% of full load, or slightly less accurately a wider envelope of loads from 10% to 100% of full load. The sensor can be correlated to a dynamic signal, as well as a static signal, or correlated to provide the most accurate data for a loading situation to provide immediate feedback to loading personnel to ensure the proper load was placed in the rail car.

With the use of the flex circuit the Smart Insert was able to provide an accurate reading of the bearing cup temperature and capable of detecting slight changes in temperature at the inboard and outboard location of the bearing. This information is useful for determining the location of a defect in the bearing. With the flex circuit capable of handling the majority of the signal conditioning onboard via the mounting locations for integrated circuity, a higher accuracy signal can be obtained, along with very minimal additional requirements needed to create a

completely self-contained sensing unit. The flex circuit also provided the essential wiring to ensure survivability and reliability to the insert during prolonged operation. The final gain used for the load sensor amplification circuitry was set at 400 V/V. The gain provided a voltage swing of four volts from the unloaded to loaded state.

Further testing should be conducted examining the sensor's response to impact loading in order to determine if the sensor would be a viable solution for detecting wheel flats or rail defects. The sensor should also be tested under lateral loading conditions in order to monitor the signal's sensitivity to this type of loading. These types of conditions would surely be experience in the field and should be reproduced in the laboratory environment to determine if any improvements in the design can be made.

Finally, detailed work should be conducted further analyzing the effects of bearing temperature on the load sensor output. Studies should be conducted determining the best method of applying a multivariable regression with the strain gauge output and the temperature of the bearing to determine the most accurate load. Improved work in this subject could lead to higher accuracies from the sensor with a larger range of loads for all conditions encountered in the field.

REFERENCES

[1] CSX, "Fuel Efficiency," CSX, [Online]. Available: http://www.csx.com/index.cfm/about-csx/projects-and-partnerships/fuel-efficiency/. [Accessed 12 May 2015].

[2] C. M. Taraneh, "Experiments and models for the thermal response of railroad tapered-roller bearings," *International Journal of Heat and Mass Transfer*, p. 5794–5803, 3 July 2008.

[3] S. White, "Wheel Defect Manual," Engineering Standard Rolling Stock, 2013.

[4] CSX Transportation, "CSXT 8100 Weighing Section IX," Jacksonville, FL, 1987.

[5] Association of American Railroad, "The Impact of the STaggers Rail Act of 1980," AAR, Washington DC, 2014.

[6] Association of American Railraods, "Positive Train Control," AAR, Washington DC, 2014.

[7] Anthea NGAI, "The Institution of Railway Signal Engineers," March 2009. [Online]. Available: http://www.irse.org.hk/eNewsletter/issue05/Technical-Articles/WILD/WILD.htm. [Accessed 27 April 2015].

[8] C. Cruceanu, Train Braking, Reliability and Safety in Railway, D. X. Perpinya, Ed., InTech, 2012.

[9] K. S. a. S. T. W., "Bearing Temperature Performance in Freight," in *ASME RTD 2007 Fall Technical Conference*, Chicago, 2007.

[10] J. A. Kypuros, "Implementation of Wireless Temperature Sensors for Continuous Condition Monitoring of Railroad Bearings," Minneapolis, 2011.

[11] L. Saenz, Calibration and Optimization of a Load Sensor Embedded in a Railroad Bearing Adapter, Master's thesis: University of Texas-Pan American, 2013.

[12] Amsted Rail, "AdapterPlus™Steering Pad System," 2012. [Online]. Available: http://www.amstedrail.com/. [Accessed 25 May 2015].

[13] DimensionEngineering, "SyRen 50A regenerative motor driver," DimensionEngineering, [Online]. Available: https://www.dimensionengineering.com/products/syren50. [Accessed 6 7 2015].

[14] J. Vincent, Structrual Biomaterials: Third Edition, New Jersey: Prinction University Press, 2012.

APPENDIX A

APPENDIX A

LOAD SENSOR BOARD SCHEMATIC

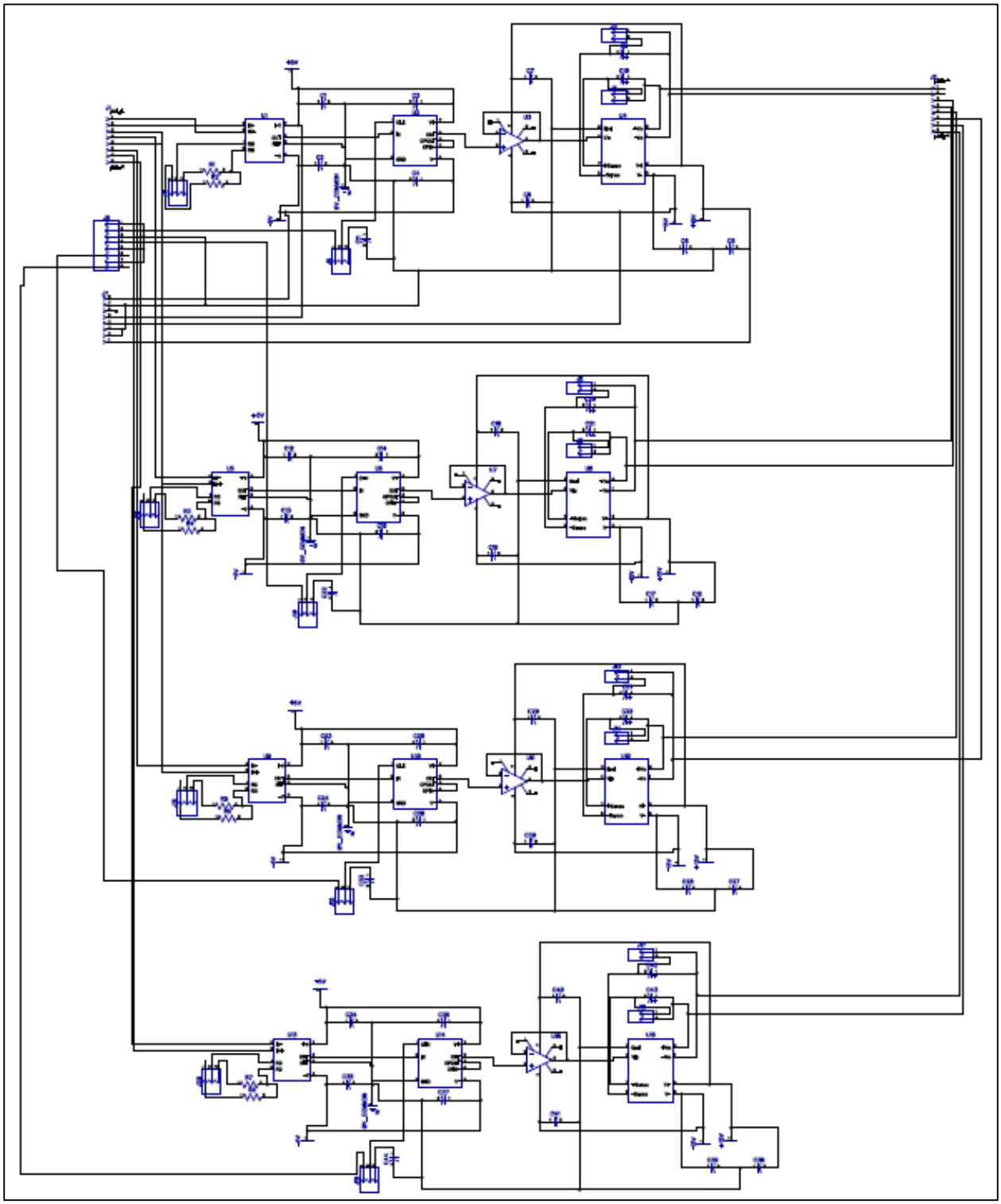

APPENDIX B

APPENDIX B

TEMPERATURE SENSOR BOARD SCHEMATIC

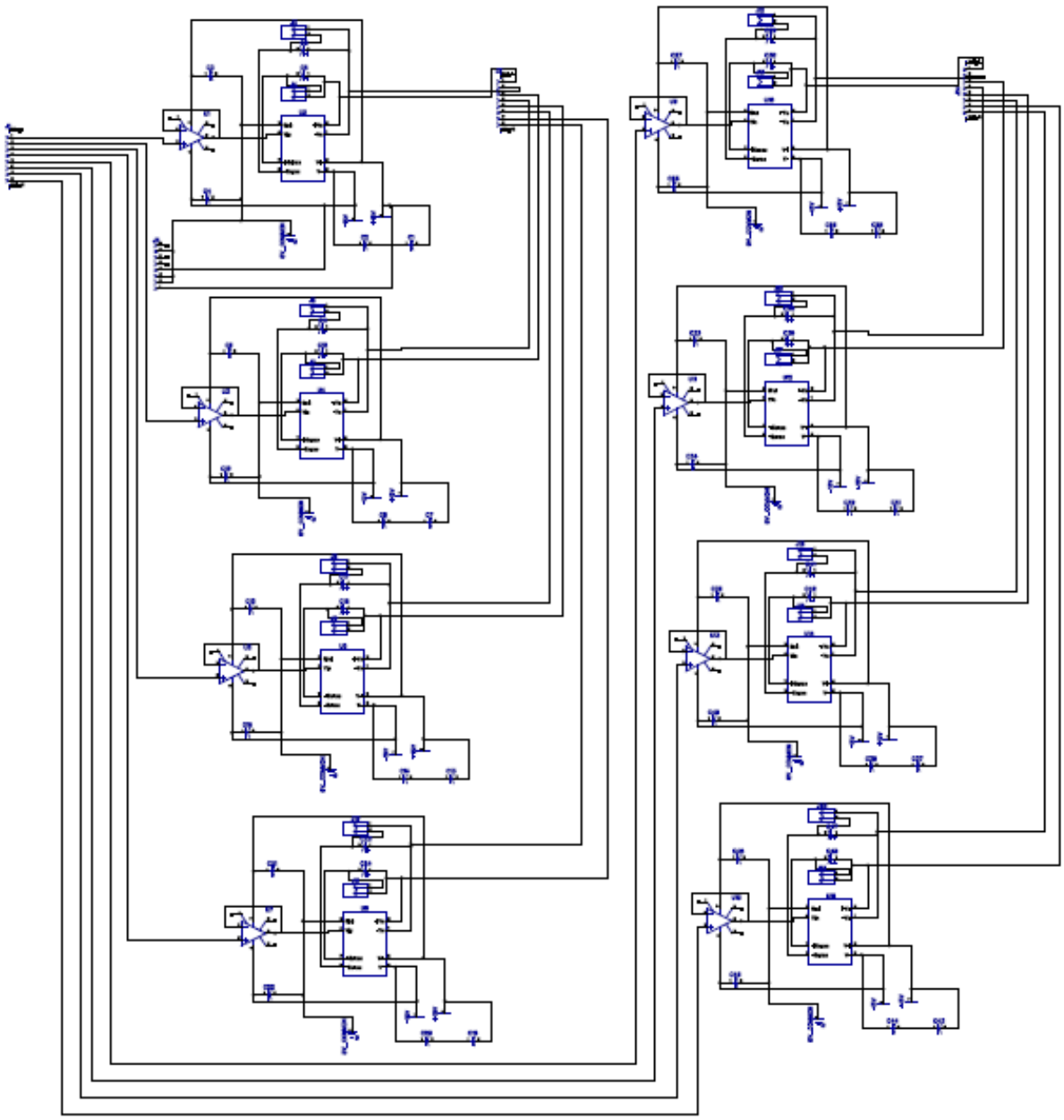

APPENDIX C

APPENDIX C

INA 129 DATASHEET

Burr-Brown Products from Texas Instruments

INA128
INA129

SBOS051B – OCTOBER 1995 – REVISED FEBRUARY 2005

Precision, Low Power INSTRUMENTATION AMPLIFIERS

FEATURES

- LOW OFFSET VOLTAGE: 50µV max
- LOW DRIFT: 0.5µV/°C max
- LOW INPUT BIAS CURRENT: 5nA max
- HIGH CMR: 120dB min
- INPUTS PROTECTED TO ±40V
- WIDE SUPPLY RANGE: ±2.25V to ±18V
- LOW QUIESCENT CURRENT: 700µA
- 8-PIN PLASTIC DIP, SO-8

APPLICATIONS

- BRIDGE AMPLIFIER
- THERMOCOUPLE AMPLIFIER
- RTD SENSOR AMPLIFIER
- MEDICAL INSTRUMENTATION
- DATA ACQUISITION

DESCRIPTION

The INA128 and INA129 are low power, general purpose instrumentation amplifiers offering excellent accuracy. The versatile 3-op amp design and small size make them ideal for a wide range of applications. Current-feedback input circuitry provides wide bandwidth even at high gain (200kHz at G = 100).

A single external resistor sets any gain from 1 to 10,000. The INA128 provides an industry-standard gain equation; the INA129 gain equation is compatible with the AD620.

The INA128/INA129 is laser trimmed for very low offset voltage (50µV), drift (0.5µV/°C) and high common-mode rejection (120dB at G ≥ 100). It operates with power supplies as low as ±2.25V, and quiescent current is only 700µA—ideal for battery-operated systems. Internal input protection can withstand up to ±40V without damage.

The INA128/INA129 is available in 8-pin plastic DIP and SO-8 surface-mount packages, specified for the –40°C to +85°C temperature range. The INA128 is also available in a dual configuration, the INA2128.

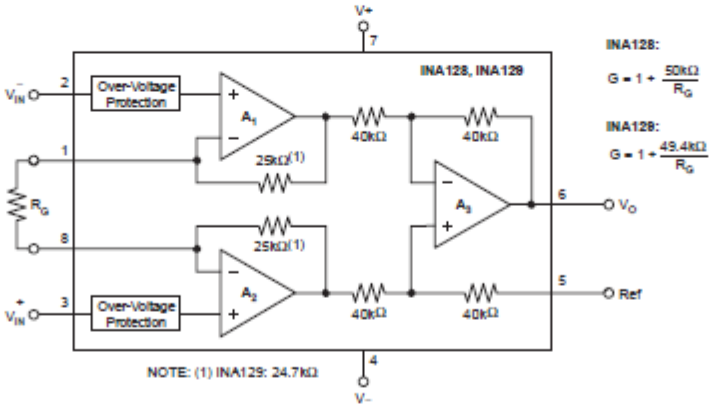

Please be aware that an important notice concerning availability, standard warranty, and use in critical applications of Texas Instruments semiconductor products and disclaimers thereto appears at the end of this data sheet.

All trademarks are the property of their respective owners.

PRODUCTION DATA information is current as of publication date. Products conform to specifications per the terms of Texas Instruments standard warranty. Production processing does not necessarily include testing of all parameters.

Texas Instruments
www.ti.com

Copyright © 1995–2005, Texas Instruments Incorporated

ABSOLUTE MAXIMUM RATINGS(1)

Supply Voltage	±18V
Analog Input Voltage Range	±40V
Output Short-Circuit (to ground)	Continuous
Operating Temperature	–40°C to +125°C
Storage Temperature Range	–55°C to +125°C
Junction Temperature	+150°C
Lead Temperature (soldering, 10s)	+300°C

(1) Stresses above these ratings may cause permanent damage. Exposure to absolute maximum conditions for extended periods may degrade device reliability. These are stress ratings only, and functional operation of the device at these or any other conditions beyond those specified is not implied.

ELECTROSTATIC DISCHARGE SENSITIVITY

This integrated circuit can be damaged by ESD. Texas Instruments recommends that all integrated circuits be handled with appropriate precautions. Failure to observe proper handling and installation procedures can cause damage.

ESD damage can range from subtle performance degradation to complete device failure. Precision integrated circuits may be more susceptible to damage because very small parametric changes could cause the device not to meet its published specifications.

ORDERING INFORMATION

For the most current package and ordering information, see the Package Option Addendum located at the end of this data sheet.

PIN CONFIGURATION

8-Pin DIP and SO-8

Top View

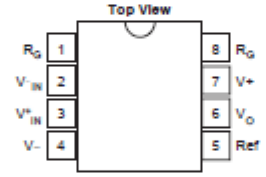

ELECTRICAL CHARACTERISTICS

At T_A = +25°C, V_S = ±15V, R_L = 10kΩ, unless otherwise noted.

PARAMETER	CONDITIONS	INA128P, U INA129P, U			INA128PA, UA INA129PA, UA			UNIT
		MIN	TYP	MAX	MIN	TYP	MAX	
INPUT								
Offset Voltage, RTI								
Initial	T_A = +25°C		±10±100/G	±50±500/G		±25±100/G	±125±1000/G	µV
vs Temperature	T_A = T_{MIN} to T_{MAX}		±0.2±2/G	±0.5±20/G		±0.2±5/G	±1±20/G	µV/°C
vs Power Supply	V_S = ±2.25V to ±18V		±0.2±20/G	±1±100/G		*	±2±200/G	µV/V
Long-Term Stability			±0.1±3/G			*		µV/mo
Impedance, Differential			10^{10} || 2			*		Ω || pF
Common-Mode			10^{11} || 9			*		Ω || pF
Common-Mode Voltage Range[1]	V_O = 0V	(V+) – 2	(V+) – 1.4		*	*		V
		(V–) + 2	(V–) + 1.7		*	*		V
Safe Input Voltage				±40			*	V
Common-Mode Rejection	V_{CM} = ±13V, ΔR_S = 1kΩ							
	G = 1	80	86		73	*		dB
	G = 10	100	106		93	*		dB
	G = 100	120	125		110	*		dB
	G = 1000	120	130		110	*		dB
BIAS CURRENT			±2	±5		*	±10	nA
vs Temperature			±30			*		pA/°C
Offset Current			±1	±5		*	±10	nA
vs Temperature			±30			*		pA/°C
NOISE VOLTAGE, RTI	G = 1000, R_S = 0Ω							
f = 10Hz			10			*		nV/√Hz
f = 100Hz			8			*		nV/√Hz
f = 1kHz			8			*		nV/√Hz
f_B = 0.1Hz to 10Hz			0.2			*		μV_{PP}
Noise Current								
f = 10Hz			0.9			*		pA/√Hz
f = 1kHz			0.3			*		pA/√Hz
f_B = 0.1Hz to 10Hz			30			*		pA_{PP}
GAIN								
Gain Equation, INA128			1 + (50kΩ/R_G)			*		V/V
INA129			1 + (49.4kΩ/R_G)			*		V/V
Range of Gain		1		10000	*		*	V/V
Gain Error	G = 1		±0.01	±0.024		*	±0.1	%
	G = 10		±0.02	±0.4		*	±0.5	%
	G = 100		±0.05	±0.5		*	±0.7	%
	G = 1000		±0.5	±1		*	±2	%
Gain vs Temperature[2]	G = 1		±1	±10		*	*	ppm/°C
50kΩ (or 49.4kΩ) Resistance[2][3]			±25	±100		*	*	ppm/°C
Nonlinearity	V_O = ±13.6V, G = 1		±0.0001	±0.001		*	±0.002	% of FSR
	G = 10		±0.0003	±0.002		*	±0.004	% of FSR
	G = 100		±0.0005	±0.002		*	±0.004	% of FSR
	G = 1000		±0.001	[4]		*	*	% of FSR

NOTE: * Specification is same as INA128P, U or INA129P, U.

(1) Input common-mode range varies with output voltage — see typical curves.

(2) Specified by wafer test.

(3) Temperature coefficient of the 50kΩ (or 49.4kΩ) term in the gain equation.

(4) Nonlinearity measurements in G = 1000 are dominated by noise. Typical nonlinearity is ±0.001%.

ELECTRICAL CHARACTERISTICS (continued)

At T_A = +25°C, V_S = ±15V, R_L = 10kΩ, unless otherwise noted.

PARAMETER	CONDITIONS	INA128P, U INA129P, U			INA128PA, UA INA129PA, UA			UNIT
		MIN	TYP	MAX	MIN	TYP	MAX	
OUTPUT								
Voltage: Positive	R_L = 10kΩ	(V+) – 1.4	(V+) – 0.9		*	*		V
Negative	R_L = 10kΩ	(V–) + 1.4	(V–) + 0.8		*	*		V
Load Capacitance Stability			1000			*		pF
Short-Circuit Current			+6/–15			*		mA
FREQUENCY RESPONSE								
Bandwidth, –3dB	G = 1		1.3			*		MHz
	G = 10		700			*		kHz
	G = 100		200			*		kHz
	G = 1000		20			*		kHz
Slew Rate	V_O = ±10V, G = 10		4			*		V/µs
Settling Time, 0.01%	G = 1		7			*		µs
	G = 10		7			*		µs
	G = 100		9			*		µs
	G = 1000		80			*		µs
Overload Recovery	50% Overdrive		4			*		µs
POWER SUPPLY								
Voltage Range		±2.25	±15	±18	*	*	*	V
Current, Total	V_{IN} = 0V		±700	±750		*	*	µA
TEMPERATURE RANGE								
Specification		–40		+85	*		*	°C
Operating		–40		+125	*		*	°C
θ_{JA} 8-Pin DIP			80			*		°C/W
SO-8 SOIC			150			*		°C/W

NOTE: * Specification is same as INA128P, U or INA129P, U.
(1) Input common-mode range varies with output voltage — see typical curves.
(2) Specified by wafer test.
(3) Temperature coefficient of the 50kΩ (or 49.4kΩ) term in the gain equation.
(4) Nonlinearity measurements in G = 1000 are dominated by noise. Typical nonlinearity is ±0.001%.

APPLICATIONS INFORMATION

Figure 1 shows the basic connections required for operation of the INA128/INA129. Applications with noisy or high impedance power supplies may require decoupling capacitors close to the device pins as shown.

The output is referred to the output reference (Ref) terminal which is normally grounded. This must be a low-impedance connection to assure good common-mode rejection. A resistance of 8Ω in series with the Ref pin will cause a typical device to degrade to approximately 80dB CMR (G = 1).

SETTING THE GAIN

Gain is set by connecting a single external resistor, R_G, connected between pins 1 and 8:

INA128:

$$G = 1 + \frac{50k\Omega}{R_G} \quad (1)$$

INA129:

$$G = 1 + \frac{49.4k\Omega}{R_G} \quad (2)$$

Commonly used gains and resistor values are shown in Figure 1.

The 50kΩ term in Equation 1 (49.4kΩ in Equation 2) comes from the sum of the two internal feedback resistors of A_1 and A_2. These on-chip metal film resistors are laser trimmed to accurate absolute values. The accuracy and temperature coefficient of these internal resistors are included in the gain accuracy and drift specifications of the INA128/INA129.

The stability and temperature drift of the external gain setting resistor, R_G, also affects gain. R_G's contribution to gain accuracy and drift can be directly inferred from the gain equation (1). Low resistor values required for high gain can make wiring resistance important. Sockets add to the wiring resistance which will contribute additional gain error (possibly an unstable gain error) in gains of approximately 100 or greater.

DYNAMIC PERFORMANCE

The typical performance curve *Gain vs Frequency* shows that, despite its low quiescent current, the INA128/INA129 achieves wide bandwidth, even at high gain. This is due to the current-feedback topology of the input stage circuitry. Settling time also remains excellent at high gain.

NOISE PERFORMANCE

The INA128/INA129 provides very low noise in most applications. Low frequency noise is approximately $0.2\mu V_{PP}$ measured from 0.1 to 10Hz (G ≥ 100). This provides dramatically improved noise when compared to state-of-the-art chopper-stabilized amplifiers.

INA128: $G = 1 + \frac{50k\Omega}{R_G}$ **INA129:** $G = 1 + \frac{49.4k\Omega}{R_G}$

DESIRED GAIN (V/V)	INA128 R_G (Ω)	INA128 NEAREST 1% R_G (Ω)	INA129 R_G (Ω)	INA129 NEAREST 1% R_G (Ω)
1	NC	NC	NC	NC
2	50.00k	49.9k	49.4k	49.9k
5	12.50k	12.4k	12.35k	12.4k
10	5.556k	5.62k	5489	5.49k
20	2.632k	2.61k	2600	2.61k
50	1.02k	1.02k	1008	1k
100	505.1	511	499	499
200	251.3	249	248	249
500	100.2	100	99	100
1000	50.05	49.9	49.5	49.9
2000	25.01	24.9	24.7	24.9
5000	10.00	10	9.88	9.76
10000	5.001	4.99	4.94	4.87

NC: No Connection

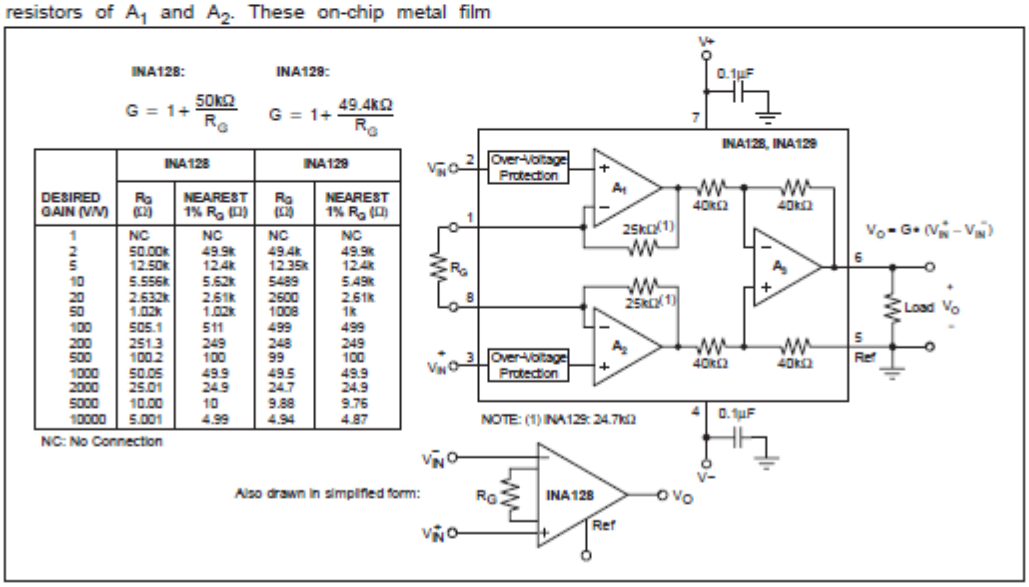

Figure 1. Basic Connections

OFFSET TRIMMING

The INA128/INA129 is laser trimmed for low offset voltage and offset voltage drift. Most applications require no external offset adjustment. Figure 2 shows an optional circuit for trimming the output offset voltage. The voltage applied to Ref terminal is summed with the output. The op amp buffer provides low impedance at the Ref terminal to preserve good common-mode rejection.

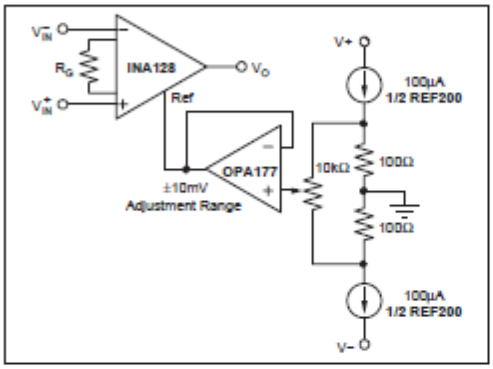

Figure 2. Optional Trimming of Output Offset Voltage

INPUT BIAS CURRENT RETURN PATH

The input impedance of the INA128/INA129 is extremely high—approximately $10^{10}\Omega$. However, a path must be provided for the input bias current of both inputs. This input bias current is approximately ±2nA. High input impedance means that this input bias current changes very little with varying input voltage.

Input circuitry must provide a path for this input bias current for proper operation. Figure 3 shows various provisions for an input bias current path. Without a bias current path, the inputs will float to a potential which exceeds the common-mode range, and the input amplifiers will saturate.

If the differential source resistance is low, the bias current return path can be connected to one input (see the thermocouple example in Figure 3). With higher source impedance, using two equal resistors provides a balanced input with possible advantages of lower input offset voltage due to bias current and better high-frequency common-mode rejection.

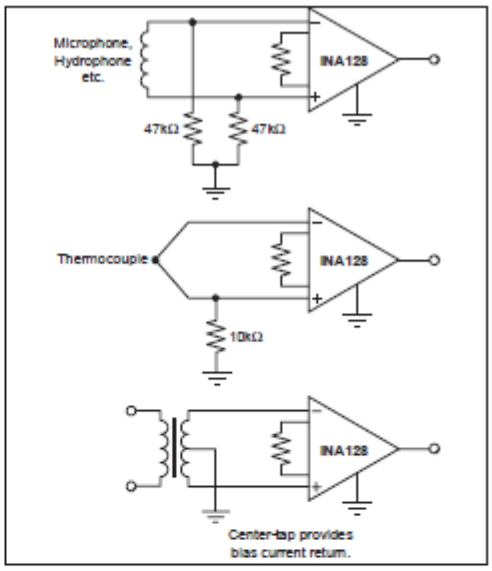

Figure 3. Providing an Input Common-Mode Current Path

INPUT COMMON-MODE RANGE

The linear input voltage range of the input circuitry of the INA128/INA129 is from approximately 1.4V below the positive supply voltage to 1.7V above the negative supply. As a differential input voltage causes the output voltage increase, however, the linear input range will be limited by the output voltage swing of amplifiers A_1 and A_2. So the linear common-mode input range is related to the output voltage of the complete amplifier. This behavior also depends on supply voltage—see performance curves, *Input Common-Mode Range vs Output Voltage*.

Input-overload can produce an output voltage that appears normal. For example, if an input overload condition drives both input amplifiers to their positive output swing limit, the difference voltage measured by the output amplifier will be near zero. The output of A_3 will be near 0V even though both inputs are overloaded.

LOW VOLTAGE OPERATION

The INA128/INA129 can be operated on power supplies as low as ±2.25V. Performance remains excellent with power supplies ranging from ±2.25V to ±18V. Most parameters vary only slightly throughout this supply voltage range—see typical performance curves.

Operation at very low supply voltage requires careful attention to assure that the input voltages remain within their linear range. Voltage swing requirements of internal nodes limit the input common-mode range with low power supply voltage. Typical performance curves, "Input Common-Mode Range vs Output Voltage" show the range of linear operation for ±15V, ±5V, and ±2.5V supplies.

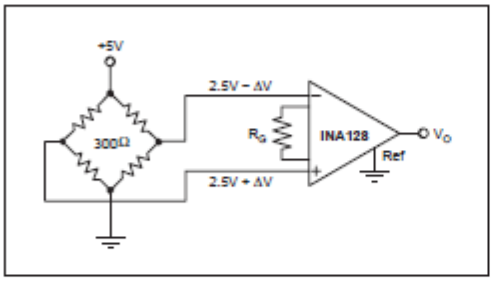

Figure 4. Bridge Amplifier

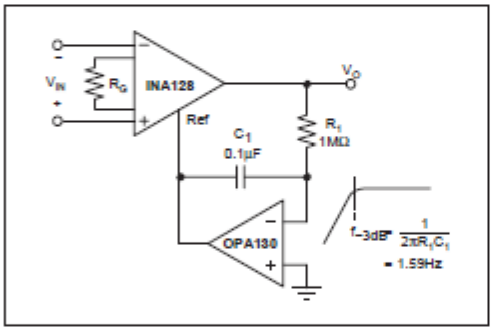

Figure 5. AC-Coupled Instrumentation Amplifier

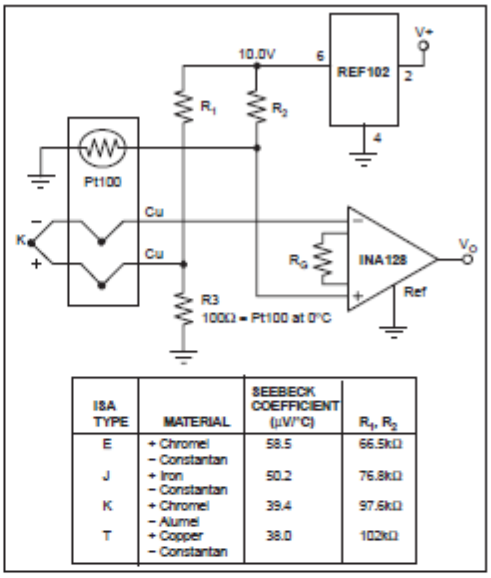

ISA TYPE	MATERIAL	SEEBECK COEFFICIENT (µV/°C)	R_1, R_2
E	+ Chromel – Constantan	58.5	66.5kΩ
J	+ Iron – Constantan	50.2	76.8kΩ
K	+ Chromel – Alumel	39.4	97.6kΩ
T	+ Copper – Constantan	38.0	102kΩ

Figure 6. Thermocouple Amplifier with RTD Cold-Junction Compensation

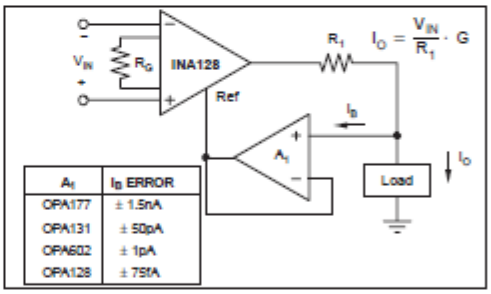

A_1	I_B ERROR
OPA177	± 1.5nA
OPA131	± 50pA
OPA602	± 1pA
OPA128	± 75fA

Figure 7. Differential Voltage to Current Converter

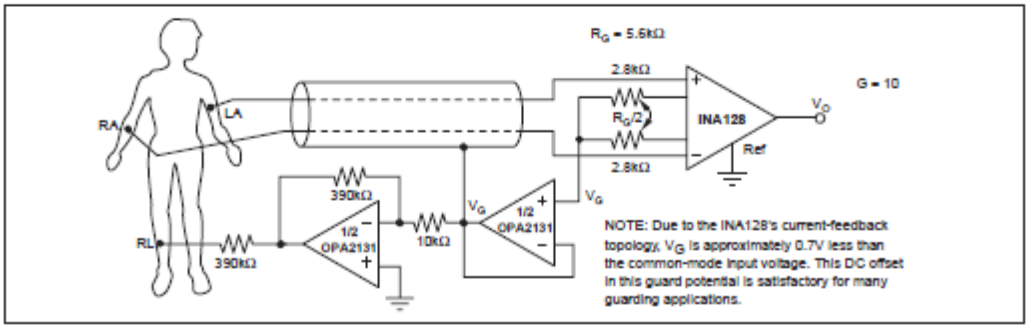

Figure 8. ECG Amplifier with Right-Leg Drive

APPENDIX D

APPENDIX D

MAX 294 DATASHEET

19-0020; Rev 2; 06/08

MAXIM

8th-Order, Lowpass, Elliptic, Switched-Capacitor Filters

General Description

The MAX293/MAX294/MAX297 are easy-to-use, 8th-order, lowpass, elliptic, switched-capacitor filters that can be set up with corner frequencies from 0.1Hz to 25kHz (MAX293/MAX294) or from 0.1Hz to 50kHz (MAX297).

The MAX293/MAX297's 1.5 transition ratio provides sharp rolloff and -80dB of stopband rejection. The MAX294's 1.2 transition ratio provides the steepest rolloff and -58dB of stopband rejection. All three filters have fixed responses, so the design task is limited to selecting the clock frequency that controls the filter's corner frequency.

An external capacitor is used to generate a clock using the internal oscillator, or an external clock signal can be used. An uncommitted op amp (noninverting input grounded) is provided for building a continuous-time lowpass filter for post-filtering or anti-aliasing. Steep rolloff and high order make these filters ideal for anti-aliasing applications that require maximum bandwidth, and for communication applications that require filtering signals in close proximity within the frequency domain.

The MAX293/MAX294/MAX297 are available in 8-pin DIP and 16-pin wide SO packages, delivering aggressive performance from a tiny area.

Applications

Data-Acquisition Systems

Anti-Aliasing

DAC Post-Filtering

Voice/Data Signal Filtering

Typical Operating Circuit

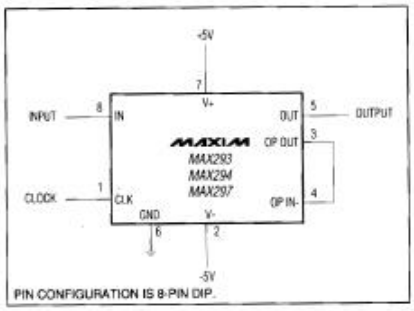

PIN CONFIGURATION IS 8-PIN DIP.

Features

- 8th-Order Lowpass Elliptic Filters
- Clock-Tunable Corner-Frequency Range:
  0.1Hz to 25kHz (MAX293/MAX294)
  0.1Hz to 50kHz (MAX297)
- No External Resistors or Capacitors Required
- Internal or External Clock
- Clock to Corner Frequency Ratio:
  100:1 (MAX293/294)
  50:1 (MAX297)
- Operate with a Single +5V Supply or Dual ±5V Supplies
- Uncommitted Op Amp for Anti-Aliasing or Clock-Noise Filtering
- 8-Pin DIP and 16-Pin Wide SO Packages

Ordering Information

PART	TEMP. RANGE	PIN-PACKAGE
MAX293CPA	0°C to +70°C	8 Plastic DIP
MAX293CWE	0°C to +70°C	16 Wide SO
MAX293C/D	0°C to +70°C	Dice*
MAX293EPA	-40°C to +85°C	8 Plastic DIP
MAX293EWE	-40°C to +85°C	16 Wide SO
MAX293MJA	-55°C to +125°C	8 CERDIP**
MAX294CPA	0°C to +70°C	8 Plastic DIP
MAX294CWE	0°C to +70°C	16 Wide SO
MAX294C/D	0°C to +70°C	Dice*

Ordering Information continued on last page.

* Contact factory for dice specifications.

** Contact factory for availability and processing to MIL-STD-883.

Pin Configurations

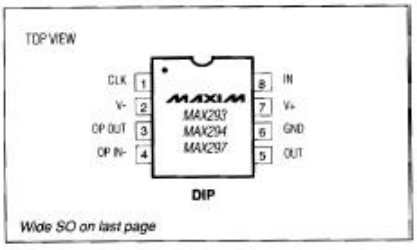

Wide SO on last page

For pricing, delivery, and ordering information, please contact Maxim Direct at 1-888-629-4642, or visit Maxim's website at www.maxim-ic.com.

8th-Order, Lowpass, Elliptic, Switched-Capacitor Filters

ABSOLUTE MAXIMUM RATINGS

Supply Voltage (V+ to V-) 12V
Input Voltage at Any Pin ..... (V- - 0.3V) ≤ V_{IN} ≤ (V+ + 0.3V)
Continuous Power Dissipation
8-Pin Plastic DIP (derate 9.09mW/°C above +70°C) ... 727mW
16-Pin Wide SO (derate 9.52mW/°C above +70°C) ... 762mW
8-Pin CERDIP (derate 8.00mW/°C above +70°C) ... 640mW

Operating Temperature Ranges:
MAX29_C_ ..... 0°C to +70°C
MAX29_E_ ..... -40°C to +85°C
MAX29_MJA ..... -55°C to +125°C
Storage Temperature Range ..... -65°C to +160°C
Lead Temperature (soldering, 10 sec) ..... +300°C

Stresses beyond those listed under "Absolute Maximum Ratings" may cause permanent damage to the device. These are stress ratings only, and functional operation of the device at these or any other conditions beyond those indicated in the operational sections of the specifications is not implied. Exposure to absolute maximum rating conditions for extended periods may affect device reliability.

ELECTRICAL CHARACTERISTICS

(V+ = 5V, V- = -5V, filter output measured at OUT pin, 20kΩ load resistor to ground at OUT, f_{CLK} = 100kHz (MAX293/MAX294) or f_{CLK} = 50kHz (MAX297) T_A = T_{MIN} to T_{MAX}, unless otherwise noted.)

PARAMETER	CONDITIONS		MIN	TYP	MAX	UNITS
FILTER CHARACTERISTICS						
Corner-Frequency Range	MAX293/MAX294			0.1-25k		Hz
	MAX297			0.1-50k		
Clock to Corner Frequency Ratio	MAX293/MAX294			100:1		
	MAX297			50:1		
Clock to Corner Frequency Tempco	MAX293			8		ppm/°C
	MAX294			7		
	MAX297			4		
Insertion Gain Relative to DC Gain (Note 1)	MAX293	f_{IN} = 0.381F_O	0.12	-0.10	-0.17	dB
		f_{IN} = 0.594F_O	0.12	0.02	-0.17	
		f_{IN} = 0.759F_O	0.12	-0.11	-0.17	
		f_{IN} = 0.866F_O	0.12	-0.03	-0.17	
		f_{IN} = 0.939F_O	0.12	-0.11	-0.17	
		f_{IN} = 0.993F_O	0.22	0.04	-0.17	
		f_{IN} = 1.000F_O	0.22	0.01	-0.17	
		f_{IN} = 1.500F_O	-73	-78		
		f_{IN} = 1.610F_O	-80	-87		
		f_{IN} = 2.020F_O	-80	-84		
		f_{IN} =4.020F_O	-80	-84		
	MAX294	f_{IN} = 0.425F_O	0.10	-0.11	-0.17	
		f_{IN} = 0.644F_O	0.10	0.02	-0.17	
		f_{IN} = 0.802F_O	0.10	-0.10	-0.17	
		f_{IN} = 0.895F_O	0.10	-0.03	-0.17	
		f_{IN} = 0.946F_O	0.10	-0.07	-0.17	
		f_{IN} = 0.994F_O	0.36	0.16	-0.17	
		f_{IN} = 1.000F_O	0.36	0.13	-0.17	
		f_{IN} = 1.200F_O	-49	-54		
		f_{IN} = 1.270F_O	-57	-62		
		f_{IN} = 1.530F_O	-57	-60		
		f_{IN} = 2.840F_O	-57	-60		

ELECTRICAL CHARACTERISTICS (continued)

(V+ = 5V, V- = -5V, filter output measured at OUT pin, 20kΩ load resistor to ground at OUT, f_{CLK} = 100kHz (MAX293/MAX294) or f_{CLK} = 50kHz (MAX297) $T_A = T_{MIN}$ to T_{MAX}, unless otherwise noted.)

PARAMETER	CONDITIONS		MIN	TYP	MAX	UNITS
Insertion Gain Relative to DC Gain (Note 1) (continued)	MAX297	$f_{IN} = 0.377F_0$	0.10	-0.11	-0.17	dB
		$f_{IN} = 0.591F_0$	0.10	0.03	-0.17	
		$f_{IN} = 0.754F_0$	0.10	-0.12	-0.17	
		$f_{IN} = 0.873F_0$	0.10	0.02	-0.17	
		$f_{IN} = 0.944F_0$	0.10	-0.07	-0.17	
		$f_{IN} = 0.996F_0$	0.30	0.11	-0.17	
		$f_{IN} = 1.000F_0$	0.30	0.10	-0.17	
		$f_{IN} = 1.500F_0$	-73	-79		
		$f_{IN} = 1.610F_0$	-80	-87		
		$f_{IN} = 2.020F_0$	-80	-84		
		$f_{IN} = 4.000F_0$	-80	-85		
Passband Ripple	MAX293			0.15		dB
	MAX294			0.27		
	MAX297			0.23		
Output DC Swing			±4			V
Output Offset Voltage	IN = GND			±150	±400	mV
DC Insertion Gain with Output Offset Removed			-0.15	±0.01	0.15	dB
Total Harmonic Distortion plus Noise	T_A = +25°C	MAX293		-71		dB
		MAX294		-69		
		MAX297		-77		
Clock Feedthrough	T_A = +25°C			5.0		mVp-p
Output Drive Capability			20	10		kΩ
CLOCK						
Internal Oscillator Frequency	C_{OSC} = 1000pF		29	35	43	kHz
Internal Oscillator Current Source/Sink	V_{CLK} = 0V or 5V			±70	±120	µA
Clock Input (Note 2) High			4.0			V
Low					1.0	
UNCOMMITTED OP AMP						
Input Offset Voltage				±10	±50	mV
Output Drive Capability			20	10		kΩ
Output DC Swing			±4			V
Gain-Bandwidth Product				4		MHz
POWER REQUIREMENTS						
Supply Voltage Dual Supply			±2.375		±5.5	V
Single Supply	V- = 0V, GND = V+/2		4.75		11.0	
Supply Current	V+ = 5V, V- = -5V, V_{CLK} = 0V to 5V			15.0	22.0	mA
	V+ = 2.375V, V- = -2.375V, V_{CLK} = -2V to 2V			7.0	12.0	

Note 1: Test frequencies selected at ripple peaks and troughs.
Note 2: Guaranteed by design.

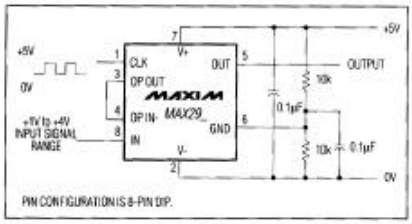

Figure 3. +5V Single-Supply Operation

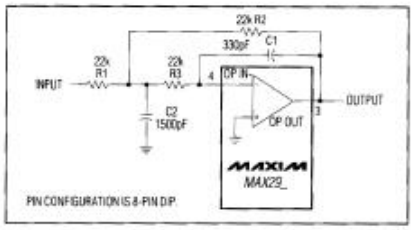

Figure 4. Uncommitted Op Amp Configured as a 2nd-Order Butterworth Lowpass Filter (F_O = 10kHz)

same mismatch in a ladder filter design will spread its error over all poles.

Clock-Signal Requirements

The MAX293/MAX294/MAX297 maximum recommended clock frequency is 2.5MHz, producing a cutoff frequency of 25kHz for the MAX293/MAX294 and 50kHz for the MAX297. The CLK pin can be driven by an external clock or by the internal oscillator with an external capacitor. For external clock applications, the clock circuitry has been designed to interface with +5V CMOS logic. Drive the CLK pin with a CMOS gate powered from 0V and +5V when using either a single supply or dual ±5V supplies. Varying the rate of an external clock will dynamically adjust the filter's corner frequency.

When using the internal oscillator, the capacitance (C_{OSC}) on the CLK pin determines the oscillator frequency:

$$f_{OSC(kHz)} = \frac{10^5}{3C_{OSC(pF)}}$$

The stray capacitance at CLK should be minimized, since it will affect the internal oscillator frequency.

Applications Information

Power Supplies

The MAX293/MAX294/MAX297 operate from either dual or single power supplies. The dual-supply voltage range is ±2.375V to ±5.5V (0.1µF bypass capacitors from each supply to GND are recommended). When using a single supply, tie the V- pin to ground and bias the GND pin to the mid-supply point using a resistor-divider network, as shown in Figure 3.

Input-Signal Amplitude Range

The ideal input-signal range is determined by observing at what voltage level the signal-to-noise plus distortion (SINAD) ratio is maximized for a given corner frequency. The *Typical Operating Characteristics* show the MAX293/MAX294/MAX297 THD + Noise response as the input signal's peak-to-peak amplitude is varied.

Uncommitted Op Amp

The uncommitted op amp has its noninverting input connected to the GND pin, and can be used to build a 1st- or 2nd-order continuous-time lowpass filter. This filter is intended for anti-aliasing applications preceding the switched-capacitor filter, but it can be used as a post-filter to reduce clock noise. Figure 4 shows one of many filters that can be built with this op amp: a 2nd-order Butterworth filter with a 10kHz corner frequency and an input impedance greater than 22kΩ. Table 1 gives alternative component values for different corner frequencies of the same Butterworth filter.

Table 1. Component Values for Figure 4's Filter

Corner Freq. (Hz)	R1 (kΩ)	R2 (kΩ)	R3 (kΩ)	C1 (F)	C2 (F)
100k	10	10	10	68p	330p
50k	20	20	20	68p	330p
25k	20	20	20	150p	680p
10k	22	22	22	330p	1.5n
1k	22	22	22	3.3n	15n
100	22	22	22	33n	150n
10	22	22	22	330n	1.5µ

NOTE: Some approximations have been made in selecting preferred component values.

The passband error caused by a 2nd-order Butterworth can be calculated using the formula:

$$\text{Gain error} = -10\log\left[1 + \left(\frac{f}{f_C}\right)^4\right] \text{ dB}$$

8th-Order, Lowpass, Elliptic, Switched-Capacitor Filters

As the passband ripple of the MAX293/MAX294/MAX297 elliptic filters is of the order of ±0.1dB, it is normally appropriate to keep the passband errors of any anti-aliasing filter at or below this level. This is achieved by choosing the corner frequency of Figure 4's Butterworth filter (f_{cB}) to be higher than the corner frequency of the elliptic switched-capacitor filter (f_{cE}) by a factor of 2.5 or more. A factor of 5 or more is recommended to avoid problems with component tolerances, i.e. $f_{cB} > (5)(f_{cE})$.

When using the uncommitted op amp as a post-filter to reduce clock noise, keep the filter's input impedance above 20kΩ to avoid excessive loading of the switched-capacitor filter. Note that the op amp experiences some clock feedthrough, so it is generally more useful for anti-aliasing than for clock-noise attenuation.

DAC Post-Filtering

When using the MAX293/MAX294/MAX297 for DAC post-filtering, synchronize the DAC and the filter clocks. If clocks are not synchronized, beat frequencies will alias into the desired passband. The DAC's clock should be generated by dividing down the switched-capacitor filter's clock.

Harmonic Distortion

Harmonic distortion arises from nonlinearities within the filter. These nonlinearities generate harmonics when a pure sine wave is applied to the filter input. Table 2 lists typical harmonic distortion values for the MAX293/MAX294/MAX297 with a 1kHz 5Vp-p sine wave input signal, a 1MHz clock frequency, and a 20kΩ load.

Table 2. Typical Harmonic Distortion (dB)

FILTER	HARMONIC			
	2nd	3rd	4th	5th
MAX293	70	90	88	92
MAX294	67	90	92	94
MAX297	84	89	93	99

Pin Configurations (continued)

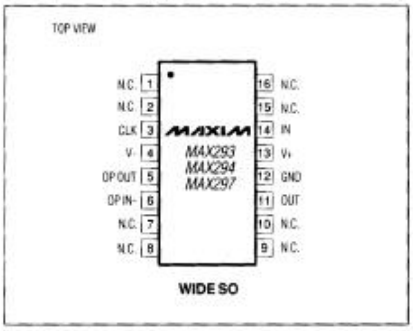

Ordering Information (continued)

PART	TEMP. RANGE	PIN-PACKAGE
MAX294EPA	-40°C to +85°C	8 Plastic DIP
MAX294EWE	-40°C to +85°C	16 Wide SO
MAX294MJA	-55°C to +125°C	8 CERDIP**
MAX297CPA	0°C to +70°C	8 Plastic DIP
MAX297CWE	0°C to +70°C	16 Wide SO
MAX297C/D	0°C to +70°C	Dice*
MAX297EPA	-40°C to +85°C	8 Plastic DIP
MAX297EWE	-40°C to +85°C	16 Wide SO
MAX297MJA	-55°C to +125°C	8 CERDIP**

** Contact factory for dice specifications.*
*** Contact factory for availability and processing to MIL-STD-883.*

Maxim cannot assume responsibility for use of any circuitry other than circuitry entirely embodied in a Maxim product. No circuit patent licenses are implied. Maxim reserves the right to change the circuitry and specifications without notice at any time.

© 2008 Maxim Integrated Products MAXIM is a registered trademark of Maxim Integrated Products, Inc.

APPENDIX E

APPENDIX E

OPA 177 DATASHEET

BURR-BROWN®

OPA177

Precision OPERATIONAL AMPLIFIER

FEATURES

- LOW OFFSET VOLTAGE: 25μV max
- LOW DRIFT: 0.3μV/°C
- HIGH OPEN-LOOP GAIN: 130dB min
- LOW QUIESCENT CURRENT: 1.5mA typ
- REPLACES INDUSTRY-STANDARD OP AMPS: OP-07, OP-77, OP-177, AD707, ETC.

APPLICATIONS

- PRECISION INSTRUMENTATION
- DATA ACQUISITION
- TEST EQUIPMENT
- BRIDGE AMPLIFIER
- THERMOCOUPLE AMPLIFIER

DESCRIPTION

The OPA177 precision bipolar op amp feature very low offset voltage and drift. Laser-trimmed offset, drift and input bias current virtually eliminate the need for costly external trimming. The high performance and low cost make them ideally suited to a wide range of precision instrumentation.

The low quiescent current of the OPA177 dramatically reduce warm-up drift and errors due to thermoelectric effects in input interconnections. It provides an effective alternative to chopper-stabilized amplifiers. The low noise of the OPA177 maintains accuracy.

OPA177 performance gradeouts are available. Packaging options include 8-pin plastic DIP and SO-8 surface-mount packages.

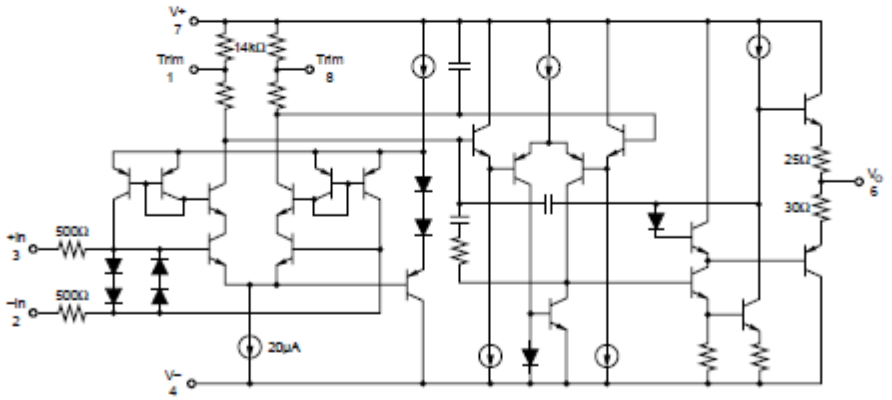

International Airport Industrial Park • Mailing Address: PO Box 11400, Tucson, AZ 85734 • Street Address: 6730 S. Tucson Blvd., Tucson, AZ 85706 • Tel: (520) 746-1111 • Twx: 910-952-1111
Internet: http://www.burr-brown.com/ • FAXLine: (800) 548-6133 (US/Canada Only) • Cable: BBRCORP • Telex: 066-6491 • FAX: (520) 889-1510 • Immediate Product Info: (800) 548-6132

©1990 Burr-Brown Corporation

PDS-1081E

Printed in U.S.A. August, 1997

SBOS008

OPA177 SPECIFICATIONS

At V_S = ±15V, T_A = +25°C, unless otherwise noted.

PARAMETER	CONDITION	OPA177F MIN	OPA177F TYP	OPA177F MAX	OPA177G MIN	OPA177G TYP	OPA177G MAX	UNITS
OFFSET VOLTAGE								
Input Offset Voltage			10	25		20	60	µV
Long-Term Input Offset[1] Voltage Stability			0.3			0.4		µV/Mo
Offset Adjustment Range	R_P = 20kΩ		±3			*		mV
Power Supply Rejection Ratio	V_S = ±3V to ±18V	115	125		110	120		dB
INPUT BIAS CURRENT								
Input Offset Current			0.3	1.5		*	2.8	nA
Input Bias Current			0.5	±2		*	±2.8	nA
NOISE								
Input Noise Voltage	1Hz to 100Hz[2]		85	150		*	*	nVrms
Input Noise Current	1Hz to 100Hz		4.5			*		pArms
INPUT IMPEDANCE								
Input Resistance	Differential Mode[3]	26	45		18.5	*		MΩ
	Common-Mode		200			*		GΩ
INPUT VOLTAGE RANGE								
Common-Mode Input Range[4]		±13	±14		*	*		V
Common-Mode Rejection	V_{CM} = ±13V	130	140		115	*		dB
OPEN-LOOP GAIN	R_L ≥ 2kΩ							
Large Signal Voltage Gain	V_O = ±10V[5]	5110	12,000		2000	6000		V/mV
OUTPUT								
Output Voltage Swing	R_L ≥ 10kΩ	±13.5	±14		*	*		V
	R_L ≥ 2kΩ	±12.5	±13		*	*		V
	R_L ≥ 1kΩ	±12	±12.5		*	*		V
Open-Loop Output Resistance			60			*		Ω
FREQUENCY RESPONSE								
Slew Rate	R_L ≥ 2kΩ	0.1	0.3		*	*		V/µs
Closed-Loop Bandwidth	G = +1	0.4	0.6		*	*		MHz
POWER SUPPLY								
Power Consumption	V_S = ±15V, No Load		40	60		*	*	mW
	V_S = ±3V, No Load		3.5	4.5		*	*	mW
Supply Current	V_S = ±15V, No Load		1.3	2		*	*	mA

At V_S = ±15V, −40°C ≤ T_A ≤ +85°C, unless otherwise noted.

OFFSET VOLTAGE								
Input Offset Voltage			15	40		20	100	µV
Average Input Offset Voltage Drift			0.1	0.3		0.7	1.2	µV/°C
Power Supply Rejection Ratio	V_S = ±3V to ±18V	110	120		106	115		dB
INPUT BIAS CURRENT								
Input Offset Current			0.5	2.2		*	4.5	nA
Average Input Offset Current Drift[6]			1.5	40		*	85	pA/°C
Input Bias Current			0.5	±4		*	±6	nA
Average Input Bias Current Drift[6]			8	40		15	60	pA/°C
INPUT VOLTAGE RANGE								
Common-Mode Input Range		±13	±13.5		*	*		V
Common-Mode Rejection	V_{CM} = ±13V	120	140		110	*		dB
OPEN-LOOP GAIN								
Large Signal Voltage Gain	R_L ≥ 2kΩ, V_O = ±10V	2000	6000		1000	4000		V/mV
OUTPUT								
Output Voltage Swing	R_L ≥ 2kΩ	±12	±13		*	*		V
POWER SUPPLY								
Power Consumption	V_S = ±15V, No Load		60	75		*	*	mW
Supply Current	V_S = ±15V, No Load		2	25		*	*	mA

* Same as specification for product to left.

NOTES: (1) Long-Term Input Offset Voltage Stability refers to the averaged trend line of V_{OS} vs time over extended periods after the first 30 days of operation. Excluding the initial hour of operation, changes in V_{OS} during the first 30 operating days are typically less than 2µV. (2) Sample tested. (3) Guaranteed by design. (4) Guaranteed by CMRR test condition. (5) To insure high open-loop gain throughout the ±10V output range, A_{OL} is tested at −10V ≤ V_O ≤ 0V, 0V ≤ V_O ≤ +10V, and −10V ≤ V_O ≤ +10V. (6) Guaranteed by end-point limits.

PIN CONFIGURATION

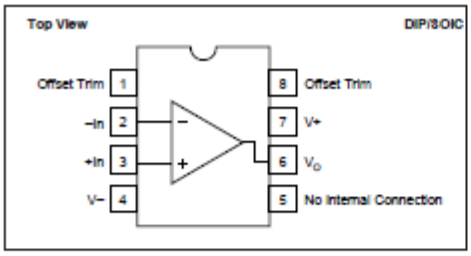

ABSOLUTE MAXIMUM RATINGS

Power Supply Voltage	±22V
Differential Input Voltage	±30V
Input Voltage	$\pm V_S$
Output Short Circuit	Continuous
Operating Temperature:	
Plastic DIP (P), SO-8 (S)	–40°C to +85°C
θ_{JA} (PDIP)	100°C/W
θ_{JA} (SOIC)	150°C/W
Storage Temperature:	
Plastic DIP (P), SO-8 (S)	–65°C to +125°C
Junction Temperature	+150°C
Lead Temperature (soldering, 10s) P packages	+300°C
(soldering, 3s) S package	+260°C

PACKAGE/ORDERING INFORMATION

PRODUCT	PACKAGE	PACKAGE DRAWING NUMBER[1]	TEMPERATURE RANGE
OPA177FP	8-Pin Plastic DIP	006	–40°C to +85°C
OPA177GP	8-Pin Plastic DIP	006	–40°C to +85°C
OPA177GS	SO-8 Surface-Mount	182	–40°C to +85°C

NOTE: (1) For detailed drawing and dimension table, please see end of data sheet, or Appendix C of Burr-Brown IC Data Book.

ELECTROSTATIC DISCHARGE SENSITIVITY

Any integrated circuit can be damaged by ESD. Burr-Brown recommends that all integrated circuits be handled with appropriate precautions. ESD can cause damage ranging from subtle performance degradation to complete device failure. Precision integrated circuits may be more susceptible to damage because very small parametric changes could cause the device not to meet published specifications.

Burr-Brown's standard ESD test method consists of five 1000V positive and negative discharges (100pF in series with 1.5kΩ) applied to each pin.

Failure to observe proper handling procedures could result in small changes to the OPA177's input bias current.

The information provided herein is believed to be reliable; however, BURR-BROWN assumes no responsibility for inaccuracies or omissions. BURR-BROWN assumes no responsibility for the use of this information, and all use of such information shall be entirely at the user's own risk. Prices and specifications are subject to change without notice. No patent rights or licenses to any of the circuits described herein are implied or granted to any third party. BURR-BROWN does not authorize or warrant any BURR-BROWN product for use in life support devices and/or systems.

APPLICATIONS INFORMATION

The OPA177 is unity-gain stable, making it easy to use and free from oscillations in the widest range of circuitry. Applications with noisy or high impedance power supply lines may require decoupling capacitors close to the device pins. In most cases 0.1µF ceramic capacitors are adequate.

The OPA177 has very low offset voltage and drift. To achieve highest performance, circuit layout and mechanical conditions must be optimized. Offset voltage and drift can be degraded by small thermoelectric potentials at the op amp inputs. Connections of dissimilar metals will generate thermal potential which can mask the ultimate performance of the OPA177. These thermal potentials can be made to cancel by assuring that they are equal in both input terminals.

1. Keep connections made to the two input terminals close together.
2. Locate heat sources as far as possible from the critical input circuitry.
3. Shield the op amp and input circuitry from air currents such as cooling fans.

OFFSET VOLTAGE ADJUSTMENT

The OPA177 has been laser-trimmed for low offset voltage and drift so most circuits will not require external adjustment. Figure 1 shows the optional connection of an external potentiometer to adjust offset voltage. This adjustment should not be used to compensate for offsets created elsewhere in a system since this can introduce excessive temperature drift.

INPUT PROTECTION

The inputs of the OPA177 are protected with 500Ω series input resistors and diode clamps as shown in the simplified circuit diagram. The inputs can withstand ±30V differential inputs without damage. The protection diodes will, of course, conduct current when the inputs are overdriven. This may disturb the slewing behavior of unity-gain follower applications, but will not damage the op amp.

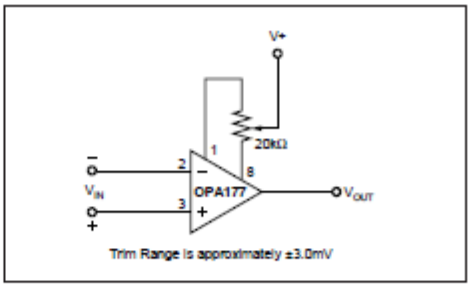

FIGURE 1. Optional Offset Nulling Circuit.

NOISE PERFORMANCE

The noise performance of the OPA177 is optimized for circuit impedances in the range of 2kΩ to 50kΩ. Total noise in an application is a combination of the op amp's input voltage noise and input bias current noise reacting with circuit impedances. For applications with higher source impedance, the OPA627 FET-input op amp will generally provide lower noise. For very low impedance applications, the OPA27 will provide lower noise.

INPUT BIAS CURRENT CANCELLATION

The input stage base current of the OPA177 is internally compensated with an equal and opposite cancellation current. The resulting input bias current is the difference between the input stage base current and the cancellation current. This residual input bias current can be positive or negative.

When the bias current is cancelled in this manner, the input bias current and input offset current are approximately the same magnitude. As a result, it is not necessary to balance the DC resistance seen at the two input terminals (Figure 2). A resistor added to balance the input resistances may actually increase offset and noise.

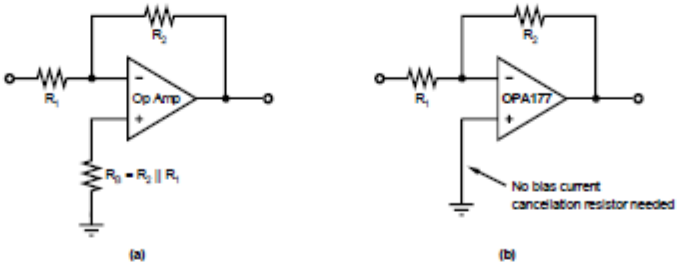

FIGURE 2. Input Bias Current Cancellation.

APPENDIX F

APPENDIX F

DRV 134 DATASHEET

TEXAS INSTRUMENTS

DRV134, DRV135

SBOS094B – JANUARY 1998 – REVISED DECEMBER 2014

DRV13x Audio-Balanced Line Drivers

1 Features

- Balanced Output
- Low Distortion: 0.0005% at f = 1 kHz
- Wide Output Swing: 17Vrms into 600 Ω
- High Capacitive Load Drive
- High Slew Rate: 15 V/µs
- Wide Supply Range: ±4.5 V to ±18 V
- Low Quiescent Current: ±5.2 mA
- 8-Pin DIP, SO-8, and SOL-16 Packages
- Companion to Audio Differential Line Receivers: INA134 and INA137
- Improved Replacement for SSM2142

2 Applications

- Audio Differential Line Drivers
- Audio Mix Consoles
- Distribution Amplifiers
- Graphic and Parametric Equalizers
- Dynamic Range Processors
- Digital Effects Processors
- Telecom Systems
- Hi-Fi Equipment
- Industrial Instrumentation

3 Description

The DRV134 and DRV135 are differential output amplifiers that convert a single-ended input to a balanced output pair. These balanced audio drivers consist of high performance op amps with on-chip precision resistors. They are fully specified for high performance audio applications and have excellent ac specifications, including low distortion (0.0005% at 1 kHz) and high slew rate (15 V/µs).

The on-chip resistors are laser-trimmed for accurate gain and optimum output common-mode rejection. Wide output voltage swing and high output drive capability allow use in a wide variety of demanding applications. They easily drive the large capacitive loads associated with long audio cables. Used in combination with the INA134 or INA137 differential receivers, they offer a complete solution for transmitting analog audio signals without degradation.

The DRV134 is available in 8-pin DIP and SOL-16 surface-mount packages. The DRV135 comes in a space-saving SO-8 surface-mount package. Both are specified for operation over the extended industrial temperature range, –40°C to +85°C and operate from –55°C to +125°C.

Device Information[1]

PART NUMBER	PACKAGE	BODY SIZE (NOM)
DRV134	SOIC (16)	10.30 mm × 7.50 mm
DRV135	SOIC (8)	4.90 mm × 3.91 mm

(1) For all available packages, see the orderable addendum at the end of the datasheet.

4 Simplified Schematic

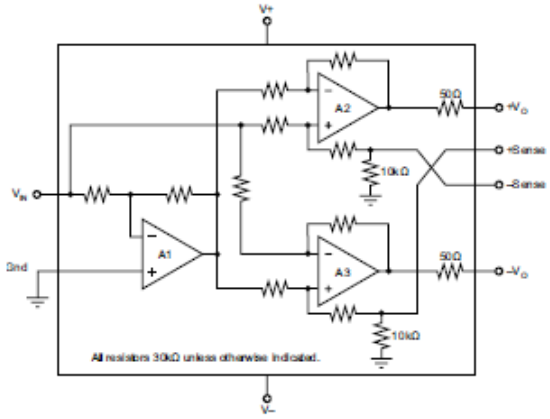

An IMPORTANT NOTICE at the end of this data sheet addresses availability, warranty, changes, use in safety-critical applications, intellectual property matters and other important disclaimers. PRODUCTION DATA.

6 Pin Configuration and Functions

Top View — 8-Pin DIP/SO-8

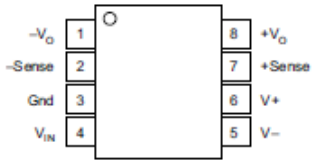

Top View — SOL-16

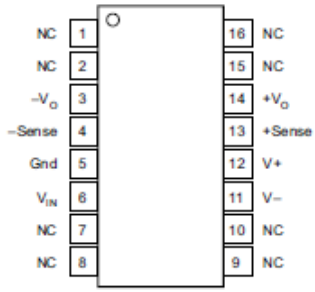

NOTE: NC - No internal connection

Pin Functions

PIN			I/O	DESCRIPTION
NAME	DIP-8 and SO-8	SOL-16		
Gnd	3	5	–	Ground
+Sense	7	13	I	Sensing, non-inverting input
–Sense	2	4	I	Sensing, inverting input
V+	6	12	–	Positive supply
V–	5	11	–	Negative supply
V_{IN}	4	6	I	Input
$–V_o$	1	3	O	Inverted, balanced differential output
$+V_o$	8	14	O	Balanced differential output
NC	–	1,2,7,8,9,10,15,16	–	These pins should be left unconnected

Copyright © 1998–2014, Texas Instruments Incorporated

7 Specifications

7.1 Absolute Maximum Ratings

over operating free-air temperature range (unless otherwise noted) (1)

	MIN	MAX	UNIT
Supply voltage, V+ to V–		40	V
Input voltage range	V–	V+	
Output short-circuit (to ground)		Continuous	
Operating temperature	–55	125	°C
Junction temperature		150	°C

(1) Stresses beyond those listed under Absolute Maximum Ratings may cause permanent damage to the device. These are stress ratings only, which do not imply functional operation of the device at these or any other conditions beyond those indicated under *Recommended Operating Conditions* . Exposure to absolute-maximum-rated conditions for extended periods may affect device reliability.

7.2 Handling Ratings

			MIN	MAX	UNIT
T_{stg}	Storage temperature range		–55	125	°C
$V_{(ESD)}$	Electrostatic discharge	Human body model (HBM), per ANSI/ESDA/JEDEC JS-001, all pins(1)	–2000	2000	V
		Charged device model (CDM), per JEDEC specification JESD22-C101, all pins(2)	–500	500	

(1) JEDEC document JEP155 states that 500-V HBM allows safe manufacturing with a standard ESD control process.
(2) JEDEC document JEP157 states that 250-V CDM allows safe manufacturing with a standard ESD control process.

7.3 Recommended Operating Conditions

over operating free-air temperature range (unless otherwise noted)

		MIN	NOM	MAX	UNIT
T_{spe}	Specification temperature range	–40		85	°C
T_A	Operation temperature range	–55		125	°C
V+	Positive supply	4.5	18	18	V
V–	Negative supply	–4.5	–18	–18	V

Copyright © 1998–2014, Texas Instruments Incorporated

7.4 Electrical Characteristics

At T_A = +25°C, V_S = ±18 V, R_L = 600 Ω differential connected between $+V_O$ and $-V_O$, unless otherwise noted.

PARAMETER			TEST CONDITIONS	MIN	TYP	MAX	UNIT
AUDIO PERFORMANCE							
THD+N	Total Harmonic Distortion + Noise		f = 20Hz to 20kHz, V_O = 10Vrms		0.001%		
			f = 1kHz, V_O = 10Vrms		0.0005%		
RTO(1)	Noise Floor		20 kHz BW THD+N < 1%		–98		dBu
RTO(1)	Headroom				27		dBu
INPUT							
Z_{IN}	Input Impedance(2)				10		kΩ
I_{IN}	Input Current		V_{IN} = ±7.07 V	–1000	±700	1000	µA
GAIN							
	Differential						
	Initial		$[(+V_O) – (–V_O)]/V_{IN}$ V_{IN} = ±10V	5.8	6		dB
	Error			–2%	±0.1%	2%	
	Error vs Temperature				±10		ppm/°C
	Single-Ended		V_{IN} = ±5V				
	Initial			5.8	6		dB
	Error			–2%	±0.7%	2%	
	Error vs Temperature				±10		ppm/°C
	Nonlinearity				0.0003		% of FS
OUTPUT							
OCMR	Common-Mode Rejection, f = 1kHz		See Figure 25	46	68		dB
SBR	Signal Balance Ratio, f = 1kHz		See Figure 26	35	54		dB
	Output Offset Voltage						
V_{OCM}(3)	Offset Voltage, Common-Mode		V_{IN} = 0	–250	±50	250	mV
	Offset Voltage, Common-Mode vs Temperature				±150		µV/°C
V_{OD}(4)	Offset Voltage, Differential		V_{IN} = 0	–10	±1	10	mV
	Offset Voltage, Differential vs Temperature				±5		µV/°C
PSRR	Offset Voltage, Differential vs Power Supply		V_S = ±4.5V to ±18V	80	110		dB
	Output Voltage Swing,	Positive	No Load(5)	(V+) – 3	(V+) – 2.5		V
		Negative		(V–) + 2	(V–) + 1.5		
	Impedance				50		Ω
C_L	Load Capacitance, Stable Operation		C_L Tied to Ground (each output)		1		µF
I_{SC}	Short-Circuit Current				±85		mA
FREQUENCY RESPONSE							
	Small-Signal Bandwidth				1.5		MHz
SR	Slew Rate				15		V/µs
	Settling Time: 0.01%		V_{OUT} = 10V Step		2.5		µs
	Overload Recovery		Output Overdriven 10%		3		µs
POWER SUPPLY							
V_S	Rated Voltage				±18		V
	Voltage Range			±4.5		±18	V
I_Q	Quiescent Current		I_O = 0	–5.5	±5.2	5.5	mA

(1) dBu = 20log (Vrms /0.7746); RTO = Referred-to-Output.
(2) Resistors are ratio matched but have ±20% absolute value.
(3) $V_{OCM} = [(+V_O) + (–V_O)] / 2$.
(4) $V_{OD} = (+V_O) – (–V_O)$.
(5) Ensures linear operation. Includes common-mode offset.

Copyright © 1998–2014, Texas Instruments Incorporated

Electrical Characteristics (continued)

At T_A = +25°C, V_S = ±18 V, R_L = 600 Ω differential connected between $+V_O$ and $-V_O$, unless otherwise noted.

PARAMETER			TEST CONDITIONS	MIN	TYP	MAX	UNIT
TEMPERATURE RANGE							
	Specification Range			–40		85	°C
	Operation Range			–55		125	°C
	Storage Range			–55		125	°C
θ_{JA}	Thermal Resistance	8-Pin DIP			100		°C/W
		SO-8 Surface mount			150		°C/W
		SOL-16 Surface mount			80		°C/W

7.5 Typical Characteristics

At T_A = 25°C, V_S = ±18 V, R_L = 600 Ω differential connected between $+V_O$ and $-V_O$, unless otherwise noted.

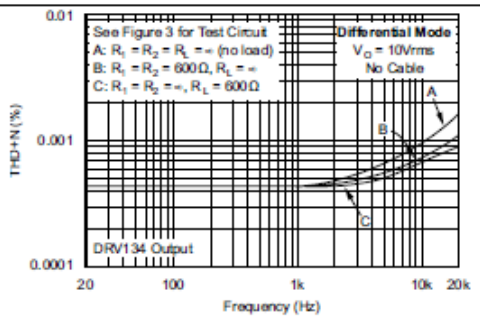

Figure 1. Total Harmonic Distortion + Noise vs Frequency

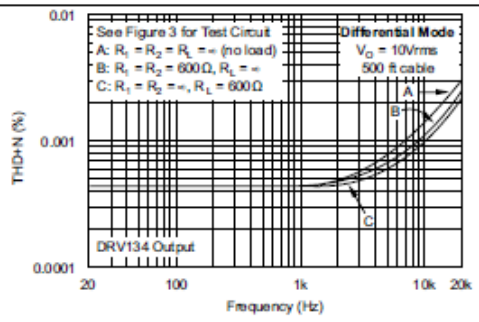

Figure 2. Total Harmonic Distortion + Noise vs Frequency

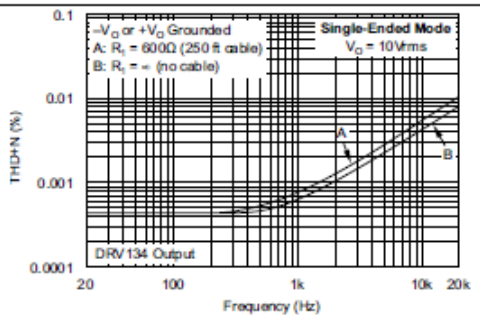

Figure 3. Total Harmonic Distortion + Noise vs Frequency

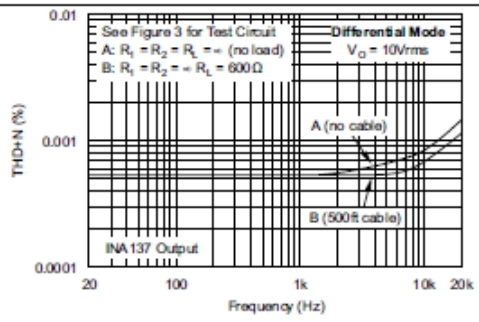

Figure 4. System Total Harmonic Distortion + Noise vs Frequency

Copyright © 1998–2014, Texas Instruments Incorporated

8 Detailed Description

8.1 Overview

The DRV134 and DRV135 consist of an input inverter driving a cross- coupled differential output stage with 50 Ω series output resistors. Characterized by low differential-mode output impedance (50 Ω) and high common-mode output impedance (1.6 kΩ), the DRV134 and DRV135 are ideal for audio applications.

Excellent internal design and layout techniques provide low signal distortion, high output level (27 dBu), and a low noise floor (–98 dBu). Laser trimming of thin film resistors assures excellent output common-mode rejection (OCMR) and signal balance ratio (SBR). In addition, low dc voltage offset reduces errors and minimizes load currents.

The *Functional Block Diagram* section shows a detailed block diagram of the DRV134 and DRV135.

8.2 Functional Block Diagram

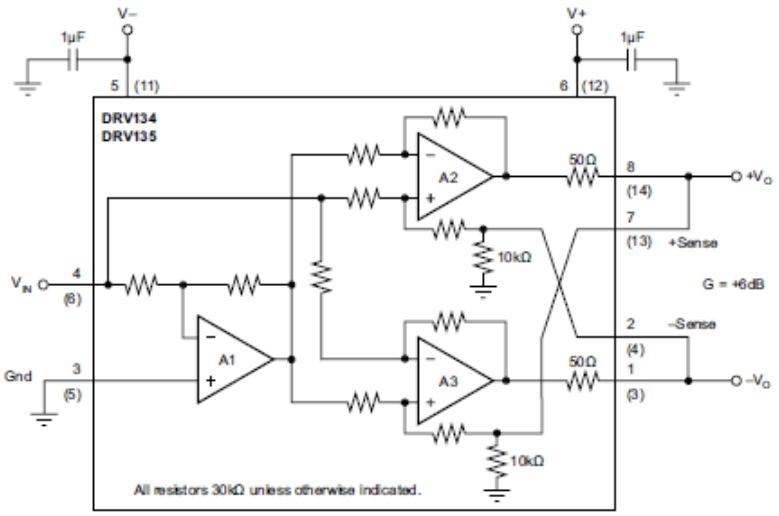

8.3 Feature Description

8.3.1 Audio Performance

The DRV134 and DRV135 were designed for enhanced ac performance. Very low distortion, low noise, and wide bandwidth provide superior performance in high quality audio applications. Laser-trimmed matched resistors provide optimum output common-mode rejection (typically 68dB), especially when compared to circuits implemented with op amps and discrete precision resistors. In addition, high slew rate (15 V/µs) and fast settling time (2.5 µs to 0.01%) ensure excellent dynamic response.

The DRV134 and DRV135 have excellent distortion characteristics. As shown in the distortion data provided in the *Typical Characteristics* section, THD+Noise is below 0.003% throughout the audio frequency range under various output conditions. Both differential and single-ended modes of operation are shown. In addition, the optional 10µF blocking capacitors used to minimize V_{OCM} errors have virtually no effect on performance. Measurements were taken with an Audio Precision System One (with the internal 80 kHz noise filter) using the THD test circuit shown in Figure 24.

Copyright © 1998–2014, Texas Instruments Incorporated

Feature Description (continued)

Up to approximately 10 kHz, distortion is below the measurement limit of commonly used test equipment. Furthermore, distortion remains relatively constant over the wide output voltage swing range (approximately 2.5 V from the positive supply and 1.5 V from the negative supply). A special output stage topology yields a design with minimum distortion variation from lot-to-lot and unit-to-unit. Furthermore, the small and large signal transient response curves demonstrate the stability under load of the DRV134 and DRV135.

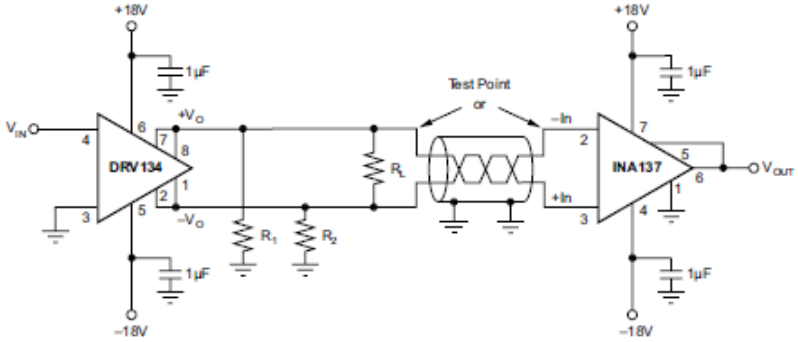

Figure 24. Distortion Test Circuit

8.3.2 Output Common-Mode Rejection

Output common-mode rejection (OCMR) is defined as the change in differential output voltage due to a change in output common-mode voltage. When measuring OCMR, V_{IN} is grounded and a common-mode voltage, VCM, is applied to the output as shown in Figure 25. Ideally no differential mode signal (VOD) should appear. However, a small mode-conversion effect causes an error signal whose magnitude is quantified by OCMR.

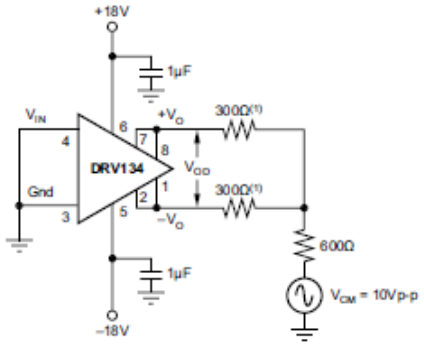

Figure 25. Output Common-Mode Rejection Test Circuit

8.3.3 Signal Balance Ratio

Signal balance ratio (SBR) measures the symmetry of the output signals under loaded conditions. To measure SBR an input signal is applied and the outputs are summed as shown in Figure 26. V_{OUT} should be zero since each output ideally is exactly equal and opposite. However, an error signal results from any imbalance in the outputs. This error is quantified by SBR. The impedances of the DRV134 and DRV135's output stages are closely matched by laser trimming to minimize SBR errors. In an application, SBR also depends on the balance of the load network.

Copyright © 1998–2014, Texas Instruments Incorporated

Feature Description (continued)

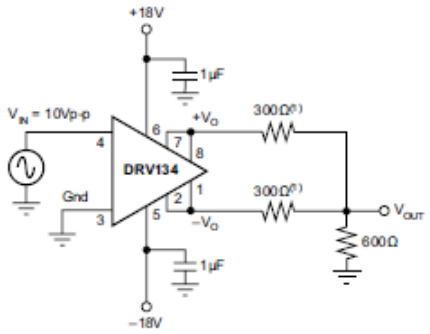

Figure 26. Signal Balance Ratio Test Circuit

8.4 Device Functional Modes

8.4.1 Differential-Output Mode

In differential-output mode, the DRV134 (and DRV135 in SO-8 package) converts a single-ended, ground-referenced input to a floating differential output with +6 dB gain (G = 2). Figure 27 shows the basic connections required for operation in differential-output mode.

Normally, $+V_O$ is connected to +Sense, $-V_O$ is connected to –Sense, and the outputs are taken from these junctions as shown in Figure 27.

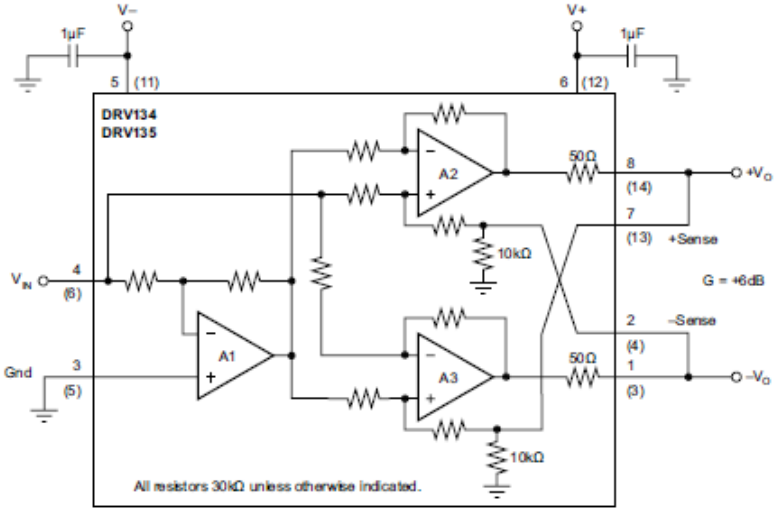

Figure 27. Basic Connections for Differential-Output Mode

Copyright © 1998–2014, Texas Instruments Incorporated

Device Functional Modes (continued)

8.4.2 Single-Ended Mode

The DRV134 can be operated in single-ended mode without degrading output drive capability. Single-ended operation requires that the unused side of the output pair be grounded (both the V_O and Sense pins) to a low impedance return path. Gain remains +6 dB. Grounding the negative outputs as shown in Figure 28 results in a non-inverted output signal (G = +2) while grounding the positive outputs gives an inverted output signal (G = –2).

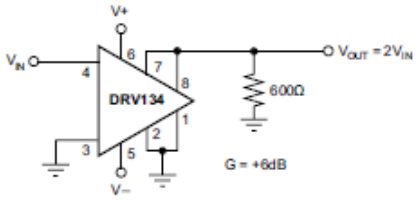

Figure 28. Typical Single-Ended Application

For best rejection of line noise and hum differential mode operation is recommended. However, single-ended performance is adequate for many applications. In general single ended performance is comparable to differential mode (see THD+N typical performance curves), but the common mode and noise rejection inherent in balanced-pair systems is lost.

Copyright © 1998–2014, Texas Instruments Incorporated

9 Application and Implementation

NOTE

Information in the following applications sections is not part of the TI component specification, and TI does not warrant its accuracy or completeness. TI's customers are responsible for determining suitability of components for their purposes. Customers should validate and test their design implementation to confirm system functionality.

9.1 Application Information

Decoupling capacitors placed close to the device pins are strongly recommended in applications with noisy or high impedance power supplies.

For best system performance, it is recommended that a high input-impedance difference amplifier be used as the receiver. Used with the INA134 (G = 0 dB) or the INA137 (G = ±6 dB) differential line receivers, the DRV134 forms a complete solution for driving and receiving audio signals, replacing input and output coupling transformers commonly used in professional audio systems (Figure 29). When used with the INA137 (G = –6 dB) overall system gain is unity.

9.2 Typical Application

9.2.1 Cable Driving Application

The DRV134 is capable of driving large signals into 600-Ω loads over long cables. Low impedance shielded audio cables such as the standard Belden 8451 or 9452 (or similar) are recommended, especially in applications where long cable lengths are required.

For applications with large dc cable offset errors, a 10-µF electrolytic nonpolarized blocking capacitor at each sense pin is recommended as shown in Figure 29.

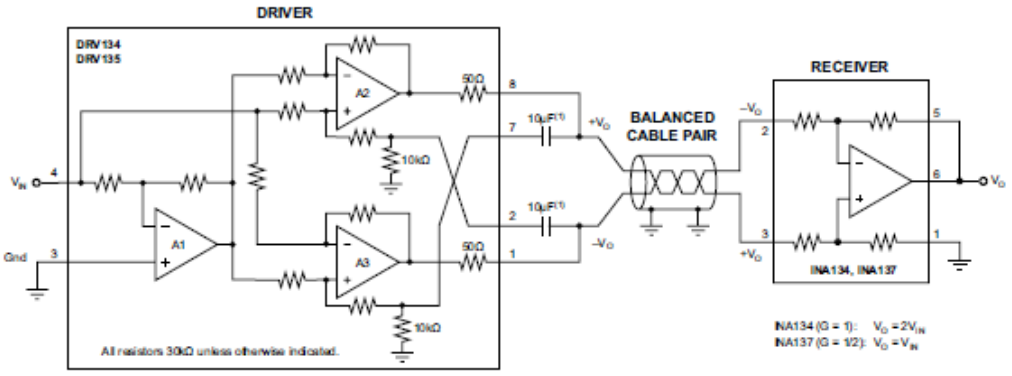

Figure 29. Complete Audio Driver and Receiver Circuit

9.2.1.1 *Design Requirements*

Consider a design with the goal of differentially transmitting a single ended signal of up to 22.2 dBu through 500 ft of cable with no load at the receiving side. The signal at the end of the cable should have no more than 0.002 percent of total harmonic distortion plus noise (THD+N) at 10 kHz and less than 0.0005 percent of THD+N for frequencies between 20 Hz and 1 kHz.

The system is required to put out a single ended signal 0 dB with respect to the input signal and accommodate inputs with peak to RMS ratios of up to 1.5 for the maximum 22.2 dBu range established above.

Copyright © 1998–2014, Texas Instruments Incorporated

Typical Application (continued)

9.2.1.2 Detailed Design Procedure

The dBu is a common unit of measurement for input sensitivity and output level of professional audio equipment. A 0 dBu signal dissipates 1 mW into a 600-Ω resistive load; therefore, a 0 dBu signal corresponds to approximately 0.775 V_{RMS}. Equation 1 shows the relationship between the signal level in dBu (denoted by L_u) and the signal level in V_{RMS} (denoted by x).

$$L_u = 20\log_{10}\left(\frac{x}{0.775}\right) \quad (1)$$

For this design, the single ended input signal of 22.2 dBu corresponds to 9.98 V_{RMS} as shown in Equation 2.

$$V_{IN} = 0.775\left(10^{\frac{L_u}{20}}\right) = 9.98\ V_{RMS} \quad (2)$$

Given that the system must accommodate for 22.2 dBu signals with up to 1.5 of peak to RMS ratio, the maximum peak input signal is 14.97 V_{PEAK} as calculated in Equation 3.

$$V_{IN\ PEAK} = 1.5(9.98) = 14.97\ V_{PEAK} \quad (3)$$

The DRV134 is chosen to convert the single ended input signal into a differential signal and the outputs of the DRV134 will be connected to one end of the 500 ft cable. In order to prevent clipping and distortion of the input signal, the power supply rails for the DRV134 are chosen as 3 V above and below the peak calculated in Equation 3. The 3 V margin is derived from the output voltage swing specification given in the *Electrical Characteristics* table. The supplies selected are 18 V for V+ and –18 V for V–.

Finally, the INA137 is used at the end of the 500 ft cable in order to convert the differential signal output of the DRV134 into a single ended signal that is 0 dB with respect to the input signal.

Figure 30 shows the system diagram.

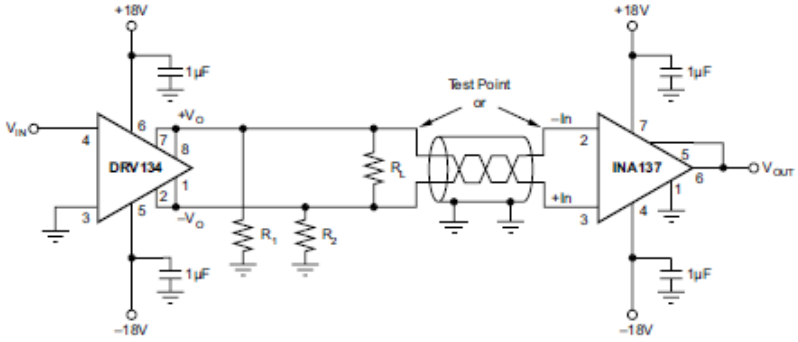

Figure 30. Diagram of System Based on DRV134 and INA137

Copyright © 1998–2014, Texas Instruments Incorporated

APPENDIX G

APPENDIX G

INSERT CAD DRAWINGS

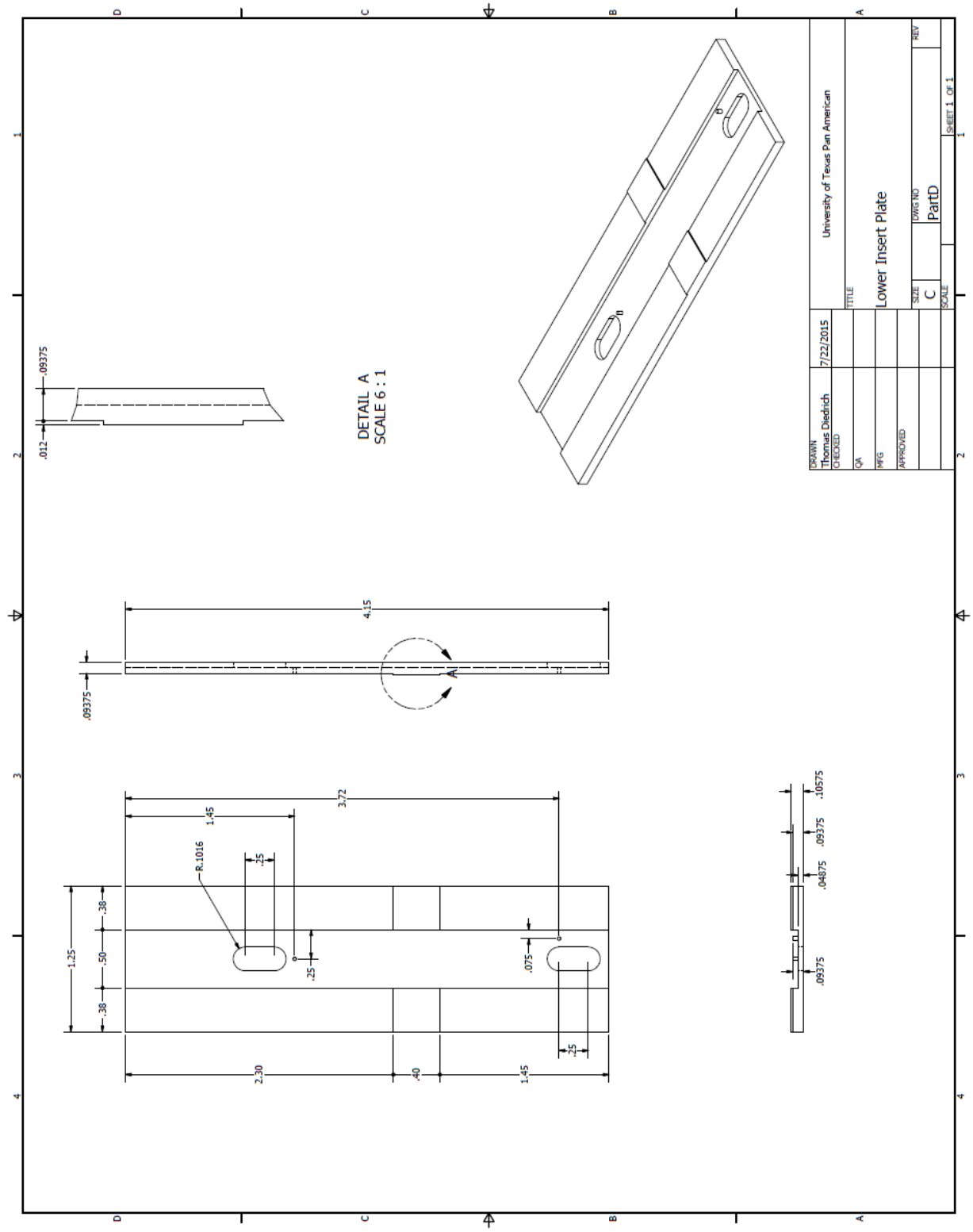

*All dimensions labeled are inches

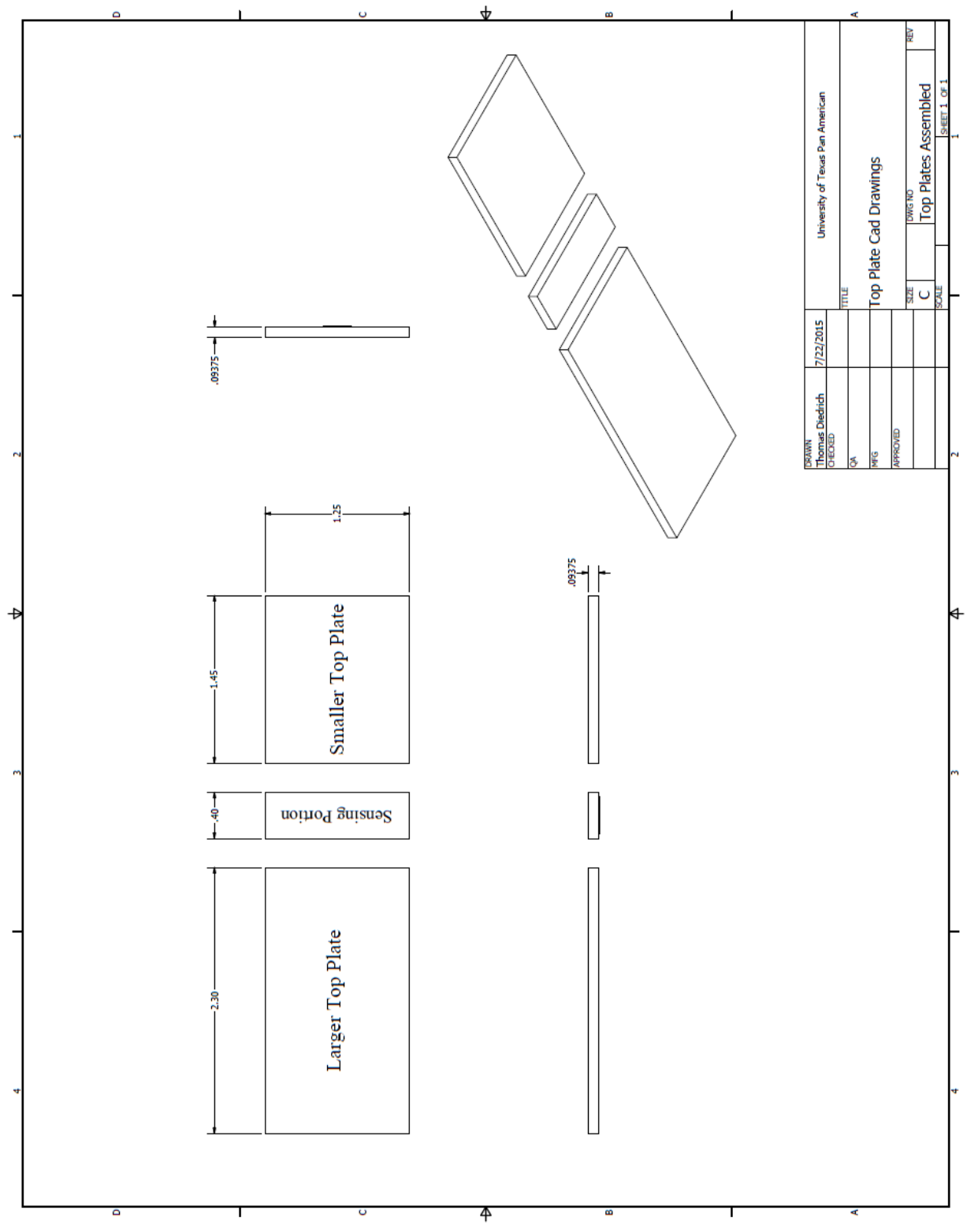

*All dimensions labeled are inches

APPENDIX H

APPENDIX H

ADDITIONAL SENSOR RAMPING FIGURES

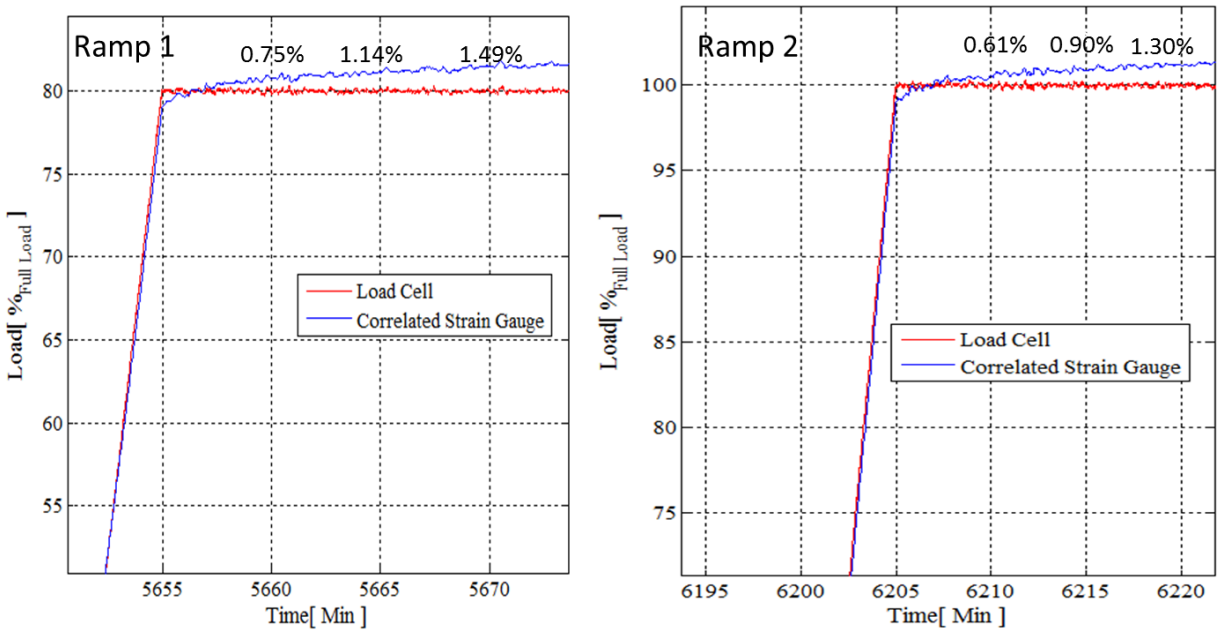

Figure 51: Ramp 1 (80% Load 15 Minute View) and Ramp 2 (100% Load 15 Minute View) for Adapter A

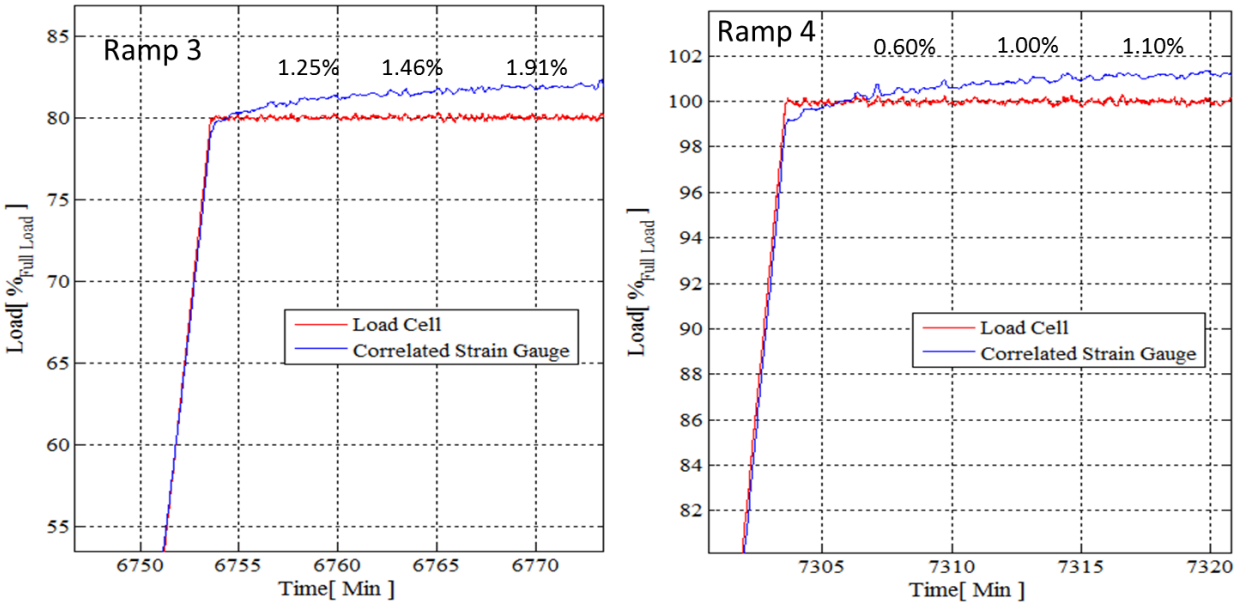

Figure 52: Ramp 3 (80% Load 15 Minute View) and Ramp 4 (100% Load 15 Minute View) for Adapter A

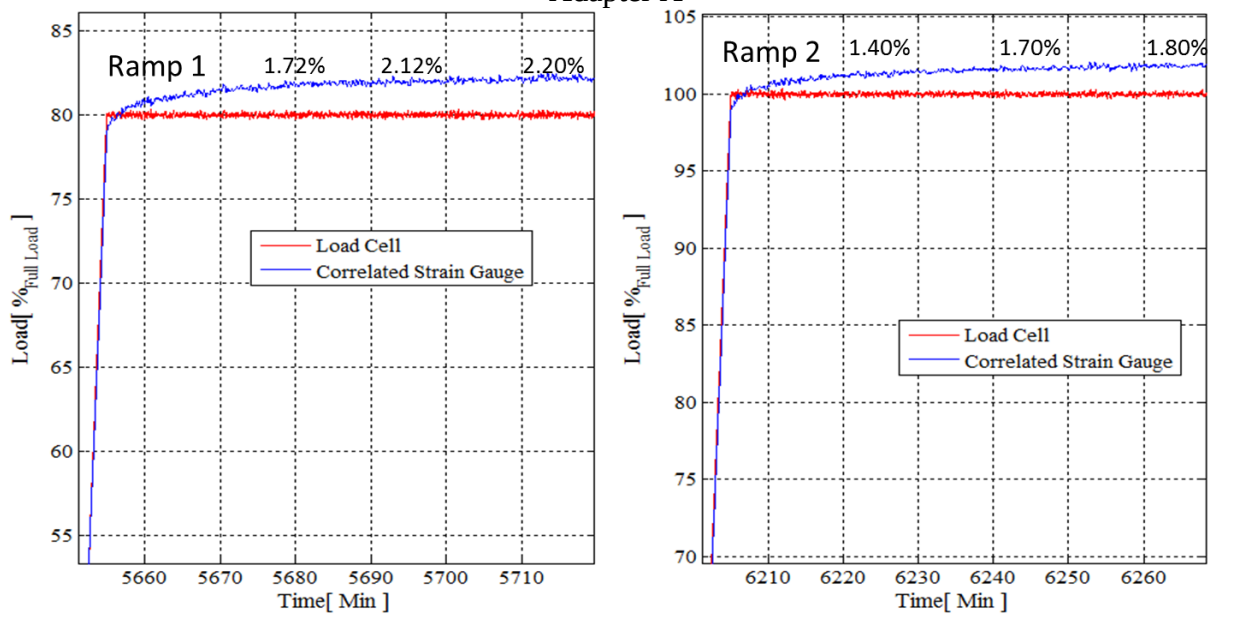

Figure 53: Ramp 1 (80% Load 1 Hour View) and Ramp 2 (100% Load 1 Hour View) for Adapter A

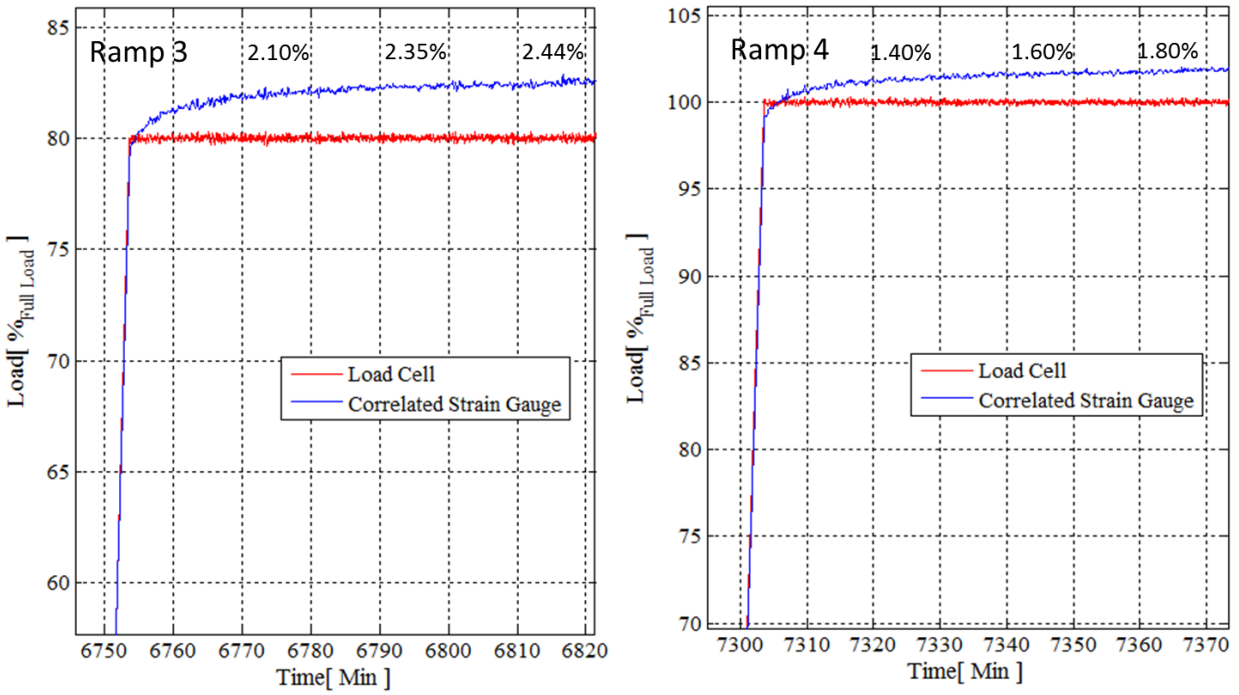

Figure 54: Ramp 3 (80% Load 1 Hour View) and Ramp 4 (100% Load 1 Hour View) for Adapter A

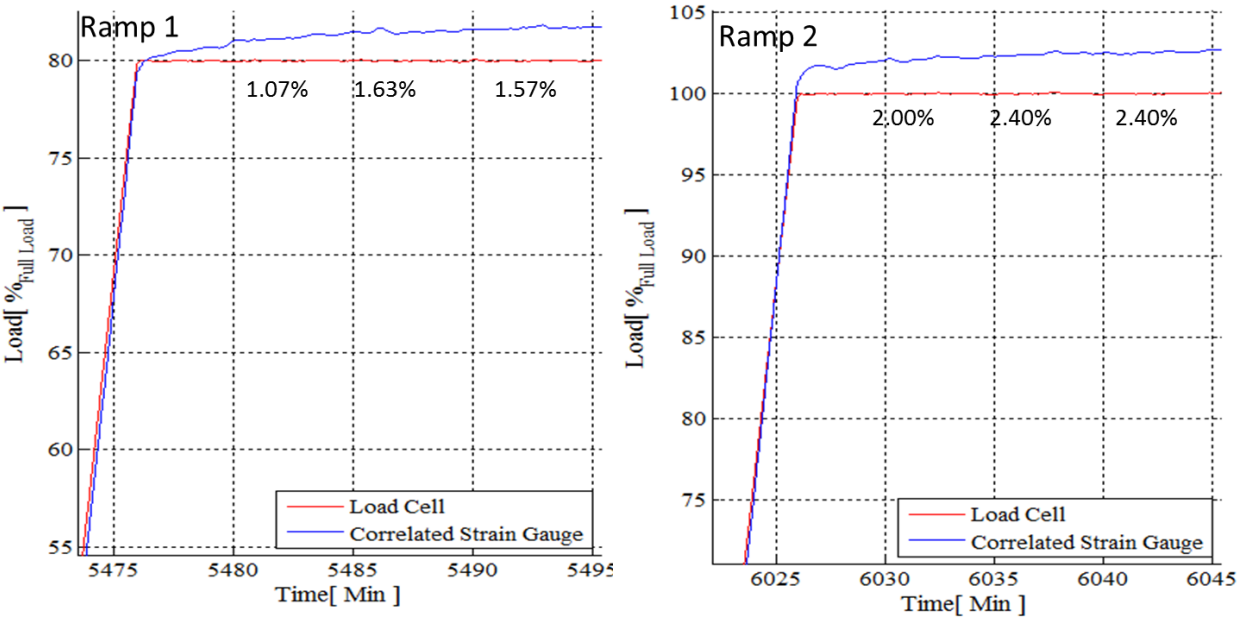

Figure 55: Ramp 1 (80% Load 15 Minute View) and Ramp 2 (100% Load 15 Minute View) for Adapter B

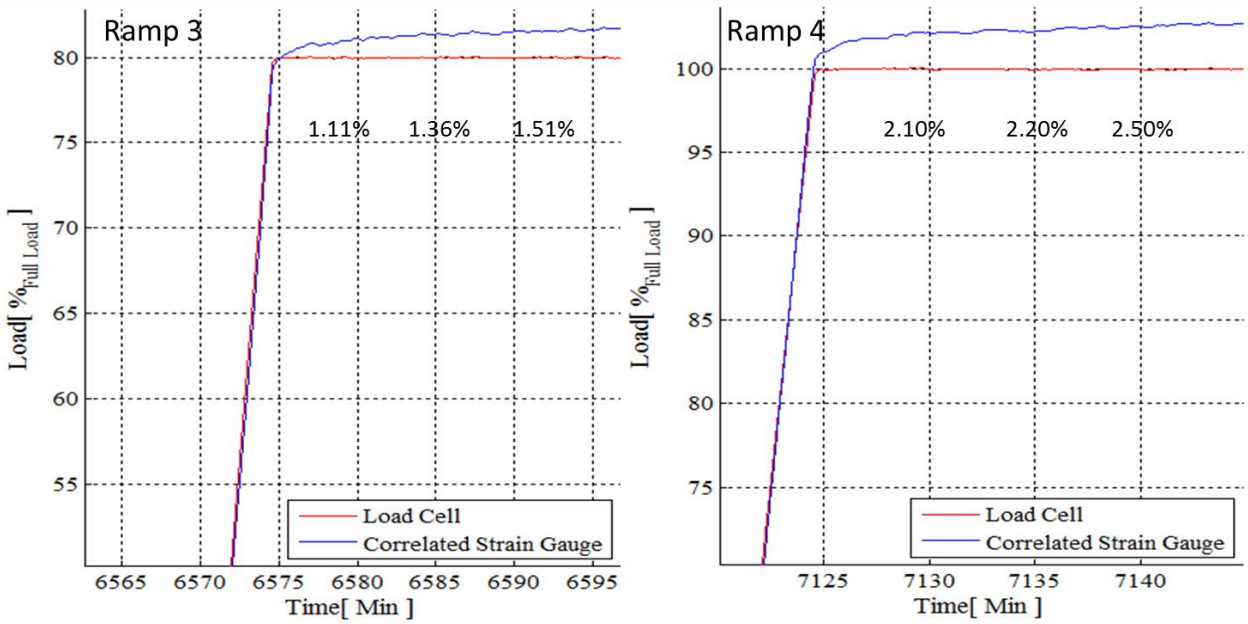

Figure 56: Ramp 3 (80% Load 15 Minute View) and Ramp 4 (100% Load 15 Minute View) for Adapter B

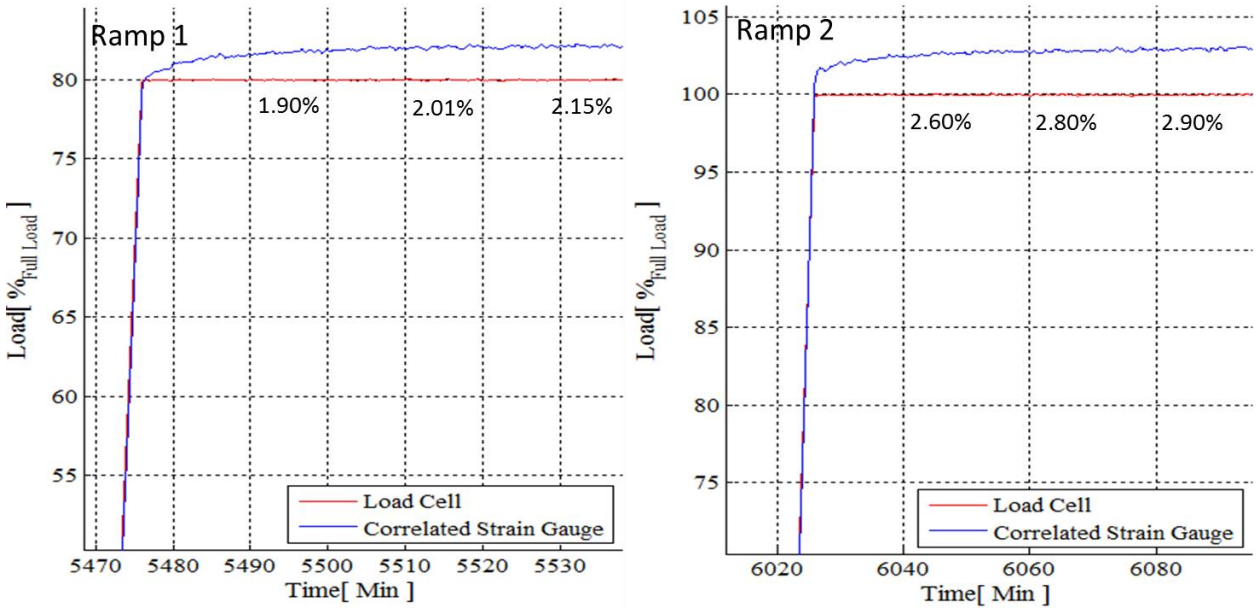

Figure 57: Ramp 1 (80% Load 1 Hour View) and Ramp 2 (100% Load 1 Hour View) for Adapter B

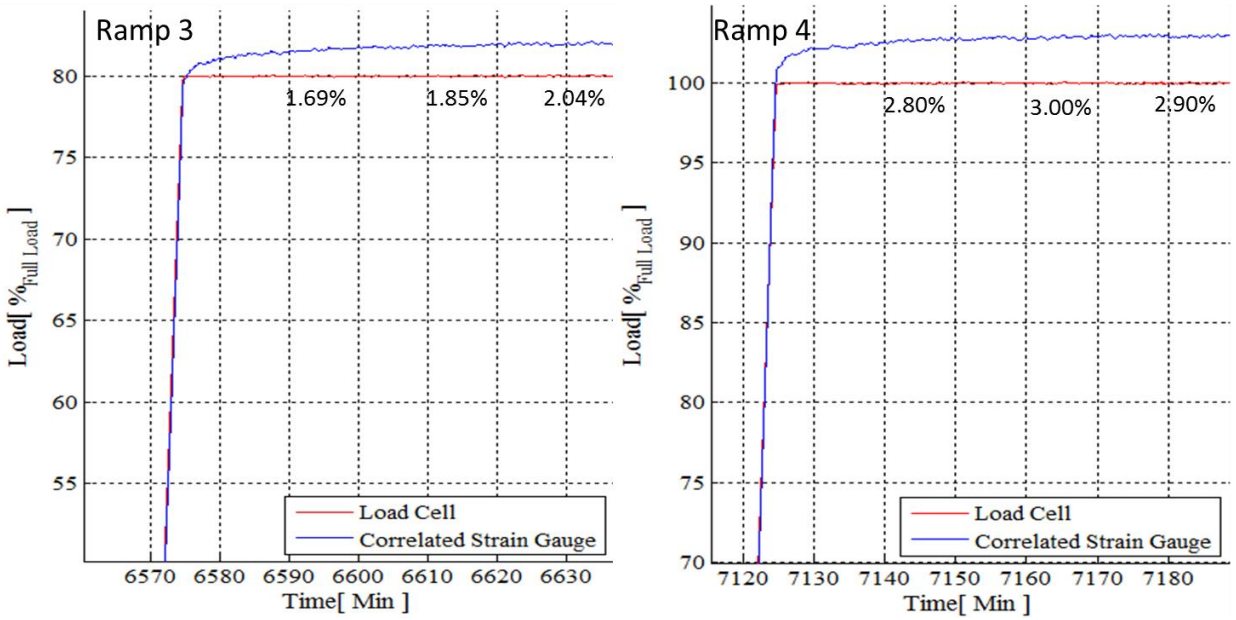

Figure 58: Ramp 3 (80% Load 1 Hour View) and Ramp 4 (100% Load 1 Hour View) for Adapter B

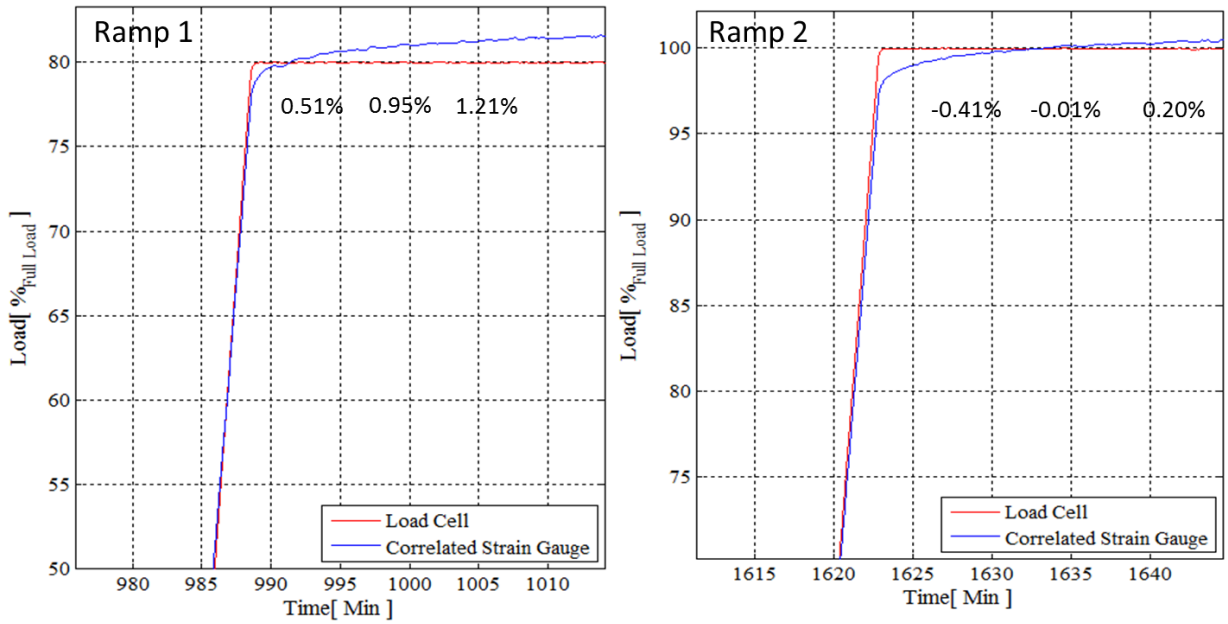

Figure 59: Ramp 1 (80% Load 15 Minute View) and Ramp 2 (100% Load 15 Minute View) for Adapter C

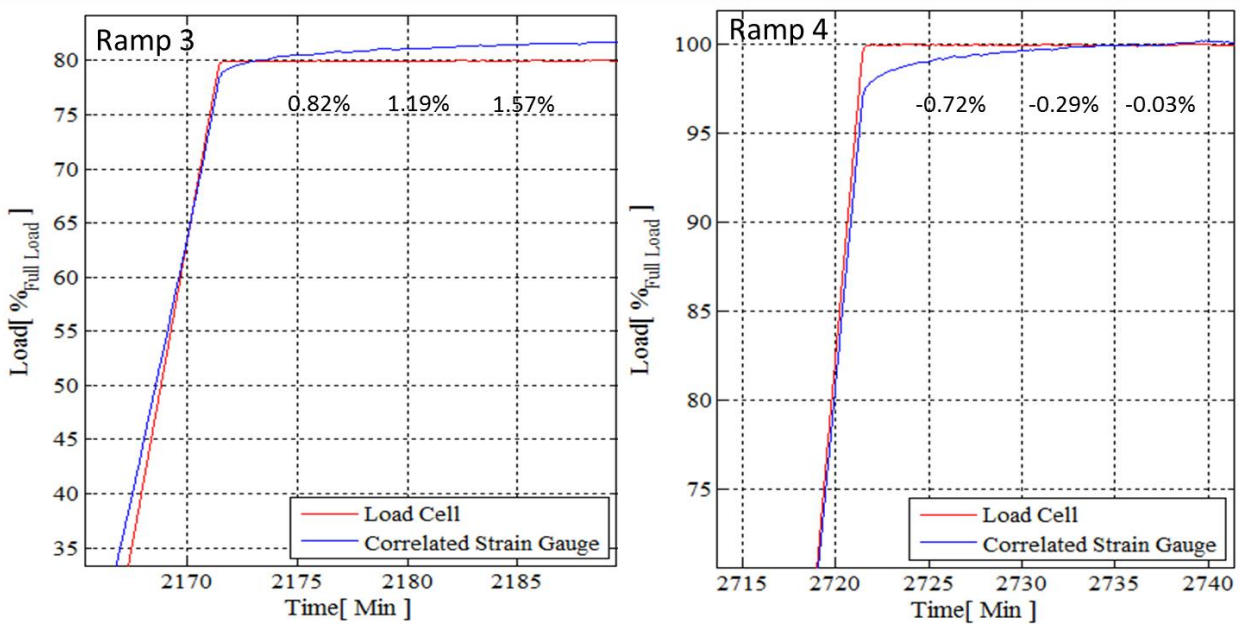

Figure 60: Ramp 3 (80% Load 15 Minute View) and Ramp 4 (100% Load 15 Minute View) for Adapter C

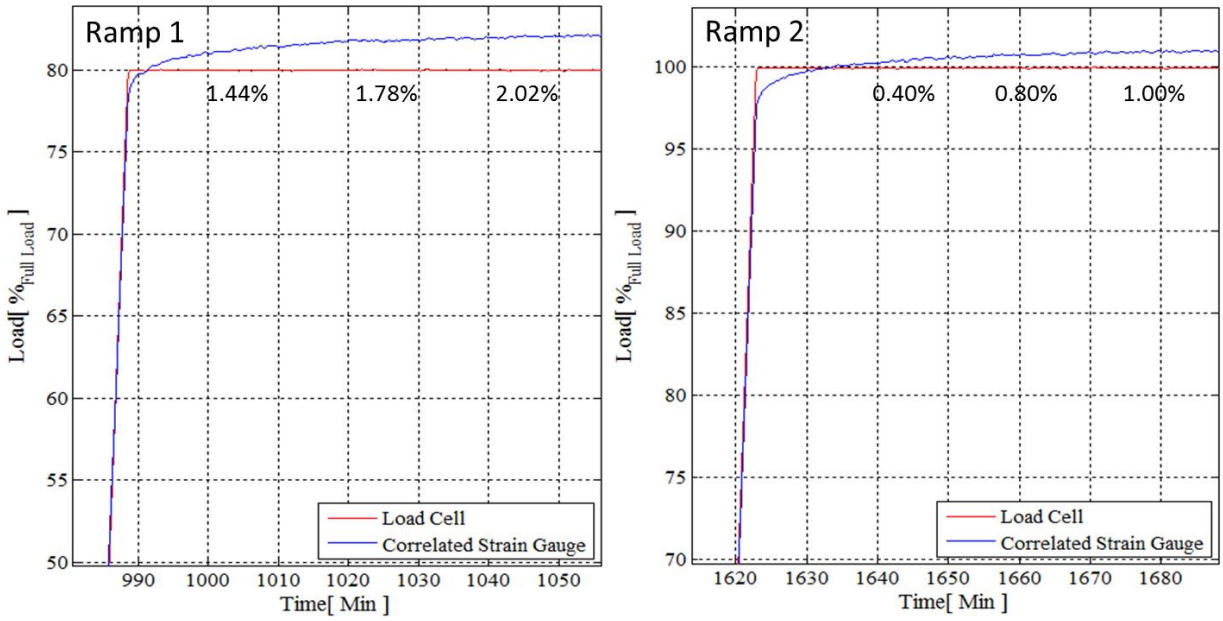

Figure 61: Ramp 1 (80% Load 1 Hour View) and Ramp 2 (100% Load 1 Hour View) for Adapter C

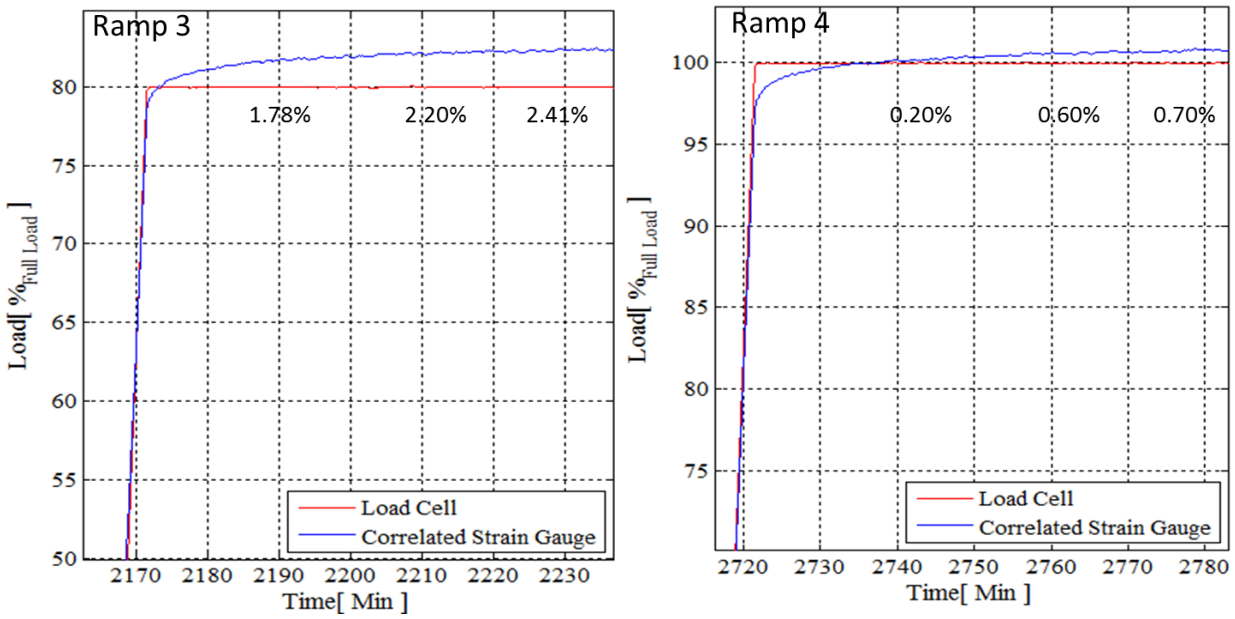

Figure 62: Ramp 3 (80% Load 1 Hour View) and Ramp 4 (100% Load 1 Hour View) for Adapter C

APPENDIX I

APPENDIX I

ADAPTER CORRELATIONS

Table 4: Second Order Adapter Correlation

	Sensor Correlation			
	X_1	X_2	X_3	Gain (V/V)
Adapter A	0.39	7.19	-15.58	400
Adapter B	0.86	-0.92	-5.83	400
Adapter C	0.03	10.00	-28.70	400

$\text{Load(Kips)} = X_1 \cdot V^2 + X_2 \cdot V + X_3$

V = voltage output of sensor

BIOGRAPHICAL SKETCH

Thomas Michael Diedrich was born on November 25, 1991 in Weslaco, TX to a Thomas and Ida Diedrich. He graduated from Weslaco East High School in 2010. After which he attended The University of Texas Pan American where he graduated with his Bachelor of Science in Mechanical Engineering in 2013. He continued his education at The University of Texas Pan American and earned a Master of Science degree in Mechanical Engineering in August 2015. His time at The University of Texas Pan American did not only included attending classes, but served as a research assistant for three years on the Railroad Research Team funded by Amsted Rail Industries, Inc. Thomas can be reached at mdiedrich.mece@gmail.com or by 1802 N. International Blvd., Weslaco, TX 78599